UNIVERSITAT ROVIRA I VIRGILI

NEW ADVANCES TO CONTROL MORPHOLOGY AND CRYSTALLINITY IN SOLUTION PROCESSED POLYMER SOLAR CELLS.

Peilin Han

Dipòsit Legal: T 256-2016

Ph.D   THESIS

New Advances to Control Morphology and Crystallinity in Solution Processed Polymer Solar Cells

Peilin Han

Supervised by: **Prof. Lluís Francesc Marsal Garví**

Departament d'Engineyeria Electrònica, Elèctrica i Automàtica

Nanoelectronic and Photonic Systems (NePhos)

UNIVERSITAT ROVIRA I VIRGILI

Tarragona
2015

Departament d'Enginyeria Electrònica, Elèctrica I Automàtica
Escola Tècnica Superior d'Enginyeria
Campus Sescelades
Avda. Països Catalans 26
43007 Tarragona, Spain
Tel. +34 977 55 96 10
Fax +34 977 55 96 05

I STATE that the present study, entitled "New advances to Control Morphology and Crystallinity in Solution Processed Polymer Solar Cells", presented by Peilin Han for the award of the degree of Doctor, has been carried out under my supervision at the Department of Electrical, Electronic and Automatic Control Engineering of this University, and that it fulfils all the requirements to be eligible for the International Doctorate Award.

Tarragona, 2th of November 2014

Doctoral thesis supervisor

Prof. Lluís Francesc Marsal Garví

Acknowledgement

After the past four years, I still remembered the scene at first time I came to spain. Even I can't image how to finish my PhD with the situation at that time without all support from you all.

First, I would owe my sincere gratitude to my supervisor Lluis Marsal. Without your friendly reply when I was applying to study PhD, I would miss a good learning opportunity in solar cells research. Thank you for all effort you have given me do independent work and it will add a heavy and thick thing in my research career.

I would like to thank Dr. Josep Ferre-Borrull for his valuable suggestion.

I would like to thank Dr. Maria Alba for her priceless assistance in my life and research, although our lines of research separated. Thank you very much for correcting my paper and thesis even though you have left and you are being busy for your postdoctoral work in Australia. I am going to remember for your kindness and friendliness.

I would like to thank Dr. Agustin Mihi for correcting my paper and suggestion in my research. I also would like to thank Dr. Victor Balderrama for directing me how to work about solar cells at the beginning.

I would also like to thank Dr. Emilio Palomares and his work team in ICIQ for your friendly technical supporting. Especially to Werther Cambarauby for the experience, the knowledge and the availability of time that they gave me.

I would like to express my gratitude to the members of Nephos group, past and present, for their collaboration and kindness. Especially to Pilar Formentin for her

technical support during my PhD, and fellow PhD candidate Chris, Jose, Maria, Agada, Gerad, Pedro, Edith, Catarina, Elisabet, et al. thank for your friendly help and discussion in the lab.

I would like to acknowledge that the staff at the Servie center of the Universitat Rovira i Virgili, Francesc, Merce, Mariana, Rita and Lucas, for their professionalism and guidance in the numerous characterization session.

Finally, I would like to thank my parents for their unconditional love and encouragement throughout my entire life. I specially thank my wife for giving me a happy life and a very important new life, my cute son Muyang.

List of Abbreviation

AFM	Atomic force microscopy
BHJ	Bulk heterojunction
CB	Chlorobenzene
CE	Charge extraction
CHN	Cyclohexanone
CT	Charge-transfer
DCB	Di-chlorobenzene
DIO	1,8-diiodoctane
EQE	External quantum efficiency
ETL	Electron transport layer
FF	Fill factor
FWHM	Full width at half-maximum
GIXS	Grazing incidence X-ray scattering
HOMO	Highest occupied molecular orbital
HTL	Hole transport layer
IQE	Internal quantum efficiency
ITO	Indium tin oxide
Jsc	Short circuit current
KPFM	Kelvin probe force microscopy
LUMO	Lowest unoccupied molecular orbital
OSC	Organic solar cells
OPV	Organic photovoltaic
$PC_{61}BM$	Phenyl-C61- butyric acid methyl ester
$PC_{71}BM$	Phenyl-C71-butyric acid methyl ester
PCE	Power conversion efficiency
PEDOT:PSS	Poly-(Ethylene dioxythiophene) doped with Poly-(Styrene

	Sulphonic acid)
P3HT	Poly (3-hexylthiophene)
PL	Photoluminescence
c-PSC	Conventional polymer solar cells
i-PSC	Inverted polymer solar cells
PTB1	Poly [[4,8-bis (octyloxy) benzo (1,2-b:4,5-b') dithiophene-2,6-diyl) (2-((dodecyloxy) carbonyl) thieno(3,4-b) thiophenediyl]]
PTB7	Poly[[4,8-bis[(2-ethylhexyl)oxy] Benzo [1,2-b:4,5-b'] dithiophene-2,6-diyl] [3-fluoro-2-[(2-ethylhexyl)carbonyl]-thieno-[3,4-b]thiophenediyl]]
SEM	Scanning electron microscopy
TEM	Transmission electron microscopy
TPV	Transient photovoltage technique
Voc	Open circuit voltage

Table of Content

Acknowledgement

List of abbreviation

List of contribution

Chapter 1

General Introduction

Energy and environment is an everlasting topic in the industrialization process of mankind. Over the past decades great efforts have focused on the development of new alternative renewable energy resources. In this chapter I mainly state the energy status in the world, work principle of polymer solar cells and factors affecting solar cells efficiency.

Chapter 1

Chapter 1

Table of content

1.1 Current energy and development of organic solar cells

1.2 Polymer solar cells and polymer materials

1.3 The working principle of solar cells

1.3.1 Light absorption and exciton generation

1.3.2 Exciton dissociation

1.3.3 Charge transport and charge collection

1.4 Characterization of solar cells performance

1.5 Factors determining performance of polymer solar cells

1.5.1 Properties of polymer

1.5.1.1 Absorption spectrum of polymer
1.5.1.2 Energy level match

1.5.2 Morphology of photoactive layer

1.5.2.1 Solvent additive and solvent mixture
1.5.2.2 Thermal annealing and post-annealing
1.5.2.3 Solvent annealing
1.5.2.4 Donor:acceptor ratio

1.5.3 The selection of electrode and interfacial layer materials

1.6 The aim of this thesis

1.7 References

Chapter 1

1.1 Current energy and development of organic solar cells

Energy and the environment is an everlasting topic in the industrialization process of mankind. Over the past decades great efforts have focused on the development of new alternative renewable energy resources. [1] In terms of globally installed capacity, solar energy is now the third most important renewable energy resource, after hydro and wind power (Figure 1.1). [2, 3] Compared to other energies, solar energy is present in abundance and its captivation requires little maintenance and no moving parts. Moreover, solar energy does not cause any environment pollution like fossil fuels and nuclear power. [4, 5] Focusing on these advantages, the preparation of different types solar cells have become one of the hottest scientific topics worldwide.
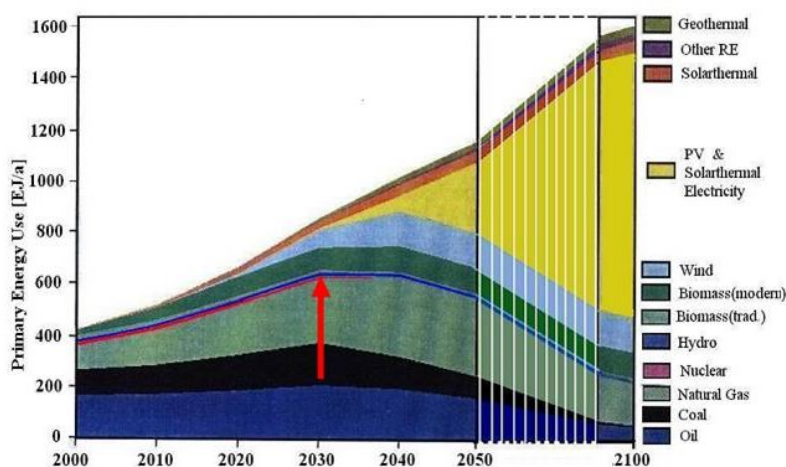
Figure 1.1. Prediction of World Future Energy structure from International Energy Agency (IEA)

Presently, thin film solar cells such as CaTe-based and silicon-based photovoltaic cells are made by depositing an active layer with a thickness of a few micrometers on a substrate. The power conversion efficiency (PCE) of crystalline silicon has reached 24% and has also been used commercially. [3, 6] Up to now, the crystalline silicon technology dominates the global PV industry with around 80%. [7] However, many drastic conditions are involved in the manufacturing process of general inorganic

Chapter 1

semiconductor-based solar cells and environmentally invasive chemicals are formed during the production. Besides, large scale preparations are difficult due to the inflexibility of general inorganic solar cells, thereby limiting further applicability. Hence, the exploitation of new molecular materials of low cost but high flexibility has become an interesting and exciting area of research.

Recently, the use of organic semiconductor materials opened a new domain of alternative energy conversion. Organic semiconductors have attracted much attention because of their fundamental scientific importance and impressive improvements in performance in a wide variety of photonic applications, such as organic light diodes (OLED), organic field-effect transistor (OFET), organic solar cells, etc.. [8-12] Compared to the general inorganic solar cells, organic solar cells (OSC) have a very bright future and they can make solar cells component with several potential advantages, including light weight, low cost production and a relatively low environmental contamination. [13, 14] In addition, OSCs have the possibility of creating devices with a large-area and flexible substrate selectivity and are therefore exploited in industrial applications (Figure 1.2).

Figure 1.2. Example of the unique properties of organic photovoltaic

Chapter 1

1.2 Polymer solar cells and polymer materials

Initial OSCs devices were based on a vapor- deposited small molecule donor and acceptor with a heterojunction structure exhibiting a PCE of ~ 1%. During the past several decades a dramatic performance increase has been achieved, particularly through the development of cell structures of bulk heterojunction (BHJ) devices and the exploitation of new materials. [15-17] In recent years OSCs based on π-conjugated polymers, so called polymer solar cells (PSCs), have attracted widespread interest in academic and commercial communities. These polymers are promising in terms of their electronic properties, low cost, chemical stability and flexible preparation, while the PCE values higher than 9% have been achieved today. [18-20]

Thin layers of high work function ITO or FTO as transparent electrode are coated onto a glass or plastic substrate during the manufacturing of typical BHJ PSC devices. The photoactive layer blend layer is sandwiched between two electrodes (cathode and anode). The top electrode is usually given by a low work function cathode, typically Al or Ag. [21, 22] In addition, the interfacial layer can be inserted between the active layer and the electrode to improve the performance of the device and to stabilize the operation. [23] The photoactive layer basically comprises an organic active layer with a conjugated polymer donor and a soluble conjugated acceptor.

To achieve cells with a high PCE and stability the materials have to be designed carefully to provide suitable highest occupied molecular orbital (HOMO)/ lowest unoccupied molecular orbital (LUMO) energy levels, large solar light absorption, and good microstructure morphology [24] as well as transport characteristics. The polymer donor serves as the main solar light absorber and as the hole transporting phase, whereas the acceptor transports electrons. Therefore these two materials possess a wide optical absorption range (to match the solar spectrum) (Figure 1.3),

Chapter 1

large extinction coefficients, and large carrier mobilities which are basic requirements toward the design of ideal photoactive blends. [25] These two materials are promising further great advantages, such as lower weight and chemical tenability.
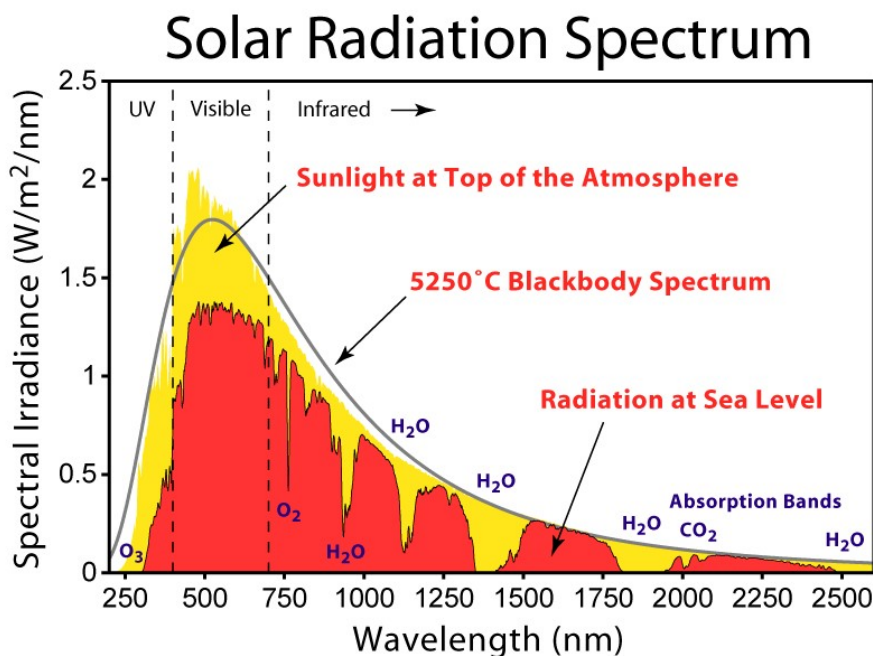
Figure 1.3. Energy distribution of ground solar spectrum

The structures of a conjugated polymer play an important role in determining the physical and chemical properties of donor and acceptor materials and further influence the performance of solar cells. Materials with a delocalized π electron system can absorb sunlight and create and transport photogenerated charge carriers. Figure 1.4 summarizes the molecular structures of some main polymer donors and acceptors. [26-28] Most donor structures are obtained from material classes such as thiophene, fluorine and carbazole based on copolymers. These low band gap polymer donors contribute to a wide spectrum response and serve as an excellent charge transporter with a high hole mobility. For example, recently, Yu and coworkers have explored a series of PTBx polymers as excellent donor materials in great detail. [29, 30] A PCE of 9% has been achieved by solar cells based on PTB7 as donor and PCBM as acceptor materials. [31]

Chapter 1
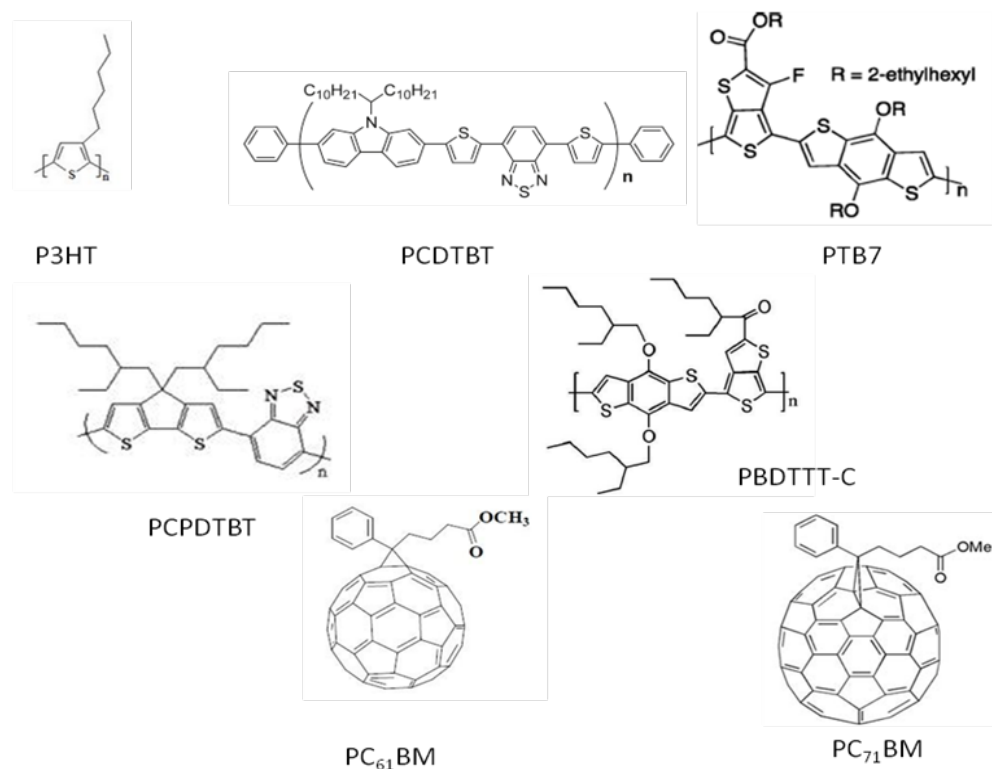
Figure 1.4. Examples of molecule structure of organic semiconductors used in organic solar cells.

Up to now, the most successful electron acceptor materials for polymer solar cells are C_{60} and its derivates phenyl-C61- butyric acid methyl ester ($PC_{61}BM$) and phenyl-C71-butyric acid methyl ester ($PC_{71}BM$). [32, 33] The ideal acceptor material for a bulk-heterojunction solar cell should have a strong absorption complementary to the absorption profile of the donor. Furthermore, one needs to optimize the LUMO-level offset of the donor to the acceptor to guarantee efficient charge transfer and a high open-circuit voltage. Finally, the acceptor needs to provide sufficient electron mobility in composites with the donor. Several acceptor molecules have been reported in bulk-heterojunction solar cells: conjugated polymers, fullerenes, carbon nanotubes, perylenes, and inorganic semiconducting nanoparticles. [34] So far, only derivatives of $PC_{61}BM$ and $PC_{71}BM$ remain highly efficient in bulk heterojunction devices, despite the fact that the position of the HOMO and LUMO levels and the optical absorption are not ideal for most of the donor polymers. [35]

9

1.3   The working principle of solar cells

The normal structure and optoelectronic conversion process of BHJ organic solar cells is divided into four steps as described in Figure 1.5. First light absorption to create hole-electron pairs (exciton), second exciton dissociation, third charge transfer and fourth charge collection.
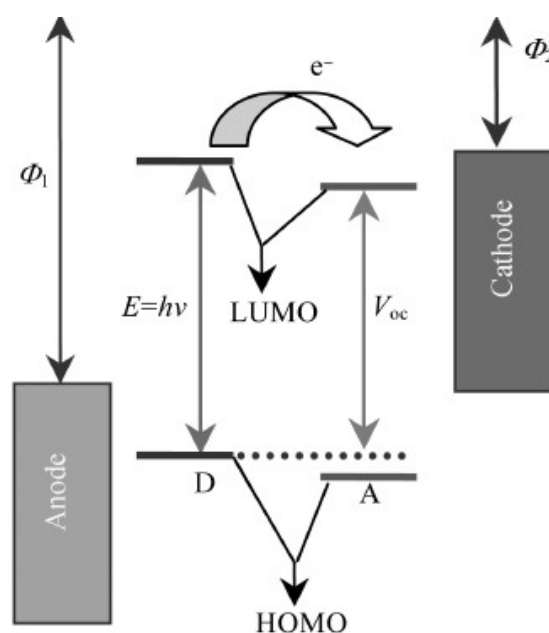
Figure 1.5. Energy level diagram of a donor/acceptor interface showing a simplified viewpoint of photoexcitation of an electron into the donor LUMO followed by electron transfer into the acceptor LUMO and migration of the separated charges away from the interface for a bulk-heterojunction photovoltaic cell.

1.3.1 Light absorption and exciton generation

The molecular structure and electron conjugation (coupling) of organic materials determine the capability of light harvesting and the absorption range in a BHJ active layer in polymer-fullerene devices. Great success in rearranging energy levels and optical band gaps and in enhancing the absorption of longer wavelengths all stem from the development of donor and acceptor conjugated polymers. [36, 37] Due to the

Chapter 1

molecular arrangement and the lack of lattice effects, organic semiconductors have an intrinsically low direct bandgap (a bandgap of 1.1 eV is capable of absorbing 77% of solar irradiation on earth). [38] Thus, organic materials exhibit very high absorption coefficients of as high as 10^{-5} cm^{-1} when compared to their inorganic counterpart and very thin layers are enough to absorb most of the photons when a reflective back contact is used. [38] The thickness of the organic layer commonly ranges from 100 to 300 nm, while the ones of polycrystalline CuInSe$_2$ and Si make up more and less than 100µm, respectively. In addition, organic semiconductors usually present narrow absorption bands which mostly absorb in the visible spectrum, favoring the use of large spectral ranges of the solar spectrum. The absorption of a photon promotes an electron to an excited state from which it reaches/jumps to the lowest excited state, due to the π-system relaxation ability. This creates a Coulomb bound electron-hole pair, the so called exciton (see Figure 1.5). It is estimated that only 10% of the photoexcitations lead to free charge carriers in conjugated polymers. [39] Thus, the design of low band gap materials to collect near infrared photons is a key to solar cells.

1.3.2 Exciton dissociation

In BHJ solar cells based on polymers combined with fullerenes, excitons are generated almost entirely in donor materials with a low band gap (Figure 1.6). Considering the interaction as a Coulombic attraction between an electron and a hole in a material allows to estimate the exciton binding energy to around 0.5 eV, which is much larger than the thermal energy contribution. At room temperature thermal energy alone is insufficient to overcome the exciton's binding energy, whereas upon light absorption singlet excitons are generated. By creating an interface between two materials with different electron affinities excitons efficiently dissociate into their charge carriers. Fullerene, as an electron acceptor, has the higher electron affinity and electrons move to its LUMO level within a polymer-fullerene active layer.
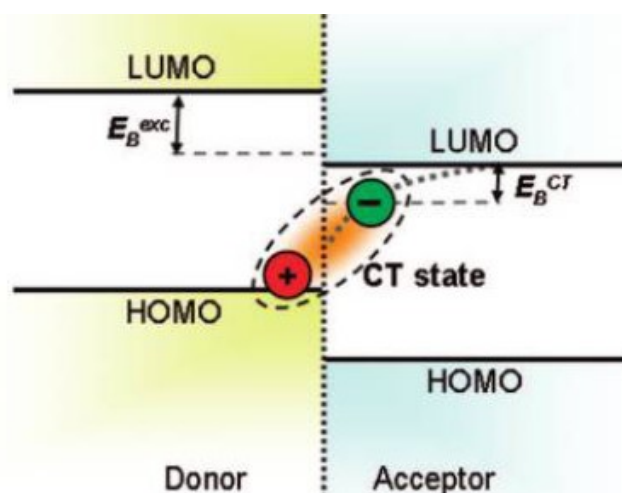
Figure 1.6. Illustration of the formation of interfacial electron-hole pairs or charge-transfer (CT) states.

The polymer of the electron donor material has the lower ionization potential and it can transport holes at the HOMO energy level. To ensure efficient exciton dissociation the LUMO level of the donor should be higher than that of the acceptor, which paves the way for the electron transfer from donor to acceptor. The energy is transferred successfully when the LUMO level of the donor is 0.5 eV higher than the one of the acceptor. In fact, the dissociation mechanism is not completely understood yet. It is often described as a two-step process. [40]

Passing through a donor/acceptor interface an exciton induces a charge-transfer (CT) where the hole resides on the donor molecule. The electron sits on the acceptor molecule but remains Coulombically bound to the donor (Figure 1.6). The ultrafast photo charge transfer from donor to acceptor takes place within 100 fs. [41] CT states have a great influence in the photocurrent generation process due to their long lifetime. In polymer-fullerene systems their lifetime spans 1-100 ns. [42] During CT state separation, geminate recombination of separated charge occurs, which can be either radiative or nonradiative.

Concerning the recombination process, the transition to the ground state is the more probable mode, even though back transfer of an electron from the acceptor to the

Chapter 1

donor is also possible. In the second case, regeneration of a donor singlet exciton or the transition to a triplet exciton state in the donor material are the mechanisms involved. Besides, when two oppositely charged polarons meet, a recombination process called non-geminate recombination may occur and CT states are again the intermediate states. The term non-geminate is used because the two polarons were generated independently from one another, while geminative recombination occurs. [43]

1.3.3 Charge transport and charge collection

After the excitons have been dissipated into electrons and holes, the free carriers can move toward their corresponding electrode via blend active layer including donor and acceptor. Drift of charge carriers is driven by using two electrodes with different work functions. The difference between the two energy levels is known as a built-in potential, it performs as a driving force for the separation and transport of free charge carriers. During the process of charge transport, the efficiency with which charge carriers reach the electrodes depends on their mobility. Organic semiconductors commonly have a low electrical transport ability compared to Si or inorganic semiconductors, which results in a strong dependence of the mobility of the charge carriers on the active layer morphology and crystallinity of polymer. The relatively low mobility in organic molecules is due to the weak electronic coupling from the intermolecular character, structural disorder effect or the large electron-vibration coupling, leading to structural relaxation. [44] Organic materials of low crystallinity possess more traps, inducing low mobility and geminate recombination. Thus enhancing the crystallinity of polymer is a great challenge for improving the transport of the free charge carriers. In addition, the morphology of both donor and acceptor components also plays an important role in determining the transportation of free charge in the blend film. A bi-continuous network structure helps to reduce the geminate recombination.

The last step before having a net current flowing in the outer external circuit is the collection of the charges at the electrodes. The process depends on the complex organic/metal electrode interfaces and the efficiency of the collection cannot be simply determined knowing the work function of the single metals, the ionization potential of the donor and the electron affinity of the acceptor. The electrode deposition process on the active layer, or vice versa, leads to several effects at the interface and the present knowledge is quite limited. Charge density redistribution, geometry modifications and chemical reactions are some of the processes that are involved, and are able to affect the position of the organic energy levels with respect to the metals Fermi level.

1.4 Characterization of solar cells performance

The current-voltage characterization of a solar cell in dark and illumination are shown in Figure 1.7. The plots are used to evaluate the device performance with some parameters including open circuit voltage (Voc), short circuit current (Jsc), the fill factor (FF) and the final PCE. The IV curve of device measured in the dark, no current flowing, shows a regular diode characterization. In the IV curve of device under light, it notes two points which present important features of the device.

The Voc corresponds to the maximum energy of the charge carriers that are extracted from the device and go into the external circuit. Generally, the Voc is determined by the difference in work function of the two electrodes. In organic solar cells, the Voc is linearly dependent on the HOMO level of the donor and LUMO level of the acceptor. [45, 46] Moreover, the Voc is also affected by the nanomorphology of the active layer and work function of the interface materials (hole transport layer and electron transport layer). [47, 48]
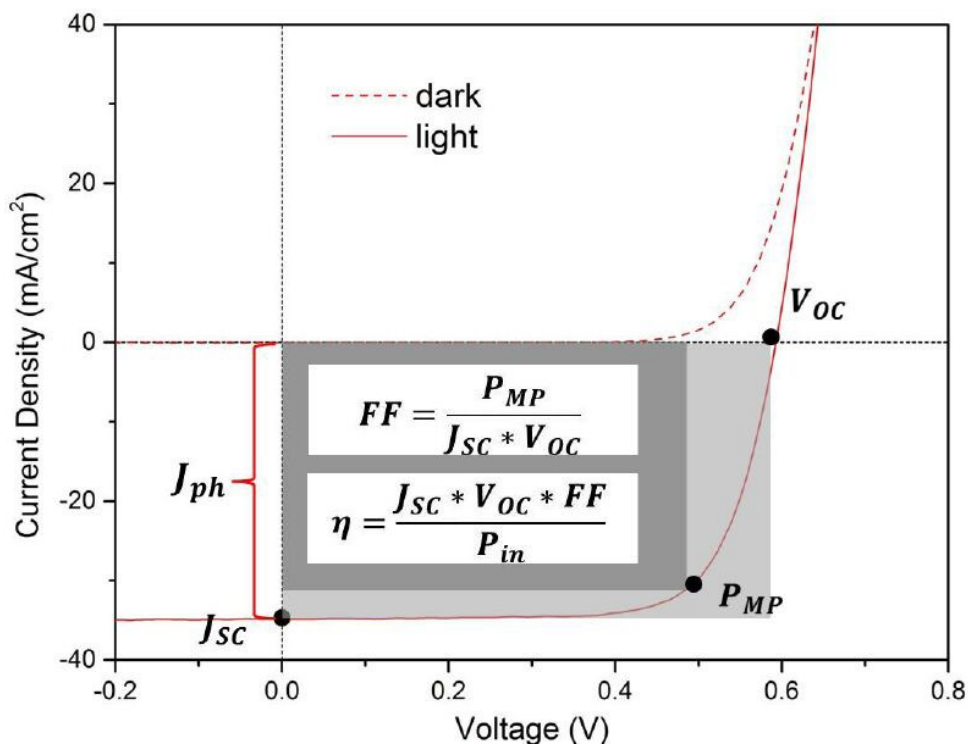
Figure 1.7. An example of the IV characterization curve for a typical PV cell.

The short circuit current corresponds to the maximum current passing through the electrodes if an ideal connection is performed. The Jsc is determined by the photoinduced charge carrier density and the charge carrier mobility. [14] Under ideal conditions, the charge carrier density depends on the donor and acceptor absorption spectra, which in turn depend on the irradiated solar spectrum and the thickness of the layer. For a specific absorption of a certain material, the charge mobility does not relate to the material but the device. It is related to the nanoscale morphology of the organic active layer. [49]

Another important parameter to characterize the performance of solar cells is the fill factor (FF). FF is an electrical property that is determined by the charge carrier reaching the electrode. It represents the ratio of the theoretical maximum producible power over the produced power.

Chapter 1

$$FF = \frac{J_{mp}\, V_{mp}}{J_{sc}\, V_{oc}} = \frac{P_{max}}{J_{sc}\, V_{oc}}$$

The power conversion efficiency (PCE) η is defined by the following formula:

$$\eta = \frac{V_{oc} J_{sc}\, FF}{P_{IN}}$$

Here, the mp is the maximum power and P_{in} is the incident light power density.

Another important performance parameter is the external quantum efficiency (EQE) or incident photo to current efficiency (IPCE) that is simply the number of electrons collected under short circuit condition, divided by the number of incident photo. EQE is calculated using the following formula:

$$EQE = \frac{1240 J_{SC}}{\lambda P_{IN}}$$

Here, λ is the incident photo wavelength with unit of nm.

1.5 Factors determining performance of polymer solar cells

1.5.1 Properties of polymer

These molecular structures of polymer donor and acceptor can influence device performance in many ways:

1.5.1.1 Absorption spectrum of polymer

It is well known that the efficiency of PSCs heavily depends on the photo response

range of the active layer to the incident light. The worse absorption of sunlight by polymer solar cells is the main restraint to the improvement of PCE.

To maximally benefit from the infinite source of solar energy, finding donor materials with a photo absorption range that covers the greater part of the solar spectrum is of utmost importance to harvest the maximum photo flux. To efficiently absorb sun light, the conjugated length and functional group of the p-type donor polymers are of critical importance and the polymers should have a smaller optical band gap. When designing a polymer, a straightforward way to reduce the band gap is by either simply inclining the HOMO or declining the LUMO level of the polymer. It is worth noting that to obtain higher efficiencies from BHJ polymer solar cells, the n-type acceptor properties of the fullerene derivatives should also be taken into account in the development process.

1.5.1.2 Energy level match

For solar cells, the short circuit current is mainly related to absorption of the active layer, which is determined by the optical band gap of the donor and the acceptor. The Voc is corresponding to the difference between the HOMO level of the donor materials and LUMO level of the acceptor materials. Figure 1.6 has shown a schematic drawing of the energy levels of polymer solar cells. Utilizing a suitable energy between LUMO of the donor and acceptor accomplishes the initial charge separation step and the dissociated electron transfer from the donor exciton state into the acceptor conduct band. The energy offset should be greater than the Coulomb binding energy of the exciton of 0.3 V, enabling the initial electron transfer to be energetically downhill. [50]

Following, the separated charges (holes and electrons) need to be transported to the appreciated electrodes whining effective lifetime. The charge carriers need a driving

force to reach the electrodes. The driving force is built in a donor ad acceptor junction, which is determined by the difference between HOMO level of the donor and LUMO of the acceptor. [51] The internal electrical field determines the maximum open circuit voltage and contributes to a field induced drift of charge carriers.

The molecular structures of polymer materials analyzed above suggest that the optimum PCEs of polymer solar cells not only depend on the smaller band gap but also the donor-acceptor level offset.

1.5.2 Morphology of photoactive layer

In polymer solar cells, the morphologies of active layers have a great effect on the device performance, which has been investigated by a number of studies. In particular, BHJ solar cells are expected to benefit from the development of efficient and controlled interfacial areas of donor-acceptor with nanoscale phase separation channels for excitons dissociation and domain sizes comparable to exciton diffusion length (~10 nm). The interpenetrating networks of donor and acceptor components including the shape, crystallinity and orientation with respect to the active layer so as to provide enough high-efficient pathways for both electrons and holes to be transported to the corresponding electrodes, play an important role in determining the device performance. Moreover, optimal phase segregation must exist to minimize geminate recombination and thus maximize charge photogeneration. For example, if the domain sizes are too large, the limited diffusion length of the photoinduced excitons means that some excitons will not reach an interface within their lifetime. Conversely, if the phase separation is too fine (and thus the interfacial area is too large), geminate and/ or bimolecular recombination might be enhanced. [52]

The morphologies of active layer can be modified by several approaches：

Chapter 1

1.5.2.1 Solvent additive and solvent mixture

Solvent selection is very important for polymer solar cells that can greatly impact the final structural arrangement in the active layer. For example, in the PTB7:PCBM system. The PCEs increases from 5.2% to 6.8% by changing the solvent from chlorobenzene (CB) to dicholorobenzene (DCB). [53] In recent years, solvent additive and solvent mixture processing have been found that are now commonly used in BHJ deposition techniques during film formation with widespread utility in high performing conjugated polymer:fullerene solar cells. For example, by mixing a few volume percent of octanedithiol (ODT) with the host solvent CB, the efficiency of [2,6-(4,4-bis(2-ethylhexyl)-4H-cyclopenta[2,1-b;3,4-b']dithiophene)-alt-4,7-(2,1,3-be nzothiadiazole)] (PCPDTBT):PCBM solar cells can be improved dramatically from 2.8% to 5.5%. [54, 55] A solvent additive can improve the device performance, mainly due to the modification of the internal order within the phase, and can increase the crystallinity of the conjugated polymer donor. [56, 57]

The effect of a solvent mixture approach for the device performance behaves very similarly to the solvent additive approach. Low vapor pressure solvents are usually used in PSCs, such as chloroform (CF) and CB, which can dissolve the polymers well in most cases. However, these vapor pressure solvents commonly lead to a low crystallinity of polymer due to the fast evaporation of solvent during the deposition process. An effective method to solve it is using solvent mixture. For example, when using the solvent mixture with a good solvent CF and a high boiling point DCB in a blend of diketopyrrolopyrrole and quaterthiophene (pDPP):PCBM, during solvent casting, the lower boiling solvent CF evaporates, continuously increasing the concentration of the DCB, thereby reducing the solubility of the polymer, while keeping the PCBM fully solubilized. [58] pDPP then crystallizes into fibrils, forcing a phase separation with the PCBM. The finally observed improvement in PCE can be directly attributed to the ordering of the pDPP enabled by the ability of DCB to

Chapter 1

selectively solubilize the PCBM. [58] According to these works, it can be concluded that crystallinity, as well as domain size, induce the phase separation in the blends which can be tuned effectively by using solvent additives or solvent mixtures, and thus bilaterally improving the performance of PSCs.

1.5.2.2 Thermal annealing and post-annealing

Thermal annealing has been proved to be an effective method for controlling the active layer morphology and enhancing the PCEs. This approach was first successfully exploited in the poly (3-hexylthiophene) (P3HT):PCBM solar cells by Padinger and coworkers, who increased the PCE up to 3.5% after thermal annealing the blend film. It was proposed that thermal annealing enhances the crystallization of P3HT and allows some of the PCBM molecules, which are embedded in the disordered P3HT region, to diffuse out and form large fullerene aggregates. [59]

Thermal annealing process can be applied in solar cells before (preannealing) or after (postannealing) electrode evaporation. Preannealing has been mentioned above. Chen et al. utilized NEXAFS technique to examine the bulk morphology and interfacial behavior of P3HT:PCBM by preannealing and postannealing. [60] The results revealed that preannealing improves the P3HT chains orientation in the active layer and reduce surface concentration of PCBM. Postannealing induces PC61BM segregation toward the cathode/active layer interface and increases the contribution by the face-on orientation.

1.5.2.3 Solvent annealing

"Solvent annealing" was first proposed for P3HT:PCBM systems by yang group. [61, 62] To induce a slow solvent evaporation the wet active layer is kept in a partially closed container, (e.g. a Petri dish), with a few drops of solvent. It is an effective

Chapter 1

method to modify the phase separation and crystallization of the blend components and alter the morphology of the BHJ film.

Controlling the growth rate of the active layer by slow evaporation of solvent results in an increased hole mobility and balanced charge transport and therefore a higher PCE (4.4%). The detailed evolution of crystallinity and morphology in P3HT:PC$_{61}$BM system during the solvent vapor treatment was also studied by Hegde et al. [63]

1.5.2.4 Donor:acceptor ratio

Except solvent selection, thermal annealing and solvent annealing, the donor and acceptor blend ratio can also influence the morphology of active layer. The ratio of donor and acceptor mainly influences the crystalline order, phase separation and morphology of the blend film. [64]

1.5.3 The selection of electrode and interfacial layer materials

In PSCs, electrodes with low work function are desirable to extract electrons/holes and block holes/electrons. [65] By tuning interfaces of light-harvesting active layers and charge-collecting electrodes to achieve the maximum performance in PSCs, buffer layers or so called interfacial layers or interlayers are essential. [66, 67] In general, the interfacial layer materials should have a suitable energy level and high charge transport properties to transport and collect electrons/holes selectively. Several materials are available as anode buffer layer, such as PEDOT:PSS, NiO, MoO$_3$, and V$_2$O$_5$ have been reported. [68-72] Regarding the extraction of electrons at the cathode, the commonly used materials are Ca, LiF, ZnO and TiOx et al.. [73-76] As materials with contact selectivity, causing an energy level mismatch with high work function donor and low work function acceptor, interfacial layers have been shown to further enhance the device efficiency by reducing the charge injection/extraction battery.

Chapter 1

1.6 Organization and objective of the thesis

As mentioned the factors determining the solar cell performance above, the morphologies and surface compositions of active layer, crystallinity of polymer and device structure are key factors to impact exciton dissociation and transport in the photovoltaic process. For these reasons, the major aim of this thesis focuses on the effect of evolution of morphologies and crystallinity of polymer on performance of PSCs based on different solution processed approaches.

Recently, a series of the wide spectral response polymer PTBx composed of thieno [3,4-b] thiophene and benzodithiophene alternating units have been widely used as a promising donor material used in solar cells. [77-79] Device based on this PTBx have continuously refreshed the record of PSCs efficiency in the last few years and exceed 9% PCE based on single junction solar cells is obtained. In chapter 3, we first applied an aging solution approach during the preparation of the PTB1:PCBM blend solution. The polymer dissolving process is also a process of polymer molecule diffusion. The interaction of donor and acceptor in the diffusion process is to be affected by solution aging. We investigate the relationship between solution aging time and evolution of morphology and polymer crystallinity structure. Furthermore, the effect of solution aging on performance of PTB1:PC_{61}BM due to the changing blend film morphologies is also discussed.

In chapter 4, a solvent mixture has been proved as an effective method to control the domain size and crystallinity of the polymer. However, the ternary solvent mixture used in the PTBx:PCBM system has been less reported on. In this part, we first use a ternary solvent including CB, DIO and the "unfriendly" solvent cyclohexanone (CHN) in PTB7:PCBM blend during the preparation of the blend solution. We detect the evolution of crystallinity structure of polymer and morphologies of the blend film in

the ternary solvent mixture treatment. In particular, for complete device, the effect of different solvent mixtures on charge carrier extraction density and charge recombination kinetics is also measured.

In chapter 5, we investigate the influence of ternary solvent mixture treatment on the surface composition of the PTB7:PC$_{71}$BM active layer. We also compare the performance of different device structures, conventional and inverted due to the variation of surface composition. The surface potential of the active layer and charge recombination kinetics of device with different structures based on a similar solvent mixture treatment is also discussed in this part.

Chapter 1

1.7 Reference

1. Deibel, C.;Dyakonov, V., Polymer–fullerene bulk heterojunction solar cells. *Reports on Progress in Physics* **2010**, *73*, 096401.

2. Poortmans, J.;Arkhipov, V., Thin film solar cells: fabrication, characterization and applications. *John Wiley & Sons*, 2006; Vol. 5.

3. Wiese, A.; Kaltschmitt, M.;Lee, W. Y., Renewable power generation–a status report. *Renewable Energy Focus* **2009**, *10*, 64-69.

4. Lewis, N. S.;Nocera, D. G., Powering the planet: Chemical challenges in solar energy utilization. *Proceedings of the National Academy of Sciences* **2006**, *103*, 15729-15735.

5. Armaroli, N.;Balzani, V., The future of energy supply: challenges and opportunities. *Angew. Chem., Int. Ed.* **2007**, *46*, 52-66.

6. 6-Takamoto, T.; Kaneiwa, M.; Imaizumi, M.;Yamaguchi, M., InGaP/GaAs-based multijunction solar cells. *Prog. Photovoltaics: Res. Appl.* **2005**, *13*, 495-511.

7. Skotheim, T. A.;Reynolds, J., *Handbook of Conducting Polymers, 2 Volume Set*; CRC press, 2007.

8. Christoph, B.; Ullrich, S.; Vladimir, D., *Organic Photovoltaics: Materials, Device Physics, and Manufacturing Technologies,* press, 2011

9. Perepichka, I. F.;Perepichka, D. F., *Handbook of thiophene-based materials: applications in organic electronics and photonics*; Wiley Online Library, 2009.

10. Lipiński, M., 10-New concepts of solar cells.

11. Price, S. C.; Stuart, A. C.; Yang, L.; Zhou, H.;You, W., Fluorine substituted conjugated polymer of medium band gap yields 7% efficiency in polymer− fullerene solar cells. *J. Am. Chem. Soc.* **2011**, *133*, 4625-4631.

12. Ren, G.; Schlenker, C. W.; Ahmed, E.; Subramaniyan, S.; Olthof, S.; Kahn, A.; Ginger, D. S.;Jenekhe, S. A., Photoinduced Hole Transfer Becomes Suppressed with Diminished Driving Force in Polymer-Fullerene Solar Cells While Electron Transfer Remains Active. *Adv. Funct. Mater.* **2013**, *23*, 1238-1249.

13. Brabec, C. J.; Cravino, A.; Meissner, D.; Sariciftci, N. S.; Fromherz, T.; Rispens, M. T.; Sanchez, L.;Hummelen, J. C., Origin of the open circuit voltage of plastic solar cells. *Adv. Funct. Mater.* **2001**,

Chapter 1

11, 374-380.

14. Günes, S.; Neugebauer, H.;Sariciftci, N. S., Conjugated polymer-based organic solar cells. *Chem. Rev.* **2007**, *107*, 1324-1338.

15. Zhang, F.; Wu, D.; Xu, Y.;Feng, X., Thiophene-based conjugated oligomers for organic solar cells. *J. Mater. Chem.* **2011**, *21*, 17590-17600.

16. Chochos, C. L.;Choulis, S. A., How the structural deviations on the backbone of conjugated polymers influence their optoelectronic properties and photovoltaic performance. *Progress in Polymer Science* **2011**, *36*, 1326-1414.

17. Zhou, H.; Yang, L.;You, W., Rational design of high performance conjugated polymers for organic solar cells. *Macromolecules* **2012**, *45*, 607-632.

18. Chu, T.-Y.; Lu, J.; Beaupré, S.; Zhang, Y.; Pouliot, J.-R.; Wakim, S.; Zhou, J.; Leclerc, M.; Li, Z.;Ding, J., Bulk heterojunction solar cells using thieno [3, 4-c] pyrrole-4, 6-dione and dithieno [3, 2-b: 2′, 3′-d] silole copolymer with a power conversion efficiency of 7.3%. *J. Am. Chem. Soc.* **2011**, *133*, 4250-4253.

19. Liang, Y.; Xu, Z.; Xia, J.; Tsai, S. T.; Wu, Y.; Li, G.; Ray, C.;Yu, L., For the bright future—bulk heterojunction polymer solar cells with power conversion efficiency of 7.4%. *Adv. Mater.* **2010**, *22*, E135-E138.

20. He, Z.; Xiao, B.; Liu, F.; Wu, H.; Yang, Y.; Xiao, S.; Wang, C.; Russell, T. P.;Cao, Y., Single-junction polymer solar cells with high efficiency and photovoltage. *Nat. Photonics* **2015**, *9*, 174-179.

21. Brabec, C. J.; Cravino, A.; Meissner, D.; Sariciftci, N. S.; Fromherz, T.; Rispens, M. T.; Sanchez, L.;Hummelen, J. C., Origin of the open circuit voltage of plastic solar cells. *Adv. Funct. Mater.* **2001**, *11*, 374-380.

22. Thompson, B. C.;Frechet, J. M., Polymer–fullerene composite solar cells. *Angew. Chem., Int. Ed.* **2008**, *47*, 58-77.

23. Brabec, C. J.; Shaheen, S. E.; Winder, C.; Sariciftci, N. S.;Denk, P., Effect of LiF/metal electrodes on the performance of plastic solar cells. *Appl. Phys. Lett.* **2002**, *80*, 1288-1290.

24. O'Neill, M.;Kelly, S. M., Ordered materials for organic electronics and photonics. *Adv. Mater.* **2011**, *23*, 566-584.

Chapter 1

25. Facchetti, A., Polymer donor–polymer acceptor (all-polymer) solar cells. *Materials Today* **2013**, *16*, 123-132.

26. Slooff, L.; Veenstra, S.; Kroon, J.; Moet, D.; Sweelssen, J.;Koetse, M., Determining the internal quantum efficiency of highly efficient polymer solar cells through optical modeling. *Appl. Phys. Lett.* **2007**, *90*, 143506.

27. Zhang, F.; Mammo, W.; Andersson, L. M.; Admassie, S.; Andersson, M. R.;Inganäs, O., Low-bandgap alternating fluorene copolymer/methanofullerene heterojunctions in efficient near-infrared polymer solar cells. *Adv. Mater.* **2006**, *18*, 2169-2173.

28. Blouin, N.; Michaud, A.;Leclerc, M., A low-bandgap poly (2, 7-carbazole) derivative for use in high-performance solar cells. *Adv. Mater.* **2007**, *19*, 2295-2300.

29. Carsten, B.; Szarko, J. M.; Son, H. J.; Wang, W.; Lu, L.; He, F.; Rolczynski, B. S.; Lou, S. J.; Chen, L. X.;Yu, L., Examining the effect of the dipole moment on charge separation in donor–acceptor polymers for organic photovoltaic applications. *J. Am. Chem. Soc.* **2011**, *133*, 20468-20475.

30. Liang, Y.;Yu, L., A new class of semiconducting polymers for bulk heterojunction solar cells with exceptionally high performance. *Acc. Chem. Res.* **2010**, *43*, 1227-1236.

31. He, Z.; Zhong, C.; Su, S.; Xu, M.; Wu, H.;Cao, Y., Enhanced power-conversion efficiency in polymer solar cells using an inverted device structure. *Nat. Photonics* **2012**, *6*, 591-595.

32. Arbogast, J. W.;Foote, C. S., Photophysical properties of C70. *J. Am. Chem. Soc.* **1991**, *113*, 8886-8889.

33. Wienk, M. M.; Kroon, J. M.; Verhees, W. J.; Knol, J.; Hummelen, J. C.; van Hal, P. A.;Janssen, R. A., Efficient methano [70] fullerene/MDMO-PPV bulk heterojunction photovoltaic cells. *Angew Chem Int Ed Engl* **2003**, *115*, 3493-3497.

34. Hoppe, H.;Sariciftci, N. S., Morphology of polymer/fullerene bulk heterojunction solar cells. *J. Mater. Chem.* **2006**, *16*, 45-61.

35. Scharber, M. C.; Muhlbacher, D.; Koppe, M.; Denk, P.; Waldauf, C.; Heeger, A. J.;Brabec, C. J., Design rules for donors in bulk-heterojunction solar cells-towards 10% energy-conversion efficiency. *ADVANCED MATERIALS-DEERFIELD BEACH THEN WEINHEIM-* **2006**, *18*, 789.

36. Cheng, Y.-J.; Yang, S.-H.;Hsu, C.-S., Synthesis of conjugated polymers for organic solar cell applications. *Chem. Rev.* **2009**, *109*, 5868-5923.

Chapter 1

37.   Li, Y., Molecular design of photovoltaic materials for polymer solar cells: toward suitable electronic energy levels and broad absorption. *Acc. Chem. Res.* **2012**, *45*, 723-733.

38.   Nunzi, J.-M., Organic photovoltaic materials and devices. *Comptes Rendus Physique* **2002**, *3*, 523-542.

39.   Zhou, X.; Blochwitz, J.; Pfeiffer, M.; Nollau, A.; Fritz, T.; Leo, K., Enhanced Hole Injection into Amorphous Hole-Transport Layers of Organic Light-Emitting Diodes Using Controlled p-Type Doping. *Adv. Funct. Mater.* **2001**, *11*, 310-314.

40.   Brédas, J.-L.; Norton, J. E.; Cornil, J.; Coropceanu, V., Molecular understanding of organic solar cells: the challenges. *Acc. Chem. Res.* **2009**, *42*, 1691-1699.

41.   Moses, D.; Wang, J.; Yu, G.; Heeger, A., Temperature-independent photoconductivity in thin films of semiconducting polymers: Photocarrier sweep-out prior to deep trapping. *Physical review letters* **1998**, *80*, 2685.

42.   Deibel, C.; Strobel, T.; Dyakonov, V., Role of the charge transfer state in organic donor–acceptor solar cells. *Adv. Mater.* **2010**, *22*, 4097-4111.

43.   Clarke, T. M.; Durrant, J. R., Charge photogeneration in organic solar cells. *Chem. Rev.* **2010**, *110*, 6736-6767.

44.   Colladet, K.; Fourier, S.; Cleij, T. J.; Lutsen, L.; Gelan, J.; Vanderzande, D.; Huong Nguyen, L.; Neugebauer, H.; Sariciftci, S.; Aguirre, A., Low band gap donor-acceptor conjugated polymers toward organic solar cells applications. *Macromolecules* **2007**, *40*, 65-72.

45.   Brabec, C. J.; Winder, C.; Sariciftci, N. S.; Hummelen, J. C.; Dhanabalan, A.; van Hal, P. A.;Janssen, R. A., A low-bandgap semiconducting polymer for photovoltaic devices and infrared emitting diodes. *Adv. Funct. Mater.* **2002**, *12*, 709-712.

46.   Potscavage Jr, W. J.; Sharma, A.;Kippelen, B., Critical interfaces in organic solar cells and their influence on the open-circuit voltage. *Acc. Chem. Res.* **2009**, *42*, 1758-1767.

47.   Liu, J.; Shi, Y.;Yang, Y., Solvation-induced morphology effects on the performance of polymer-based photovoltaic devices. *Adv. Funct. Mater.* **2001**, *11*, 420.

48.   Kontturi, E.; Thüne, P.;Niemantsverdriet, J., Novel method for preparing cellulose model surfaces by spin coating. *Polymer* **2003**, *44*, 3621-3625.

49.   Martens, T.; D'Haen, J.; Munters, T.; Beelen, Z.; Goris, L.; Manca, J.; D'Olieslaeger, M.;

Chapter 1

Vanderzande, D.; De Schepper, L.;Andriessen, R., Disclosure of the nanostructure of MDMO-PPV: PCBM bulk hetero-junction organic solar cells by a combination of SPM and TEM. *Synthetic Metals* **2003**, *138*, 243-247.

50. Koster, L.; Mihailetchi, V.;Blom, P., Bimolecular recombination in polymer/fullerene bulk heterojunction solar cells. *Appl. Phys. Lett.* **2006**, *88*, 052104.

51. Campos, L. M.; Tontcheva, A.; Günes, S.; Sonmez, G.; Neugebauer, H.; Sariciftci, N. S.;Wudl, F., Extended photocurrent spectrum of a low band gap polymer in a bulk heterojunction solar cell. *Chemistry of materials* **2005**, *17*, 4031-4033.

52. Dang, M. T.; Hirsch, L.; Wantz, G.;Wuest, J. D., Controlling the morphology and performance of bulk heterojunctions in solar cells. Lessons learned from the benchmark poly (3-hexylthiophene):[6, 6]-phenyl-C61-butyric acid methyl ester system. *Chem. Rev.* **2013**, *113*, 3734-3765.

53. Hu, X.; Dong, Y.; Huang, F.; Gong, X.;Cao, Y., Solution-processed high-detectivity near-infrared polymer photodetectors fabricated by a novel low-bandgap semiconducting polymer. *J. Phys. Chem. C* **2013**, *117*, 6537-6543.

54. Peet, J.; Soci, C.; Coffin, R.; Nguyen, T.; Mikhailovsky, A.; Moses, D.;Bazan, G. C., Method for increasing the photoconductive response in conjugated polymer/fullerene composites. *Appl. Phys. Lett.* **2006**, *89*, 252105.

55. Peet, J.; Kim, J. Y.; Coates, N. E.; Ma, W. L.; Moses, D.; Heeger, A. J.;Bazan, G. C., Efficiency enhancement in low-bandgap polymer solar cells by processing with alkane dithiols. *Nat. Mater.* **2007**, *6*, 497-500.

56. Rogers, J. T.; Schmidt, K.; Toney, M. F.; Kramer, E. J.;Bazan, G. C., Structural order in bulk heterojunction films prepared with solvent additives. *Adv. Mater.* **2011**, *23*, 2284-2288.

57. Sun, Y.; Welch, G. C.; Leong, W. L.; Takacs, C. J.; Bazan, G. C.;Heeger, A. J., Solution-processed small-molecule solar cells with 6.7% efficiency. *Nat. Mater.* **2012**, *11*, 44-48.

58. Liu, F.; Gu, Y.; Wang, C.; Zhao, W.; Chen, D.; Briseno, A. L.;Russell, T. P., Efficient Polymer Solar Cells Based on a Low Bandgap Semi-crystalline DPP Polymer-PCBM Blends. *Adv. Mater.* **2012**, *24*, 3947-3951.

59. Padinger, F.; Rittberger, R. S.;Sariciftci, N. S., Effects of postproduction treatment on plastic solar cells. *Adv. Funct. Mater.* **2003**, *13*, 85-88.

Chapter 1

60. Chen, D.; Nakahara, A.; Wei, D.; Nordlund, D.;Russell, T. P., P3HT/PCBM bulk heterojunction organic photovoltaics: correlating efficiency and morphology. *Nano Lett.* **2010**, *11*, 561-567.

61. Li, G.; Shrotriya, V.; Huang, J.; Yao, Y.; Moriarty, T.; Emery, K.;Yang, Y., High-efficiency solution processable polymer photovoltaic cells by self-organization of polymer blends. *Nat. Mater.* **2005**, *4*, 864-868.

62. Li, G.; Yao, Y.; Yang, H.; Shrotriya, V.; Yang, G.;Yang, Y., " Solvent annealing" effect in polymer solar cells based on poly (3-hexylthiophene) and methanofullerenes. *Adv. Funct. Mater.* **2007**, *17*, 1636.

63. Hegde, R.; Henry, N.; Whittle, B.; Zang, H.; Hu, B.; Chen, J.; Xiao, K.;Dadmun, M., The impact of controlled solvent exposure on the morphology, structure and function of bulk heterojunction solar cells. *Sol. Energy Mater. Sol. Cells* **2012**, *107*, 112-124.

64. Chirvase, D.; Parisi, J.; Hummelen, J. C.;Dyakonov, V., Influence of nanomorphology on the photovoltaic action of polymer–fullerene composites. *Nanotechnology* **2004**, *15*, 1317.

65. Zhou, Y.; Fuentes-Hernandez, C.; Shim, J.; Meyer, J.; Giordano, A. J.; Li, H.; Winget, P.; Papadopoulos, T.; Cheun, H.;Kim, J., A universal method to produce low–work function electrodes for organic electronics. *Science* **2012**, *336*, 327-332.

66. Yip, H.-L.;Jen, A. K.-Y., Recent advances in solution-processed interfacial materials for efficient and stable polymer solar cells. *Energy & Environmental Science* **2012**, *5*, 5994-6011.

67. Po, R.; Carbonera, C.; Bernardi, A.;Camaioni, N., The role of buffer layers in polymer solar cells. *Energy & Environmental Science* **2011**, *4*, 285-310.

68. Jørgensen, M.; Norrman, K.;Krebs, F. C., Stability/degradation of polymer solar cells. *Sol. Energy Mater. Sol. Cells* **2008**, *92*, 686-714.

69. Meyer, J.; Kröger, M.; Hamwi, S.; Gnam, F.; Riedl, T.; Kowalsky, W.;Kahn, A., Charge generation layers comprising transition metal-oxide/organic interfaces: Electronic structure and charge generation mechanism. *Appl. Phys. Lett.* **2010**, *96*, 193302.

70. Shrotriya, V.; Li, G.; Yao, Y.; Chu, C.-W.;Yang, Y., Transition metal oxides as the buffer layer for polymer photovoltaic cells. *Appl. Phys. Lett.* **2006**, *88*, 073508.

71. Steirer, K. X.; Ndione, P. F.; Widjonarko, N. E.; Lloyd, M. T.; Meyer, J.; Ratcliff, E. L.; Kahn, A.; Armstrong, N. R.; Curtis, C. J.;Ginley, D. S., Enhanced efficiency in plastic solar cells via energy matched solution processed NiOx interlayers. *Advanced Energy Materials* **2011**, *1*, 813-820.

72. Murase, S.;Yang, Y., Solution processed MoO$_3$ interfacial layer for organic photovoltaics prepared by a facile synthesis method. *Adv. Mater.* **2012**, *24*, 2459-2462.

73. Steim, R.; Kogler, F. R.;Brabec, C. J., Interface materials for organic solar cells. *J. Mater. Chem.* **2010**, *20*, 2499-2512.

74. Ratcliff, E. L.; Zacher, B.;Armstrong, N. R., Selective interlayers and contacts in organic photovoltaic cells. *The Journal of Physical Chemistry Letters* **2011**, *2*, 1337-1350.

75. Zhang, F.; Gadisa, A.; Inganäs, O.; Svensson, M.;Andersson, M., Influence of buffer layers on the performance of polymer solar cells. *Appl. Phys. Lett.* **2004**, *84*, 3906-3908.

76. Mihailetchi, V.; Koster, L.;Blom, P., Effect of metal electrodes on the performance of polymer: fullerene bulk heterojunction solar cells. *Appl. Phys. Lett.* **2004**, *85*, 970-972.

77. Liang, Y.; Wu, Y.; Feng, D.; Tsai, S.-T.; Son, H.-J.; Li, G.;Yu, L., Development of new semiconducting polymers for high performance solar cells. *J. Am. Chem. Soc.* **2008**, *131*, 56-57.

78. Liang, Y.; Feng, D.; Wu, Y.; Tsai, S.-T.; Li, G.; Ray, C.;Yu, L., Highly efficient solar cell polymers developed via fine-tuning of structural and electronic properties. *J. Am. Chem. Soc.* **2009**, *131*, 7792-7799.

79. Hammond, M. R.; Kline, R. J.; Herzing, A. A.; Richter, L. J.; Germack, D. S.; Ro, H.-W.; Soles, C. L.; Fischer, D. A.; Xu, T.;Yu, L., Molecular order in high-efficiency polymer/fullerene bulk heterojunction solar cells. *ACS nano* **2011**, *5*, 8248-8257.

Chapter 2

Experimental Technique and Principle

In this chapter, the basic experimental techniques employed for preparation of polymer solar cells, such as substrate cleaning, film deposition, and its corresponding characterization in general are described.

Chapter 2

Chapter 2

Table of content

2.1 Reagents and materials

2.2 Solar cells devices preparation

2.2.1 Substrate cleaning

2.2.2 Device preparation

2.3 Device performance measurements

2.3.1 Power conversion efficiency (PCE)

2.3.2 External quantum efficiency (EQE)

2.4 Optical properties characterization

2.5 Electronic properties characterization

2.5.1 Charge extraction (CE)

2.5.2 Transient photovoltage technique (TPV)

2.6 Morphology and crystallinity structure characterization of polymer

2.6.1 Atomic force microscopy (AFM)

2.6.2 Transmission electron microscopy (TEM)

2.6.3 Grazing incidence X-ray scattering (GIXS)

2.7 Surface energy measurements

2.8 Reference

Chapter 2

Chapter 2

2.1 Reagents and materials

In the thesis, the following reagents and materials are used in fabrication of solar cells and performance characterization

Poly-(Ethylene dioxythiophene) doped with Poly-(Styrene Sulphonic acid) (PEDOT:PSS) FHC was acquired from Ossila Ltd.,

Poly (3-hexylthiophene) (P3HT), Poly [[4,8-bis (octyloxy) benzo (1,2-b:4,5-b') dithiophene-2,6-diyl) (2-((dodecyloxy) carbonyl) thieno(3,4-b) thiophenediyl]] (PTB1) and Poly[[4,8-bis[(2-ethylhexyl)oxy] Benzo [1,2-b:4,5-b'] dithiophene-2,6-diyl] [3-fluoro-2-[(2-ethylhexyl)carbonyl]-thieno-[3,4-b]thiophenediyl]] (PTB7) were purchased from one material.

Fullerene [6,6]-phenyl C61-butyric acid methyl ester (PC$_{61}$BM) (Mw: 910.9 g mol^{-1}) and [6,6]-phenyl-C71 butyric acid methyl ester (PC$_{71}$BM) (Mw: 1030.99 g mol^{-1}) were purchased from and Nano-C Inc and Solenne B.V., respectively.

Indium tin oxide (ITO) coated glass substrates (with nominal sheet resistance of 15 Ohm/square and 120 nm of thickness) were purchased from PsiOTec Ltd.

High-purity (99.99%) silver (Ag) wires were obtained from Testbourne Ltd., and calcium (Ca) pellets with high-purity (99.99%) was purchased from Kurt J. Lesker.

The reagents including dichlorobenzene (DCB), chlorobenzene (CB), 1,8-diiodooctane (DIO), cyclohexanone (CHN) Ethylene glycol, Diiodomethane are obtained from Sigma-Aldrich.

The common donor polymer molecules structure used in my thesis are shown in Figure 2.1

Chapter 2
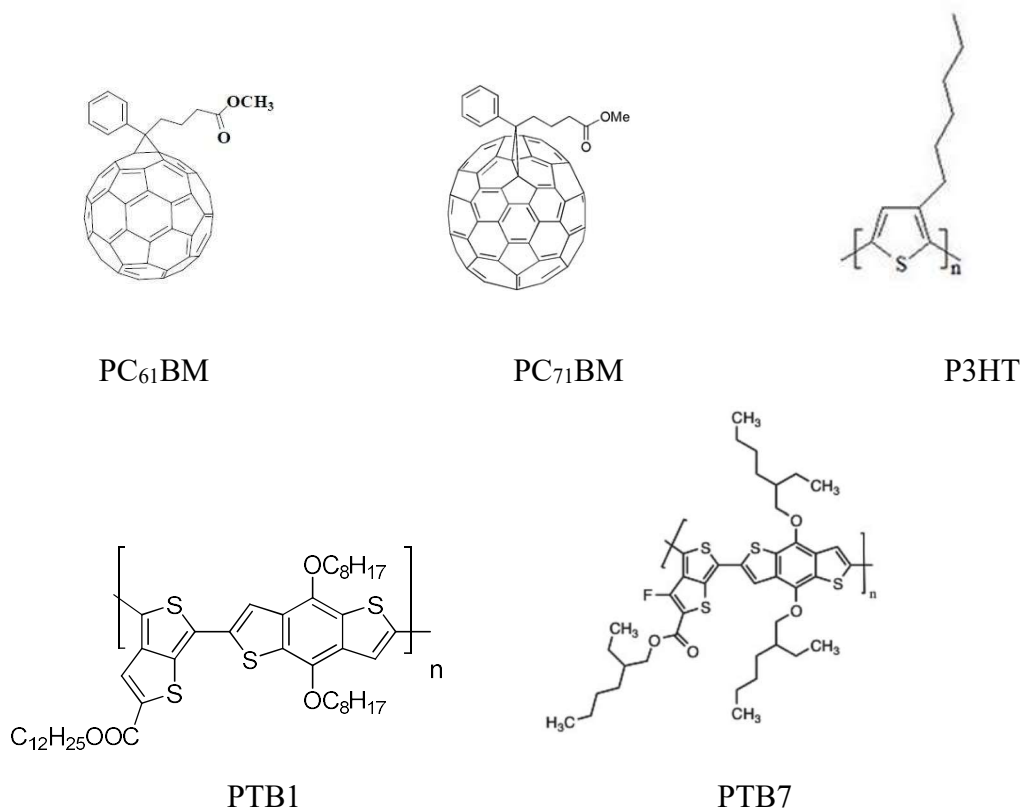
Figure 2.1. Molecular structures of some of the donor and acceptor polymers used in our experiment.

2.2 Solar cells devices preparation

2.2.1 Substrate cleaning

ITO substrates are first rinsed by acetone to remove the initial covered photoresin. Then ITO are cleaned in detergent, water, acetone, and isopropyl alcohol under ultrasonication for 15 min each and subsequently dried in an oven at 120 ℃ for 5 h in air. It is important note that before spin-coating hole or electron transport layer materials, the ITO surface pre-treated by ultraviolet ozone for 15 min in order to remove organic remains.

Chapter 2

2.2.2 Devices preparation

In the case of conventional solar cells devices, PEDOT:PSS was spin-coated onto an cleaned ITO surface, and the spin coating conditions are first 4800 rpm for 30 s followed by 30 s at 3500 rpm in atmospheric conditions. Low conductivity PEDOT:PSS was chosen to minimize measurement error from device area due to lateral conductivity of PEDOT:PSS. After being baked at 120 °C for 20 min, the substrates were transferred into a nitrogen-filled glove box (< 0.1 ppm O_2 and H_2O). Following that, the blend solution composites layer was deposited by spin casting at 1000 rpm for 30s on the ITO/PEDOT:PSS substrate without further special treatments. The substrate is covered with an inverted petri dish allowing a slow evaporation of solvent. Subsequently the samples were transferred into a thermal evaporator located in the same glove box. A Ca layer and an Ag layer were deposited in sequence under the vacuum of 1×10^{-6} mbar. The effective area of the device was 0.09 cm^2.

In the case of inverted solar cells, first, The ZnO as a hole transport layer is obtained by spin coating the ZnO Precursor solution on top of ITO glass substrate at 3000 rpm for 40 s. After that, the film is heated at 200 ℃ for 1 h in air. Following that, the blend solution composites layer was deposited by spin coating at 1000 rpm for 30s on the ITO/ZnO substrate without further special treatments. The substrate is covered with an inverted petri dish allowing a slow evaporation of solvent. Subsequently the samples were transferred into a thermal evaporator located in the same glove box. A MoO_3 layer (10 nm) and an Ag layer (100 nm) were deposited in sequence under the vacuum of 1×10^{-6} mbar. The effective area of the device was 0.09 cm^2.

2.3 Device performance measurements

Device performance parameters of solar cells include open circuit voltage, short circuit

Chapter 2

current, fill factor and corresponding photo-current conversion efficiency. External quantum efficiency is also measure in the section.

2.3.1 Power conversion efficiency

I-V characterization was performed with a Keithley 2400 source measure unit under AM 1.5G illumination at 100 mW cm^{-2} with a solar simulator (Abet Technologies model 11000 class type A, Xenon arc). The light density was calibrated by a monosilicon detector (NREL) to reduce spectral mismatch. The applied voltage and cell current curves were obtained automatically with homebuilt labview software.

2.3.2 External quantum efficiency

The EQE values were carried out with a home-made setup consisting of a 150 W Oriel xenon lamp, a motorized monochromator and a Keithley 2400 digital source meter. An integrating sphere was used to provide homogeneous monochromatic light distribution over the active area of the devices. In addition, the photocurrent and irradiated light intensity were measured simultaneously.

2.4 Optical properties characterization

Photoluminescence (PL) is useful technique in solar cells characterization that provides a direct evidence for exciton dissociation and transport in the donor/acceptor system.[1,2] In our experiment, PL was measured in a fluorescence spectrophotometer from Photon Technology International Inc. for the three kinds of structures. A Xe lamp was used as the excitation light source at room temperature.

In addition, absorption spectrum of the blend active layer was measured at room

temperature with a Perkin Elmer Lambda 950 UV/VIS/NIR spectrometer.

2.5 Electronic properties characterization

2.5.1 Charge extraction (CE)
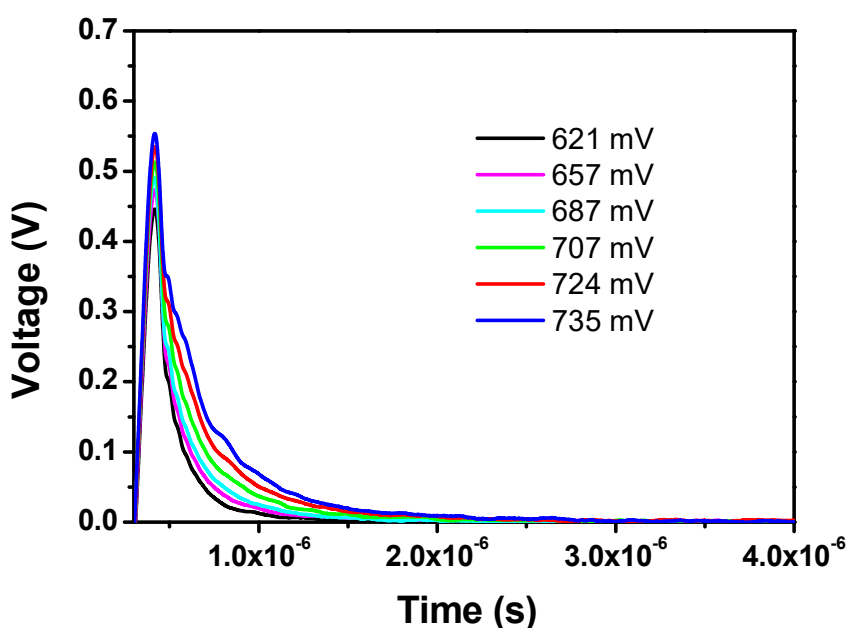
Figure 2.2. Charge carrier extraction data corresponds to decays at different light bias.

CE is a useful time domains technique to measure the charge accumulating and extracting distribution within the complete bulk device at different applied bias.[3-5] The general CE procedure is first to leave the device in open circuit conditions while illuminated at different intensities. Then, the cell is short-circuited and the decay in the photocurrent is measured through a small external load resistor and integrated to obtain the extracted charge. The desired illumination intensity is achieved with a white light LED ring from LUXEON® Lumileds connected to a DC power supply and a TGP110 function generator that allows the LEDs to reach a background illumination up to 1 sun on the ITO side of the device. The LEDs were typically turned on for approximately 100 ms so that they could reach steady state conditions. The LEDs have a rise/fall time of <100 ns. After the light is switched off and the circuit is temporally closed, while

charges are forced to pass through a TDS 2022 Oscilloscope from Tektronix© that traces the drop in voltage across a 50 Ω resistance. Figure 2.2 shows charge extraction data corresponds to the decays. The acquired signal is processed by applying the equation:

$$n = \frac{1}{Aqd}\frac{1}{R}\int V(t)dt$$

Where A is the device effective area, d is the device thickness, R is the resistance connected to the circuit, V is measure voltage, n is the charge density. The resulting point represents the charge carrier density accumulated on the device due to the photovoltaics process with respect to the light bias.

2.5.2 Transient photovoltage technique (TPV)

Information on the charge carrier recombination dynamics and carrier lifetime dependency on voltage is obtained by TPV measurements.[3-5] The complete devices are connected to the 1M input terminal of a Tektronix© TDS2022 oscilloscope and the background illumination was obtained from a ring of 6 white LEDs from LUXEON®. The small perturbation (5mV) was applied through a light pulse (N2 laser nominal wavelength, 50 ns pulses). The charge recombination rate was calculated for illumination intensities ranging from 0.1 to 1 sun.

2.6 Morphology and crystallinity structure characterization of polymer

2.6.1 Atomic force microscopy

AFM topographic and phase images of the row sample were obtained in the tapping

Chapter 2

mode on a molecular imaging model Pico SPM II (pico +). The images of all samples were collected in air using silicon probes with a typical spring constant of 1–5 nN m^{-1} and a resonant frequency of 75 kHz.

2.6.2 Transmission electron microscopy

Transmission Electron Microscopy (TEM) was carried out in a JEOL JEM-1011 microscope operating at 100 kV and equipped with a SIS Megaview III CCD camera. A few droplets of the sample suspended in ethanol were placed on a carbon-coated copper grids followed by evaporation at ambient conditions.

2.6.3 Grazing incidence X-ray scattering (GIXS)

Grazing incidence X-ray scattering (GIXS) is a scattering technique used to elucidate film morphology and the nanostructure of thin films. GIXS is carried out at a storage ring producing synchrotron X-radiation, which can provide the required high flux and collimation of the X-ray photons.[6-9] In the GIXS approach, X-rays impinge on the sample at a small grazing angle and a 2D detector is typically used to detect the scattered X-rays.[10] Grazing incidence wide angle X-ray scattering (GIWAXS) is relevant for structural characterization of BHJ films due to its large sampling volume and statistical information provided (a characteristic shared with all scattering techniques). It is commonly used on organic films to determine both the crystalline lattice spacing from the diffraction peaks and the crystalline correlation length from peak widths and to determine the orientation order parameters (Hermans orientation parameter) of the crystal planes. Grazing incidence small angle X-ray scattering (GISAXS) can give the size, shape, and interdomain correlation of the BHJ components. In our present study, GIWAXR and GISAXR measurements were made using a Bruker-AXS D8-Discover diffractometer equipped with parallel incident beam (Göbel mirror), vertical θ-θ goniometer, XYZ motorized stage and with a GADDS (General

Area Diffraction System). Samples of blend film on Si substrate were placed directly on the sample holder for reflection mode. An X-ray collimator system close-to-the-sample allows to analyzing areas of 500 μm width. The X-ray diffractometer was operated at 40 kV and 40 mA to generate Cu kα radiation. The GADDS detector was a HI-STAR (multiwire proportional counter of 30×30 cm with a 1024×1024 pixel) placed at 15 and 30 cm from the sample.

Scattering intensities were expressed as a function of the scattering vector q:

$$q = 4\pi\sin\theta/\lambda$$

Where θ is the half of the scattering angle and $\lambda = 1.5406$ Å is the wavelength of the incident radiation. The d-spacing of peak corresponding to the interstack space is expressed by Bragg equation:

$$2d\sin\theta = n\lambda$$

2.7 Surface energy measurements

Surface energy components are evaluated by utilizing advancing contact angle measurements.[11,12] Surface energy components were extracted from each data set with a fitting routine based on the acid–base model,[13] which is given by

$$(1+\cos\theta_{adv})\gamma_L^T = 2\left(\sqrt{\gamma_S^{LW}\gamma_L^{LW}} + \sqrt{\gamma_S^+\gamma_L^-} + \sqrt{\gamma_S^-\gamma_L^+}\right)$$

Where γ^T, γ^{LW}, γ^+, and γ^- denote the total, Lifshitz-van der Waals (dispersive), Lewis acid and base surface energy components, while the subscripts S and L refer to the solid surface and probe liquid. Thus, full description of an unknown surface energy requires contact angle measurements using at least three well-characterized probe liquids, one of which must be purely dispersive (i.e., a polar).

Chapter 2
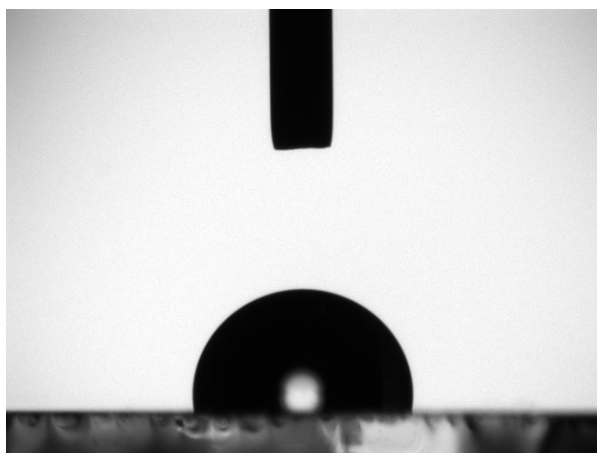
Figure 2.3. Contact angle measurements scheme.

Contact angle measurements were collected on a VCA Optima (AST Products) where 5 μL droplets were applied to the surface and left equilibrating for 15 s before measuring the advancing contact angle (θadv) (the scheme is shown in Figure 2.3). The equilibration time was selected as the time needed for a nonabsorbing, highly wetting liquid to yield a stable contact angle (e.g., diiodomethane on UVO ITO). A minimum of 6 droplets were measured for each liquid−solid combination with outliers.

Chapter 2

2.8 Reference

1. Li, G.; Yao, Y.; Yang, H.; Shrotriya, V.; Yang, G.;Yang, Y., " Solvent annealing" effect in polymer solar cells based on poly (3-hexylthiophene) and methanofullerenes. *Adv. Funct. Mater.* **2007**, *17*, 1636.

2. Duval, M.;Sarazin, D., Properties of PEO in dilute solution under stirring. *Macromolecules* **2003**, *36*, 1318-1323.

3. Maurano, A.; Hamilton, R.; Shuttle, C. G.; Ballantyne, A. M.; Nelson, J.; O'Regan, B.; Zhang, W.; McCulloch, I.; Azimi, H.;Morana, M., Recombination dynamics as a key determinant of open circuit voltage in organic bulk heterojunction solar cells: a comparison of four different donor polymers. *Adv. Mater.* **2010**, *22*, 4987-4992.

4. Sánchez-Díaz, A.; Burtone, L.; Riede, M.;Palomares, E., Measurements of efficiency losses in blend and bilayer-type zinc phthalocyanine/C60 high-vacuum-processed organic solar cells. *J. Phys. Chem. C* **2012**, *116*, 16384-16390.

5. Spoltore, D.; Oosterbaan, W. D.; Khelifi, S.; Clifford, J. N.; Viterisi, A.; Palomares, E.; Burgelman, M.; Lutsen, L.; Vanderzande, D.;Manca, J., Effect of polymer crystallinity in P3HT: PCBM solar cells on band gap trap states and apparent recombination order. *Advanced Energy Materials* **2013**, *3*, 466-471.

6. Rivnay, J.; Mannsfeld, S. C.; Miller, C. E.; Salleo, A.;Toney, M. F., Quantitative determination of organic semiconductor microstructure from the molecular to device scale. *Chem. Rev.* **2012**, *112*, 5488-5519.

7. DeLongchamp, D. M.; Kline, R. J.; Fischer, D. A.; Richter, L. J.;Toney, M. F., Molecular characterization of organic electronic films. *Adv. Mater.* **2011**, *23*, 319-337.

8. Rogers, J. T.; Schmidt, K.; Toney, M. F.; Bazan, G. C.;Kramer, E. J., Time-resolved structural evolution of additive-processed bulk heterojunction solar cells. *J. Am. Chem. Soc.* **2012**, *134*, 2884-2887.

9. Huang, Y.; Liu, F.; Guo, X.; Zhang, W.; Gu, Y.; Zhang, J.; Han, C. C.; Russell, T. P.;Hou, J., Manipulating backbone structure to enhance low band gap polymer photovoltaic performance. *Advanced Energy Materials* **2013**, *3*, 930-937.

10. Fuoss, P.;Brennan, S., Surface sensitive X-ray scattering. *Annual Review of Materials Science* **1990**, *20*, 365-390.

11. Ma, D.; Lv, M.; Lei, M.; Zhu, J.; Wang, H.;Chen, X., Self-organization of amine-based cathode

interfacial materials in inverted polymer solar cells. *ACS nano* **2014**, *8*, 1601-1608.

12. Clark, M. D.; Jespersen, M. L.; Patel, R. J.;Leever, B. J., Predicting vertical phase segregation in polymer-fullerene bulk heterojunction solar cells by free energy analysis. *ACS applied materials & interfaces* **2013**, *5*, 4799-4807.

13. Van Oss, C.; Ju, L.; Chaudhury, M.;Good, R., Estimation of the polar parameters of the surface tension of liquids by contact angle measurements on gels. *Journal of Colloid and Interface Science* **1989**, *128*, 313-319.

Chapter 2

Chapter 3

Improving the Efficiency of PTB1: PCBM BHJ Solar Cells by Polymer Blend Solution Aging

In this chapter, we state the effect on performance of PTB1: PCBM BHJ solar cells by solution aging processing. The aging process is performed by storing the completely dissolved blend solution of the donor and acceptor for certain periods of time before device fabrication. Increased aging times improves microphase separation morphology and bi-continuous interpenetrating network of active layer as proven by close inspection of the polymer mixture. As a consequence of such a synergistic increase, the resulting solar cells show an enhancement in short circuit current. Power conversion efficiencies (PCE) as high as 5.16% are found in devices fabricated with aged blends, a significant improvement exceeding 19% over the efficiency of 4.32% obtained in devices without polymer blend solution aging. This simple procedure has the potential to boost the maximum efficiencies exhibited by this technology.

Chapter 3

UNIVERSITAT ROVIRA I VIRGILI
NEW ADVANCES TO CONTROL MORPHOLOGY AND CRYSTALLINITY IN SOLUTION PROCESSED POLYMER SOLAR CELLS.
Peilin Han
Dipòsit Legal: T 256-2016

Chapter 3

Table of content

Chapter 3

3.1 Introduction

Bulk heterojunction (BHJ) solar cells based on polymer:fullerene are currently regarded as the one of most promising organic photovoltaic (OPV) devices due to the ease of fabrication and low processing costs.[1-3] In the recent years, power conversion efficiency (PCE) of organic solar cells has been continuously improved. PCE as high as 11.3% has been achieved, an appealing value for any commercial application.[4] Despite their numerous advantages, there are still other factors that limit the performance of polymer solar cells (PSCs) such as charge transport towards the interface between donor and acceptor, and exciton dissociation, determined by crystallinity and the interpenetrating networks formed between donor and acceptor. In order to improve the photovoltaic performance, great effort has been made for designing new polymers [5-8] and using additives or interfacial materials. [9-12] Furthermore, the morphology of active layer has also been optimized, [13-16] including thermal annealing [17] and the use of different solvent mixtures. [18, 19]

For BHJ solar cells, the electron-hole pairs (excitons) generated through light absorption in the donor, diffuse to the heterointerface formed by the donor/acceptor. There, they are dissociated into free charges and transported to their respective electrodes. The built in field appearing at the interface between donor and acceptor is key for exciton dissociation in the photovoltaic process. [20, 21] Several groups have found enhanced interfacial charge transfer in devices with large interface area and strongly interpenetrating morphology. [22-26] In 2005, Yang et al. achieved a significant improvement of the performance of poly (3-hexylthiophene) (P3HT): [6,6]-phenyl-C_{61}-butyric acid methyl ester ($PC_{61}BM$) blend solar cells by using the solvent annealing approach. [27, 28] This solution-processed method efficiently increased the interfacial charge transfer between the P3HT and PCBM by controlling the evaporation rate of the solvent after spin-coating. This process allowed for a better

Chapter 3

arrangement of the polymers in the blend improving exciton dissociation and charge transport efficiency, resulting in high short circuit current (Jsc) and fill factor (FF).

Recently, a series of the wide spectral response polymer PTBx composed of thieno [3,4-b] thiophene and benzodithiophene alternating units have been widely used as a promising donor material used in solar cells. Device based on this PTBx have been continuously refreshed the record of PSCs efficiency in the last few years. [6], [9], [29-31] PTB1 (poly((4,8-bis (octyloxy) benzo (1,2-b:4,5-b') dithiophene-2,6-diyl) (2-((dodecyloxy) carbonyl) thieno(3,4-b) thiophenediyl)), is selected into solar cells here as the single PTB1 structure includes the basic electro-optic properties and molecular structures of the other PTBx polymers.[31] The PTB1 has a broad absorption band in the solar spectrum and an excellent charge mobility for charge transport. [9] In addition, the PTB1 backbone planes lie parallel to the substrate surface and result in a large contact area with the acceptor or the interfacial layer. [32] The structure orientation character of PTB1 in the active layer is beneficial to transport the charge across the interface.

In this work, we want to demonstrate how charge separation and transport at the interface between donor and acceptor can be improved in the blend solution, even before the active layer is spin coated. Right after the blend solution is prepared, the donor and acceptor diffuse into each other. This is why solution aging is found to be a key method to procure optimal interpenetration between donor and acceptor. This processing step is performed by leaving the complete blend solution rest for a certain period of time before being spun. An essential part of treatment is that the blend solution must be sealed completely without heating and stirring, to avoid solvent evaporation and affect the concentration of solution or aggregation as seen in long stirring times.[33] We investigated the impact of solution aging on the efficiency of PTB1:PC$_{61}$BM BHJ solar cells. We analyzed the morphology and structure of PTB1:PC$_{61}$BM blend films using atomic force microscopy (AFM), grazing incidence

small angle X-ray scattering (GISAXS) and wide angle X-ray scattering (GIWAXS). The performance of PTB1:PC$_{61}$BM BHJ solar cells was analyzed by current-voltage, external quantum efficiency and absorbance measurements. This study revealed that optimum blend aging times prior to spin casting lead to power conversion efficiency enhancements over 19% in solar cells as compared to devices made with readily prepared blends.

3.2 Experiment Section

Ortho-dichlorobenzene (ODCB) was used as solvent. The polymer PTB1 and PC$_{61}$BM were co-dissolved in ODCB in the weight ratio of 1:1. The dispersion was carried out by magnetic stirring at 40 ºC for 15 hours. Solution aging process was performed by putting the sealed bottle with the completely dissolved blend solution without stirring and heating for different times in the glove box. The ITO covered glass clean and devices fabrication are followed in experimental section in chapter 2. The final devices are completed by depositing a Ca layer (25 nm) and an Ag layer (100nm) on the active layer. The related characterization techniques including optical property (PL, UV-vis), AFM, GIXS and performance of solar cells has also been described in experimental section in chapter 2.

3.3 Results and Discussion

3.3.1 Measurements of solar cells performance

BHJ solar cells were fabricated with the structure of ITO/PEDOT:PSS/PTB1:PC$_{61}$BM/Ca/Ag, as described in the experimental section. Different aging times were investigated: 0 h, 24 h, 48 h and 72 h. The optimal blend ratio PTB1/PC$_{61}$BM 1:1 wt. was used with a PTB1 concentration of 15 mg mL^{-1} (the optimal operation conditions were obtained in our previous study [34]). Figure 3.1a shows the current density versus voltage (J-V) curves of devices corresponding to solution aging times of 0, 24, 48 and 72 h. the performance parameters are

summarized in Table 3.1. Devices made with just prepared polymer blends (0 h), showed PCE of 4.32% obtained with a Voc of 590 mV, a Jsc of 10.58 mA cm^{-2} and a good FF of 69.2%. When the blend mixture is aged 24 h, the Jsc and Voc slightly increased to 11.20 mA cm^{-2} and 600 mV, respectively. The fill factor changes along with the increased aging time to 68.4%. As a result, the PCE improves to 4.60%. After aging the solution for 48 h, the Jsc improves significantly to 12.61 mA cm^{-2}, while maintaining the Voc and the FF at 600 mV and 68.2%, respectively. Consequently, the PCE of the PSC reaches 5.16%. When the blend solution is aged for 72 h, the Jsc of the PSCs increases to 12.92 mA cm^{-2}, although the PCE decreases to 4.8% due to a decrease in the Voc to 570 mV and the FF to 65.2%.
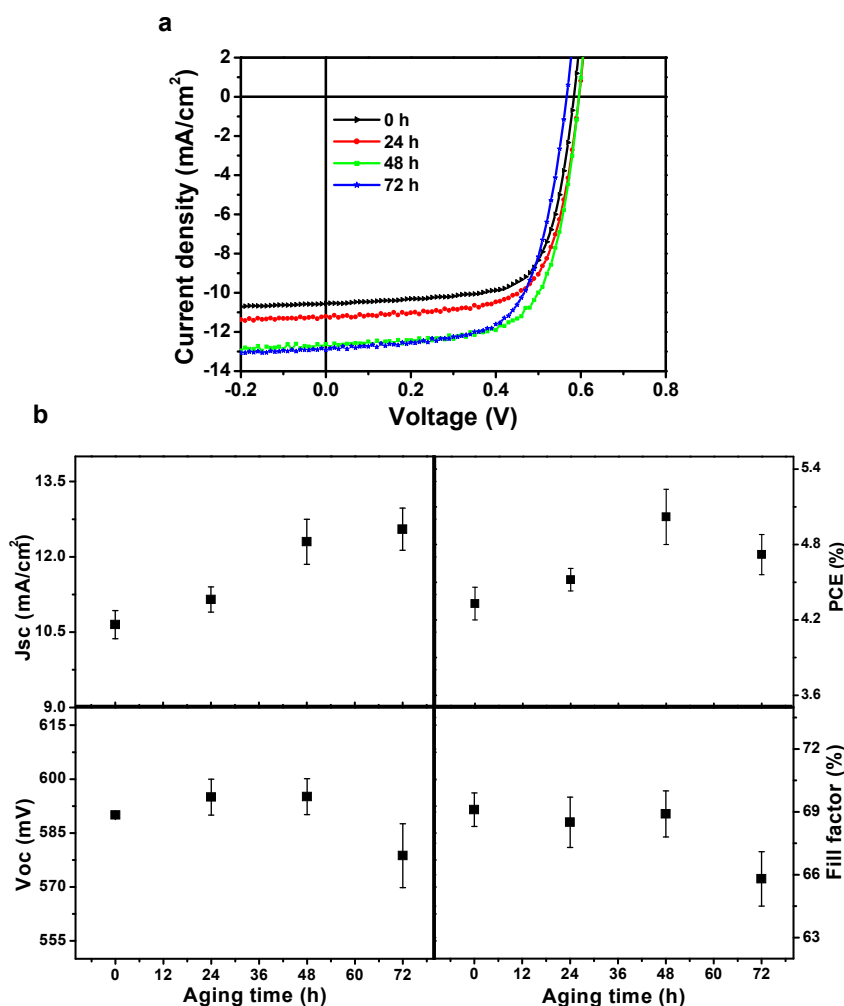
Figure 3.1. (a) Current-voltage curves under AM 1.5 G illumination at 1 sun. Devices were fabricated from PTB1:PC$_{61}$BM solutions (15 mg mL^{-1}) aged for 0, 24, 48, 72 hours, respectively. (b) Figures of merit from the PTB1:PC$_{61}$BM solar cell devices fabricated. At least six devices were measured for each aged solution to obtain the statistics presented therein.

Chapter 3

The photovoltaic performance data (including Voc, Jsc, FF) of the PTB1:PC$_{61}$BM solar cells for each aging time (6 devices each) are summarized in Figure 3.1b. The trend seen in the PCE improvement from solution aging is mainly due to the increase Jsc.

Table 3.1. Performance parameters of our devices

Aging time	V$_{OC}$ (mV)	J$_{SC}$ (mA/cm^2)	FF (%)	PCE (%)
0 h	590.0±0.0	10.65±0.28	69.1±0.8	4.33±0.13
24 h	595.0±5.0	11.15±0.25	68.5±1.2	4.52±0.09
48 h	595.1±5.0	12.30±0.45	68.9±1.1	5.02±0.22
72 h	578.7±9.9	12.55±0.42	65.8±1.3	4.72±0.16

In order to investigate the origin of this improved photocurrent, the spectral response of the champion devices for each blend aging time was studied. Figure 3.2a shows the external quantum efficiency (EQE) measurements for the corresponding devices. The EQE is enhanced over the wavelength range of 500-720 nm with increasing blend aging times, in good agreement with the Jsc results from the current voltage characterization of our devices. The maximum EQE enhancement is found at a wavelength of 640 nm, going from 60% to 70% by increasing the blend aging time from 0 h to 72 h.

In general, enhanced EQE and Jsc may originate from the efficient charge dissociation and transport or increased absorption of photons. [35, 36] To investigate any absorption changes in the PTB1:PC$_{61}$BM blends aged for different periods of time, the absorption spectra of the different solutions is measured (Figure 3.2b) showing virtually the same spectral characteristics in intensity and absorption range. The internal quantum efficiency (IQE) spectrum is obtained from the absorption spectrum (not shown) and the EQE of the PTB1:PC$_{61}$BM solar cells shown in Figure 3.2c. The results are in good agreement with the characteristics of EQE and Jsc, close to 90% in 650 nm-750 nm. The high IQE indicates that the most of separated excitons is

collected at the electrode. Comparing films with the same thickness (ca.110 nm, the cross sectional micrograph of device by scanning electron microscopy (SEM) shows
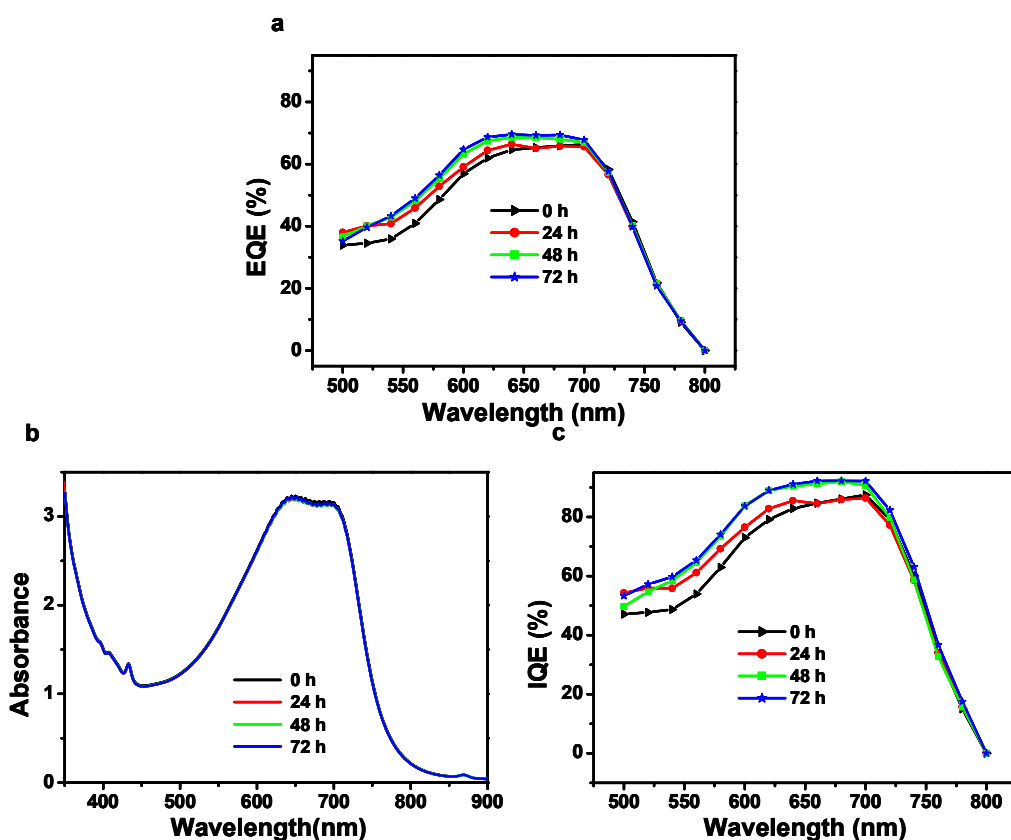
Figure 3.2. (a) EQE spectra of the devices fabricated with $PTB1:PC_{61}BM$ blends aged 0, 24, 48 and 72 hours. (b) Absorption spectrum of $PTB1:PC_{61}BM$ blend solutions with different aging times. (c) IQE spectra calculated from the corresponding EQE and absorption spectra of each device.
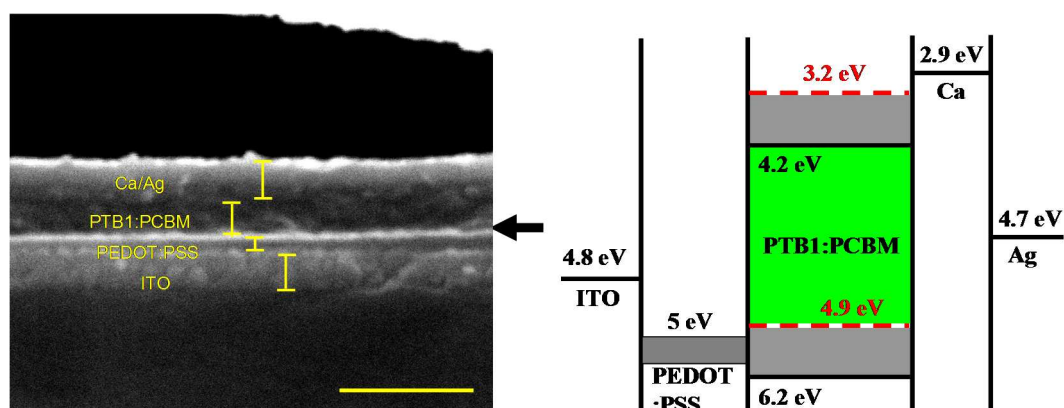
Figure 3.3. Cross sectional SEM image of device structure with corresponding energy level diagram of the device architecture. The scale bar is 500 nm.

in Figure 3.3) deposited from solutions with different aging times, we observe that the aging process did not change light absorption but instead, increases Jsc likely due to a more efficient exciton dissociation and charge transfer at the interface PTB1/PC$_{61}$BM.

3.3.2 Photoluminescence quenching upon the solution aging

Photoluminescence (PL) quenching provides direct evidence for photogenerated exciton dissociation and transport in the donor/acceptor blend system. [28] Photo excitation promotes the electron from the donor's HOMO into LUMO and produces the charge transfer state. In the process, the exciton (charge transfer state) either can be recombined by relaxing back to ground state or quenched by dissociated electron transfers to acceptor at the interface of donor/acceptor. In present work, the normalized PL spectra from PTB1:PC$_{61}$BM blend solution with different solution aging time are shown in Figure 3.4. We try to understand the dissociation of photogenerated excitons by solution aging processed before blend solution is spin-coated. All solutions were excited using 500 nm wavelength. The PTB1:PC$_{61}$BM blend solution exhibits an emission band centred at 810 nm that is from PTB1 emission. Furthermore, it is noteworthy that photoluminescence quenching takes place clearly after solution aging of the blend solution, whereas there are no observable changes in the absorption spectrum (Figure 3.2b). The significant PL quenching observed by solution aging path ensures either the efficient exciton dissociation or the dissociated charge transport in the interfacial PTB1/PC$_{61}$BM. It also implies that solution process increases extent of intertwined and collision between PTB1 and PC$_{61}$BM, further resulting in the large interface area and the electron interaction, and subsequently improving photocurrent generation efficiency. By PL analysis, we demonstrates that the solution aging can improve the electron transfer of PTB1 and PC$_{61}$BM and mediate more photo induced charge transfer from PTB1 to PC$_{61}$BM, it is a possible reason to further increase the Jsc and PCE.

Chapter 3
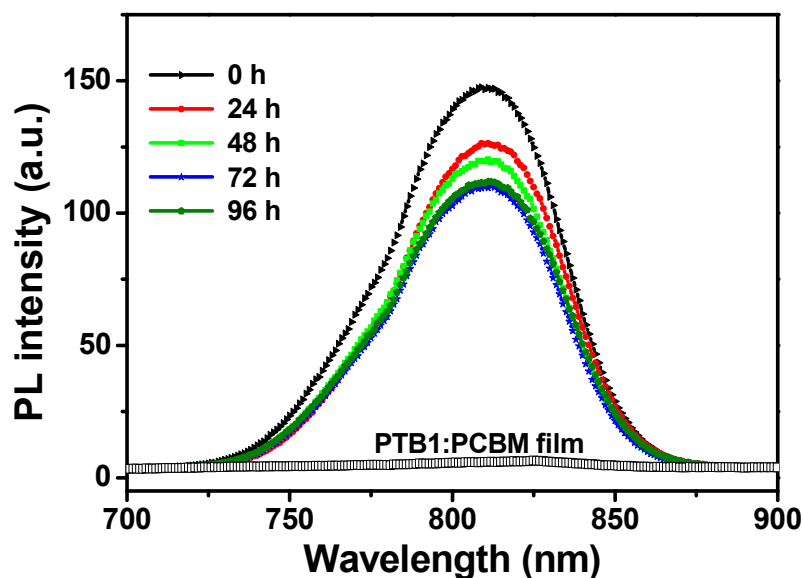
Figure 3.4. PL spectra of PTB1:PC$_{61}$BM solution with different aging time and film.

3.3.3 Morphological characterization with AFM

Once the photogenerated exciton has diffused to a donor/acceptor interface, it can be dissociated by an interfacial electron transfer reaction. Unfortunately, although increasing the aging times of the blends produces an increase in the photocurrent, J-V results indicate that 72 h aging times cause reduces Voc and FF. The device fabricated after 72 h solution aging prior spin casting shows Voc and FF value of 570 mV and 65.2%, respectively, lower values than those obtained with 48 h solution aging, leading to a decreased PCE of 4.8%. It is possible that letting the mixture rest in for periods longer than 48 h results in the formation of aggregates in the active layer due to diffusion superimposes of PTB1 and PC$_{61}$BM as indicated by the AFM measurements (Figure 3.5). Subsequently, the ohmic contact between active layer and metal electrode will be further reduced resulting in an increased non-geminate charge carrier recombination. 72 h solution aging changes the formation of stable nanoscale and bi-continuous interpenetrating donor-acceptor networks morphology in the film,

58

Chapter 3

which is crucial for exciton separation and charge transport to their respective electrode.
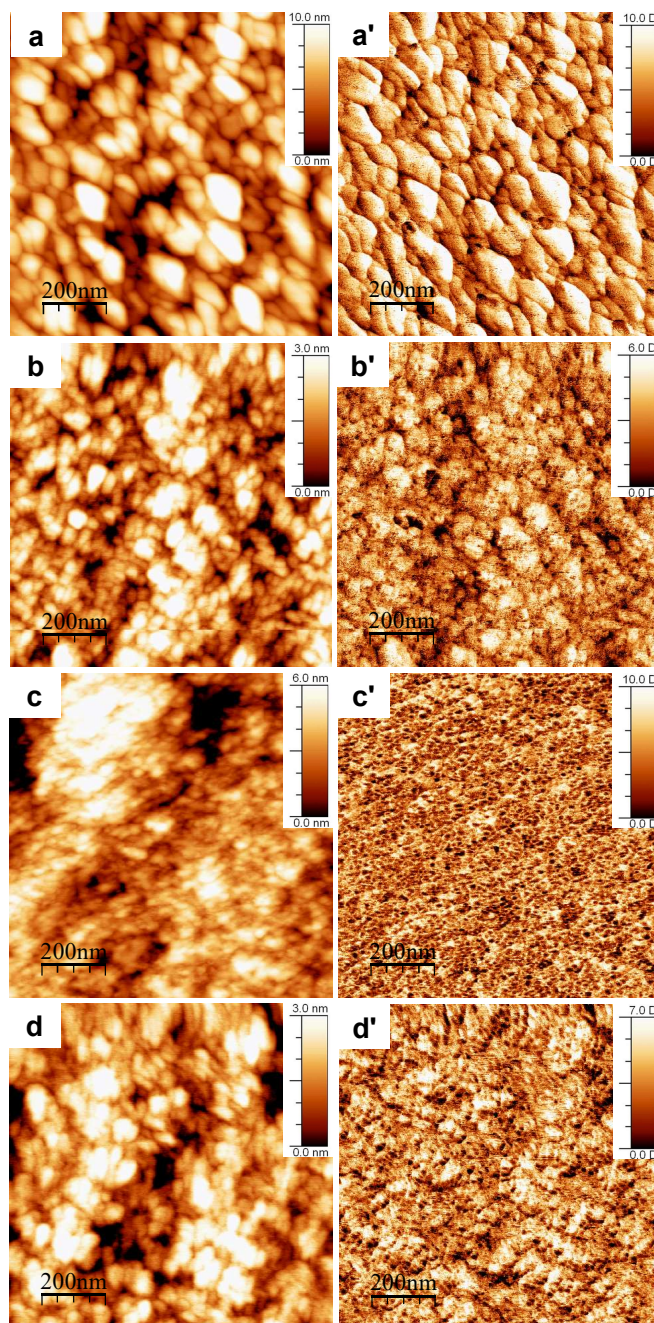
Figure 3.5. AFM topographic (right) and phase images (left) of thin films fabricated from PTB1:PCBM blend solutions (15 mg mL^{-1}) with different aging times: (a, a') 0 h, (b, b') 24 h, (c, c') 48 h and (d, d') 72 h.

AFM is used to investigate the nanoscale morphology of PTB1:PC$_{61}$BM blend film cast from solution of 15 mg mL^{-1} aged for different periods of time (Figure 3.5a-d').

Chapter 3

The surface topography of blend film from the as prepared solution (0 h) displays feature dimensions of 40-100 nm with an average roughness of 2 nm (Figure 3.5a). The phase image (Figure 3.5a') shows large phase separation and the poor interpenetrating network morphology of PTB1:$PC_{61}BM$ film. The surface of film spin casted from a 24 h aged blend mixture changed significantly, with a visible decrease in the roughness and domain size (Figure 3.5b,3.5b'). When the solution aging time increases to 48 h, the surface of the blend film shows a small grain domain size (< 20 nm) with an average roughness of 1.1 nm (Figure 3.5c). The interpenetrating network and micro-phase separation of PTB1:PCBM blend layer are improved (Figure 3.5c'). The change in the active layer morphology indicates that an aging the blend solutions for more than 48 h increased the degree of diffusion of the donor and acceptor into each other's domain. In Figure 3.6, we show a process schematic diagram of donor
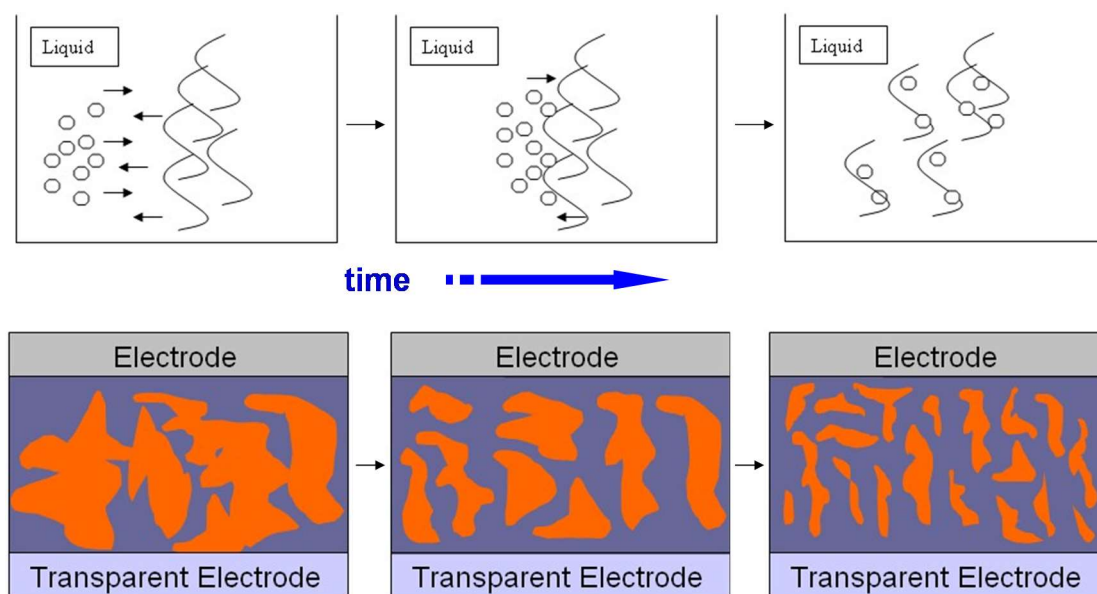
Figure 3.6. Process schematic diagram of donor and acceptor blend solution aging and morphology variation of blend film

and acceptor blend solution aging and a schematic morphology variation of blend film along with the increased time. By relating to the results with the device performance, smaller scale phase separation increases interface area between PTB1 and $PC_{61}BM$ where exciton separation will take place more efficiently (charge diffusion length is generally less than 10 nm). Meanwhile, the smaller nanoscale structure is also beneficial to increase the contact area with the metal electrode and improve the

efficiency of electron extraction from active layer, thereby leading to an increased Jsc and FF.

However, in the film deposited from a solution aged for 72 h, the performance of the cell is deteriorated respect to shorter aging times. This deterioration in fill factor and Voc is probably originated in the increased phase aggregation for long aging times from the surface topography images (Figure 3.5d,d') indicating a reduction in the interpenetration of the network, leading to inefficient charge percolation and poor 'wiring' to the device electrodes. In addition, the phase aggregation may weaken the strength of π–π interactions through the polymer backbone stacking in the film, further decreasing the fill factor of OPV device. [6] The decreased interchain interaction of the donor will also lead to the enrichment of the $PC_{61}BM$ and PTB1. The significant phase aggregation from the rich $PC_{61}BM$ and PTB1 disrupts the balance of interpenetrating network and reduces the ohmic contact between active layer and electrode. Finally, it affects the charge injection process to the electrodes, and increases the recombination reaction at the interface induced the lower Voc, [37] although the efficient exciton separation enhanced the Jsc.

3.3.4 Crystal structure arrangements from solution aging processing

It should be noted that the blend layer morphology discussed above is relative to the molecular packing structure. Grazing incidence small angle X-ray scattering and wide angle X-ray scattering can provide information about the structural arrangements in a film based on the elastic scattering of incident X-rays with the blend film. [38, 39] In order to measure the $PTB1:PC_{61}BM$ blend samples using the GISAXS, it is necessary to prepare a thick film as the amount of scattered intensity is very low. Figure 3.7a-d shows 2D GIWAXS and GISAXS molecular packing patterns of PTB1 and $PC_{61}BM$ blends with solution aging times of 0 h and 48 h with their corresponding q_y and q_z

Chapter 3

scans. The π-conjugated backbones and the interstack separation is defined by the side chains extended outward from the backbone parallel to the substrate (Figure. 3.7e).[32]
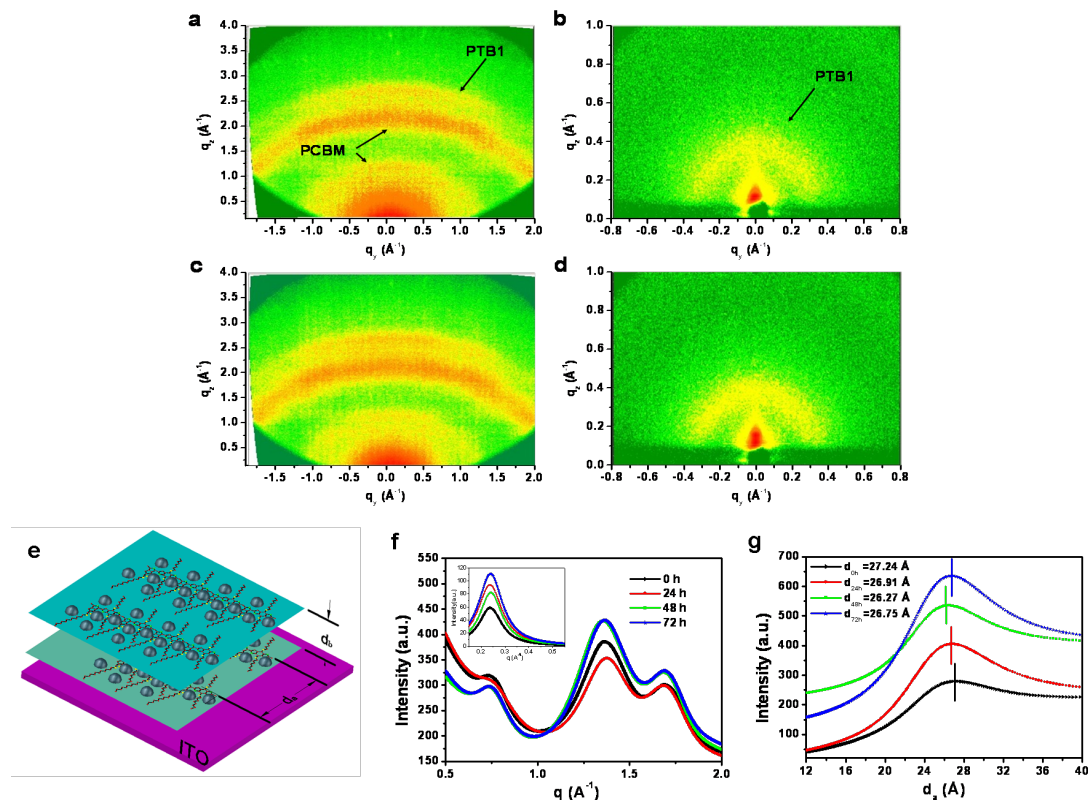
Figure 3.7. GIWAXS and GISAXS images acquired from PTB1: $PC_{61}BM$ blend films fabricated from solutions aged during: (a, b) 0 h and (c, d) 48 h. (e) PTB1 and $PC_{61}BM$ backbone interstack model. (f) GIWAXS data; inset is the GISAXS of samples. (g) Interstack spacing of PTB1 from GISAXS data.

Figure 3.7f shows a distinct in-plane peak transformed from Figure. 3.7a-d. The peaks at $q_y = 0.23$ Å^{-1} and $q_z = 1.71$ Å^{-1} corresponds to interstack d-spacing of $d_a = 27.2$ Å and $d_b = 3.67$ Å are from PTB1. [32] Additional broad rings in the scattering pattern at $q_{y,z} = 1.41$ Å^{-1} (d = 4.46 Å) and $q_{y,z} = 0.73$ Å^{-1} (d = 8.6 Å) are from (311) and (111) Bragg diffractions coming from neat C_{60} structures. [40] The samples before and after solution aging showed similar scattering profiles, indicating the PTB1 crystal structure remained unchanged. Nevertheless, a slight d-spacing decrease in GIWAXS patterns of the solution aged films was observed. The corresponding peak q_y reveals a decrease in the interchain interstack spacing direction parallel to the substrate from $d_a = 27.2$ Å to $d_a = 26.2$ Å by aging the blend solution for 48 h (Figure 3.7g). The peak

Chapter 3

corresponding to the π-stacking spacing (d_b = 3.7 Å) in the vertical direction stays unchanged. For PTB1-PC$_{61}$BM blend, the dominant element reacting with PC$_{61}$BM is the thienothiophene unit of the PTB1 molecule (the π- π stacking distance is not changed significantly because benzodithiophene dominates the π- π stacking interaction). The linear alkyl side chains attached to the thienothiophene unit in PTB1 may not affect the π- π stacking interaction, but affect PC$_{61}$BM reaction with the PTB1 side chains. [6] The PTB1 crystallized initially in solution. These reduced interchain d-spacing (d_a) indicate that interaction of PTB1 and PC$_{61}$BM along the direction parallel to the substrate increases after solution aging. The results lead to the enhanced electron-hole separation between donor and acceptor directly, in agreement with the small micro-phase separation morphology of blend film after solution aging.
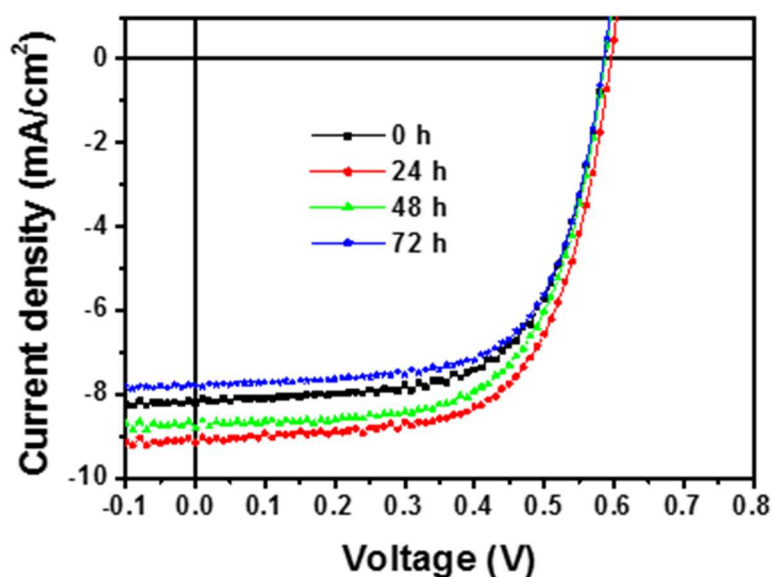
Figure 3.8. (a) Current-voltage curves under AM 1.5 G illumination at 1 sun. Devices were fabricated from P3HT:PCBM solutions (15 mg mL^{-1}) aged for 0, 24, 48, 72 hours, respectively.

In order to verify the validity of solution aging, the approach is also verified in P3HT:PC$_{61}$BM system. The I-V curve is shown in Figure 3.8 and the performance parameter is summarizes in Table 3.2. The fabrication of P3HT:PC$_{61}$BM solar cells is similar to PTB1:PC$_{61}$BM solar cells and different aging times are performer with 0 h, 24 h, 48 h and 72 h. the results show that the optimal PCE of 3.5 % with Jsc of 9.14

mA/cm^2 is obtained from solution aging for 24 h comparison with PCE of 3.1 % obtained without solution aging. We believe that this efficient method can be applied to other organic devices such as photodetectors, field-effect transistors and light emitting diodes.

Table 3.2. Performance parameters of our best devices.

Aging time	V_{OC} (mV)	J_{SC} (mA/cm^2)	FF (%)	PCE (%)
0 h	590	8.19	64	3.09
24 h	600	9.13	63.5	3.34
48 h	590	8.8	63.3	3.28
72 h	590	7.8	65.2	3.0

3.4 Conclusions

We have shown the importance of solution aging in the fabrication of polymer solar cells. The novel method affects the exciton separation, morphology of blend film and impacts device performance. Compared to the blend film without solution aging, the aged films present significantly improved small nanoscale domain morphology and a bi-continuous interpenetrating network which in turn result in higher interface area and efficient charge generation between the donor and acceptor. GIWAXS and GISAXS of films show favorable charge transport pathways due to the increase of interaction between $PC_{61}BM$ and the thienothiophene unit of PTB1. All effects give rise to the better charge collection and higher short circuit current. Finally, we obtained the best performance of 5.16% with blend solutions aged for 48 h, a significant improvement exceeding 19% over the efficiency of 4.32% obtained in devices without polymer blend solution aging.

Chapter 3

3.5 References

1.   Thompson, B. C.;Frechet, J. M., Polymer–fullerene composite solar cells. *Angew. Chem., Int. Ed.* **2008**, *47*, 58-77.

2.   Kim, Y.; Cook, S.; Tuladhar, S. M.; Choulis, S. A.; Nelson, J.; Durrant, J. R.; Bradley, D. D.; Giles, M.; McCulloch, I.;Ha, C.-S., A strong regioregularity effect in self-organizing conjugated polymer films and high-efficiency polythiophene: fullerene solar cells. *Nat. Mater.* **2006**, *5*, 197-203.

3.   Li, G.; Zhu, R.;Yang, Y., Polymer solar cells. *Nat. Photonics* **2012**, *6*, 153-161.

4.   Bin Mohd Yusoff, A. R.; Kim, D.; Kim, H. P.; Shneider, F. K.; da Silva, W. J.;Jang, J., A high efficiency solution processed polymer inverted triple-junction solar cell exhibiting a power conversion efficiency of 11.83%. *Energy & Environmental Science* **2015**, *8*, 303-316.

5.   Blouin, N.; Michaud, A.; Gendron, D.; Wakim, S.; Blair, E.; Neagu-Plesu, R.; Belletete, M.; Durocher, G.; Tao, Y.;Leclerc, M., Toward a rational design of poly (2, 7-carbazole) derivatives for solar cells. *J. Am. Chem. Soc.* **2008**, *130*, 732-742.

6.   Szarko, J. M.; Guo, J.; Liang, Y.; Lee, B.; Rolczynski, B. S.; Strzalka, J.; Xu, T.; Loser, S.; Marks, T. J.;Yu, L., When function follows form: effects of donor copolymer side chains on film morphology and BHJ solar cell performance. *Adv. Mater.* **2010**, *22*, 5468-5472.

7.   Zhou, H.; Yang, L.; Stuart, A. C.; Price, S. C.; Liu, S.;You, W., Development of fluorinated benzothiadiazole as a structural unit for a polymer solar cell of 7% efficiency. *Angew Chem Int Ed Engl* **2011**, *123*, 3051-3054.

8.   Zhou, E.; Cong, J.; Zhao, M.; Zhang, L.; Hashimoto, K.;Tajima, K., Synthesis and application of poly (fluorene-alt-naphthalene diimide) as an n-type polymer for all-polymer solar cells. *Chem. Commun.* **2012**, *48*, 5283-5285.

9.   Liang, Y.; Wu, Y.; Feng, D.; Tsai, S.-T.; Son, H.-J.; Li, G.;Yu, L., Development of new semiconducting polymers for high performance solar cells. *J. Am. Chem. Soc.* **2008**, *131*, 56-57.

10.   You, J.; Chen, C. C.; Dou, L.; Murase, S.; Duan, H. S.; Hawks, S. A.; Xu, T.; Son, H. J.; Yu, L.;Li, G., Metal Oxide Nanoparticles as an Electron-Transport Layer in High-Performance and Stable Inverted Polymer Solar Cells. *Adv. Mater.* **2012**, *24*, 5267-5272.

11.   Oostra, A. J.; van den Bos, K. H.; Blom, P. W.;Michels, J. J., Disruption of the electrical

Chapter 3

conductivity of highly conductive poly (3, 4-ethylenedioxythiophene): poly (styrene sulfonate) by hypochlorite. *J. Phys. Chem. B* **2013**, *117*, 10929-10935.

12.   Tan, Z. a.; Li, L.; Cui, C.; Ding, Y.; Xu, Q.; Li, S.; Qian, D.;Li, Y., Solution-processed tungsten oxide as an effective anode buffer layer for high-performance polymer solar cells. *J. Phys. Chem. C* **2012**, *116*, 18626-18632.

13.   Jo, J.; Na, S.-I.; Kim, S.-S.; Lee, T.-W.; Chung, Y.; Kang, S.-J.; Vak, D.;Kim, D.-Y., Three-dimensional bulk heterojunction morphology for achieving high internal quantum efficiency in polymer solar cells. *Adv. Funct. Mater.* **2009**, *19*, 2398.

14.   Peet, J.; Kim, J. Y.; Coates, N. E.; Ma, W. L.; Moses, D.; Heeger, A. J.;Bazan, G. C., Efficiency enhancement in low-bandgap polymer solar cells by processing with alkane dithiols. *Nat. Mater.* **2007**, *6*, 497-500.

15.   Ren, B.-Y.; Ou, C.-J.; Zhang, C.; Chang, Y.-Z.; Yi, M.-D.; Liu, J.-Q.; Xie, L.-H.; Zhang, G.-W.; Deng, X.-Y.;Li, S.-B., Diarylfluorene-modified fulleropyrrolidine acceptors to tune aggregate morphology for solution-processable polymer/fullerene bulk-heterojunction solar cells. *J. Phys. Chem. C* **2012**, *116*, 8881-8887.

16.   Dang, M. T.; Hirsch, L.; Wantz, G.;Wuest, J. D., Controlling the morphology and performance of bulk heterojunctions in solar cells. Lessons learned from the benchmark poly (3-hexylthiophene):[6, 6]-phenyl-C61-butyric acid methyl ester system. *Chem. Rev.* **2013**, *113*, 3734-3765.

17.   Padinger, F.; Rittberger, R. S.;Sariciftci, N. S., Effects of postproduction treatment on plastic solar cells. *Adv. Funct. Mater.* **2003**, *13*, 85-88.

18.   Wienk, M. M.; Turbiez, M.; Gilot, J.;Janssen, R. A., Narrow-Bandgap Diketo-Pyrrolo-Pyrrole Polymer Solar Cells: The Effect of Processing on the Performance. *Adv. Mater.* **2008**, *20*, 2556-2560.

19.   Ma, W.; Tumbleston, J. R.; Ye, L.; Wang, C.; Hou, J.;Ade, H., Quantification of Nano-and Mesoscale Phase Separation and Relation to Donor and Acceptor Quantum Efficiency, Jsc, and FF in Polymer: Fullerene Solar Cells. *Adv. Mater.* **2014**, *26*, 4234-4241.

20.   Clarke, T. M.;Durrant, J. R., Charge photogeneration in organic solar cells. *Chem. Rev.* **2010**, *110*, 6736-6767.

21.   Graetzel, M.; Janssen, R. A.; Mitzi, D. B.;Sargent, E. H., Materials interface engineering for solution-processed photovoltaics. *Nature* **2012**, *488*, 304-312.

Chapter 3

22.   Chen, S.; Manders, J. R.; Tsang, S.-W.;So, F., Metal oxides for interface engineering in polymer solar cells. *J. Mater. Chem.* **2012**, *22*, 24202-24212.

23.   Xin, H.; Reid, O. G.; Ren, G.; Kim, F. S.; Ginger, D. S.;Jenekhe, S. A., Polymer nanowire/fullerene bulk heterojunction solar cells: how nanostructure determines photovoltaic properties. *Acs Nano* **2010**, *4*, 1861-1872.

24.   Chen, H.-Y.; Yang, H.; Yang, G.; Sista, S.; Zadoyan, R.; Li, G.;Yang, Y., Fast-grown interpenetrating network in poly (3-hexylthiophene): methanofullerenes solar cells processed with additive. *J. Phys. Chem. C* **2009**, *113*, 7946-7953.

25.   Jailaubekov, A. E.; Willard, A. P.; Tritsch, J. R.; Chan, W.-L.; Sai, N.; Gearba, R.; Kaake, L. G.; Williams, K. J.; Leung, K.;Rossky, P. J., Hot charge-transfer excitons set the time limit for charge separation at donor/acceptor interfaces in organic photovoltaics. *Nat. Mater.* **2013**, *12*, 66-73.

26.   Zhou, H.; Zhang, Y.; Seifter, J.; Collins, S. D.; Luo, C.; Bazan, G. C.; Nguyen, T. Q.;Heeger, A. J., High-Efficiency Polymer Solar Cells Enhanced by Solvent Treatment. *Adv. Mater.* **2013**, *25*, 1646-1652.

27.   Li, G.; Shrotriya, V.; Huang, J.; Yao, Y.; Moriarty, T.; Emery, K.;Yang, Y., High-efficiency solution processable polymer photovoltaic cells by self-organization of polymer blends. *Nat. Mater.* **2005**, *4*, 864-868.

28.   Li, G.; Yao, Y.; Yang, H.; Shrotriya, V.; Yang, G.;Yang, Y., " Solvent annealing" effect in polymer solar cells based on poly (3-hexylthiophene) and methanofullerenes. *Adv. Funct. Mater.* **2007**, *17*, 1636.

29.   Chen, W.; Xu, T.; He, F.; Wang, W.; Wang, C.; Strzalka, J.; Liu, Y.; Wen, J.; Miller, D. J.;Chen, J., Hierarchical nanomorphologies promote exciton dissociation in polymer/fullerene bulk heterojunction solar cells. *Nano Lett.* **2011**, *11*, 3707-3713.

30.   Lou, S. J.; Szarko, J. M.; Xu, T.; Yu, L.; Marks, T. J.;Chen, L. X., Effects of additives on the morphology of solution phase aggregates formed by active layer components of high-efficiency organic solar cells. *J. Am. Chem. Soc.* **2011**, *133*, 20661-20663.

31.   Liang, Y.;Yu, L., A new class of semiconducting polymers for bulk heterojunction solar cells with exceptionally high performance. *Acc. Chem. Res.* **2010**, *43*, 1227-1236.

32.   Guo, J.; Liang, Y.; Szarko, J.; Lee, B.; Son, H. J.; Rolczynski, B. S.; Yu, L.;Chen, L. X., Structure, dynamics, and power conversion efficiency correlations in a new low bandgap polymer: PCBM solar

Chapter 3

cell. *J. Phys. Chem. B* **2010**, *114*, 742-748.

33.   Duval, M.;Sarazin, D., Properties of PEO in dilute solution under stirring. *Macromolecules* **2003**, *36*, 1318-1323.

34.   Balderrama, V.; Estrada, M.; Han, P.; Granero, P.; Pallarés, J.; Ferré-Borrull, J.;Marsal, L., Degradation of electrical properties of PTB1: PCBM solar cells under different environments. *Sol. Energy Mater. Sol. Cells* **2014**, *125*, 155-163.

35.   Lin, L. B.; Jenekhe, S.;Borsenberger, P., High electron mobility in bipolar composites of organic molecules. *Appl. Phys. Lett.* **1996**, *69*, 3495-3497.

36.   Hu, Z.; Zhang, J.;Zhu, Y., High-performance and air-processed polymer solar cells by room-temperature drying of the active layer. *Appl. Phys. Lett.* **2013**, *102*, 043307.

37.   Yang, L.; Zhou, H.;You, W., Quantitatively analyzing the influence of side chains on photovoltaic properties of polymer− fullerene solar cells. *J. Phys. Chem. C* **2010**, *114*, 16793-16800.

38.   Rivnay, J.; Mannsfeld, S. C.; Miller, C. E.; Salleo, A.;Toney, M. F., Quantitative determination of organic semiconductor microstructure from the molecular to device scale. *Chem. Rev.* **2012**, *112*, 5488-5519.

39.   DeLongchamp, D. M.; Kline, R. J.; Fischer, D. A.; Richter, L. J.;Toney, M. F., Molecular characterization of organic electronic films. *Adv. Mater.* **2011**, *23*, 319-337.

40.   Woo, C. H.; Thompson, B. C.; Kim, B. J.; Toney, M. F.; Fréchet, J. M., The influence of poly (3-hexylthiophene) regioregularity on fullerene-composite solar cell performance. *J. Am. Chem. Soc.* **2008**, *130*, 16324-16329.

Chapter 3

Chapter 4

Morphology Formation and Charge Recombination in Ordered Construction Bulk Heterojunction Solar Cells via the Role of multiple Solvent Mixture Processing

In the chapter, a ternary solvent treatment including DIO, CB, cyclohexanone (CHN) has first been employed in PTB7:PC$_{71}$BM blends. We observed that upon the addition of CHN significantly increased chain alignment of polymer and phase separation. In-situ study of the crystallization film by X-ray scattering reveals the formation of oriented crystalline domains and increase of interchain stacking distance and π-π stacking between PTB7 polymer backbones along with increase of CHN in solution, which consequently leads to an increase in photo-generated current. Combined with increased polymer crystallinity and big phase separation in blend film, enlarged charge extraction and charge recombination kinetics based on bimolecular recombination are obtained. All the effects based on CHN/CB of different ratio treatment induce a simultaneous enhancement in short circuit current and relatively reduction in device fill factor.

Chapter 4

Table of content

Chapter 4

Chapter 4

4.1 Introduction

In the past decade, bulk heterojunction (BHJ) polymer solar cells (PSC) with high efficiencies have been fabricated and hold great promise for many commercial applications due to their advantages of mechanical flexibility and low cost. [1-3] Although the power conversion efficiency (PCE) over 9% in PSCs has been obtained, [4-6] the challenge to further their efficiency for commercially application still remains. Recent years, many studies have focus on the exploitation of new materials with suitable molecular energy level including donor materials, acceptor materials and charge transport layer materials between the active layer and electrode. [7-11] In addition, device optimization by utilizing different device structure or controlling morphology of the active layer are also successful strategies to improve PCE. [12-14]

In organic photovoltaic (OPV), improving the crystallinity of the polymer and obtaining well dispersed domains between the donor and acceptor fullerene can enhance charge separation and transport. A large interfacial area between donor and acceptor provides a favorable morphology that benefits phase separation and charge collection at the corresponding electrode. [15, 16] Thus, controlling the morphologies of BHJ films plays a key role in the improvement of solar cells efficiency.

It has also been reported that the nanomorphologies of blend films can be tuned by thermal annealing and solvent annealing. [17-19] These approaches effectively improve the crystallization and chain alignment orientation of the polymers by controlling of the solvent evaporation rate. [17-19] Moreover, the use of different solvent mixtures and the addition of additives have also been studied as successful ways to change the active layer morphology and the polymer crystallinity in the modification of solar cells. [20-23] For example, the use of high boiling point solvents such as dichlorobenzene (DCB) mixed with the favorable solvent chloroform (CF) or the solvent additive 1,8-diiodoctane (DIO) can effectively improve the efficiency of

Chapter 4

solar cells respect to device made with a single solvent, increasing the crystallinity and solubility of the polymer in solution. [24, 25] In addition, the ternary solvent mixture such as DCB/CF/DIO has also been employed successfully to optimize the morphology of active layer in PDPP3T/PCBM solar cells. [26] Compared to single solvent and binary solvent, ternary solvent mixture DCB/CF/DIO treated PDPP3T/PCBM blend film gives a more favorable morphology and rougher domain interfaces and thus improve the PCE of solar cells. [26]

Poly[[4,8-bis[(2-ethylhexyl)oxy]benzo[1,2-b:4,5-b′]dithiophene-2,6-diyl][3-fluoro-2-[(2-ethylhexyl) carbonyl] thieno[3,4-b]thiophenediyl]] (PTB7) as a breakthrough donor material has exhibited excellent photovoltaic properties in recent years, [27-30] typically combined with [6,6]-phenyl-C71-butyric acid methyl ester (PC$_{71}$BM) as acceptor material. [27-32] PCEs of 7 to 9% have also been obtained by several strategies, including the use of different electron or hole transport layers or the modification of the device structure. [4, 27-28, 33, 34] Furthermore, the use of additive and solvent mixture treatment of the blend surface have been reported to have an effect on performance of solar cells. So far, the self-assembly film formation via ternary solvent mixture processing on morphology, crystallinity structure of blend film for PTB7:PCBM solar cells have not yet been surveyed. Especially, the effect of variation morphology on charge extraction and recombination from ternary solvent mixture treatment for PTB7:PCBM solar cells device still is a blank area. In the present study, ternary solvent including a good solubility solvent CB, a solvent additive DIO and a marginal solvent cyclohexanone (CHN) are chosen to understand the effect on the morphology of PTB7:PC$_{71}$BM blend film and crystallinity structure of polymer. Good solvent CB and good additive DIO have been reported as an excellent combination used in PTB7:PC$_{71}$BM solar cells. [28] CHN as an "unfriend" solvent has ever been investigated during the film formation in poly(3-hexylthiophene) (P3HT):PCBM system from CB and CHN mixture, which displays a strong action for P3HT self-assembly, further inducing the enhanced P3HT crystallization and charge

transport in P3HT:PCBM device. [35] In this work, we examine the optoelectronic conversion performance of device based on PTB7:PC$_{71}$BM processed with CB and CB/CHN solvent mixture of different ratio treatment. A dramatic morphology change of active layer and solidified of polymers due to Addition of unfriendly solvent CHN are demonstrated by atomic force microscopy (AFM). Crystallinity structure evolution of polymer in ternary solvent mixture is determined by grazing incidence X-ray scattering (GIXS). For the final complete device, we use the transient photovoltaic (TPV) and charge extraction (CE) techniques to measure the effect of different solvent mixture on charge carrier extraction density and charge recombination kinetics.

4.2 Experiment section

The blend solution of PTB7 and PC$_{71}$BM (1:1.5, w/w) is prepared using CB (Sigma-Aldrich) and stirred for 15 h at 40 ℃ in glove box. CHN (Sigma-Aldrich) is added into PTB7:PC$_{71}$BM solution by 3:1, 2:1, 1:1 in ratio of CHN/CB without stirring and heating. The final concentration of PTB7 is 10 mg/ml. after 1 h, the blend solution is stirred for another 2 h. The solution aging processed is also performed for in present experiment. The additive of DIO (Sigma-Aldrich) is added into blend solution and stirred for 10 min before film deposition. And then the solutions are spin coated on ITO substrate covered by PEDOT:PSS. The ITO covered glass clean and devices fabrication are followed in experimental section in chapter 2. The final devices are completed by depositing a Ca layer (20 nm) and an Ag layer (100nm) on the active layer. The related characterization techniques including AFM, GIXS, TPV, CE and performance measurements of solar cells have also been described in experimental section in chapter 2.

4.3 Result and Discussion

4.3.1 Measurements of solar cells performance

When using multiple solvent systems, the volume ratio of each solvent ingredient is a key to performance optimization. An optimal D/A ratio (1:1.5 in w/w) of PTB7 and $PC_{71}BM$ and a solvent additive (3% DIO in volume in total solvent) have been reported in previous study. [26] Here, $PTB7:PC_{71}BM$ blend solutions are prepared using CB and solvent mixtures of CB/CHN in different ratios of 3:1, 2:1 and 1:1 and a constant 3% DIO in volume in total solvent is used for all devices. The devices were fabricated in the configuration $(ITO/PEDOT:PSS/PTB7:PC_{71}BM/Ca/Ag)$ and performance was investigated under AM 1.5G illumination. A solution aging [36] process is also applied in the experiment and the best performance is found in solution aging for 24 h (Figure 4.1). As shown in Figure 4.2a, for devices obtained from the CB/DIO, it exhibits a PCE of 6.86 % with an open circuit voltage (Voc) of 0.73 V, a short circuit current (Jsc) of 14.55 mA/cm^2 and a 64.5 % of fill factor (FF). All the devices fabricated with and without CHN treatment exhibited similar Voc values
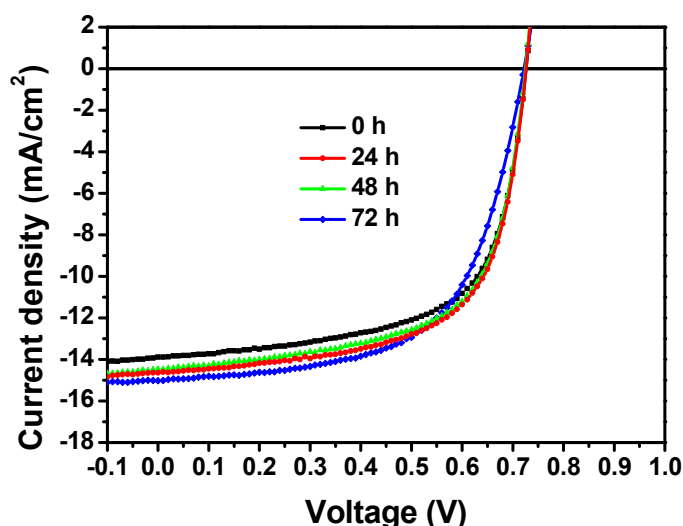
Figure 4.1. Current-voltage curve of devices fabricated from $PTB7:PC_{71}BM$ solution aged for 0 h, 24 h, 48 h, 72 h. The device aged for 24 h displays a best PCE of 6.86 % with a Jsc of 14.55 mA/cm^2, a Voc of 0.73 V and a FF of 64.5%.

Chapter 4
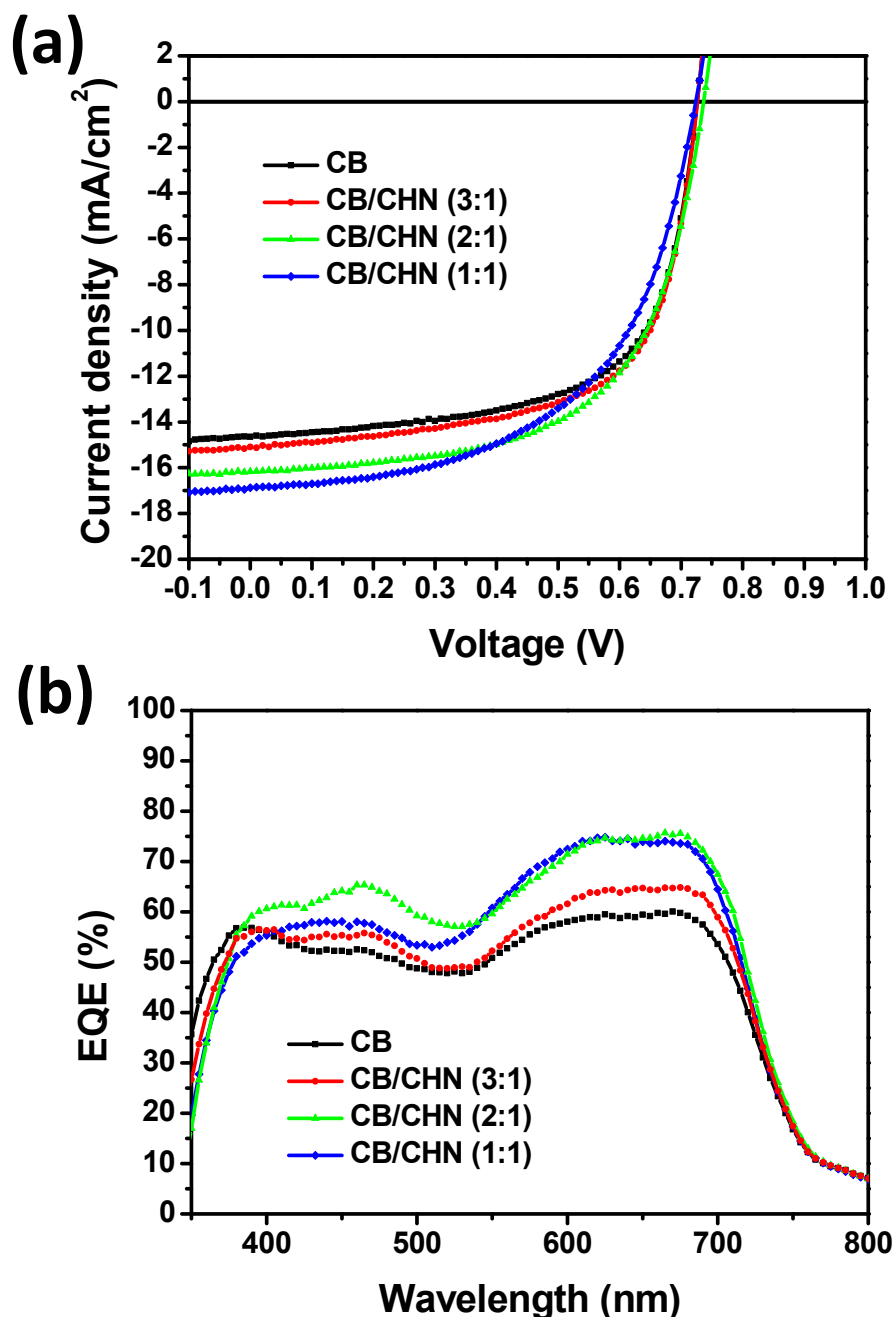
Figure 4.2. (a) Current-voltage curves under AM 1.5 G illumination at 1 sun. Devices processed from different solvents: CB, CB/CHN (3:1), CB/CHN (2:1) and CB/CHN (1:1). 3 % DIO in volume is contained in all solvents. (b) EQE spectra of devices processed with different solvents.

ranging between 0.72 V and 0.74 V. The performance data extracted from the J-V curves is summarized in Table 1. Upon the introduction of CHN into the solvent mixture, the performance improved significantly mostly due to an increase in the Jsc. Devices processed from CB/CHN at a ratio of 3:1, exhibit a short circuit current of 15.24 mA/cm^2 with a corresponding PCE of 7.1 %, although FF decreases to 63.7%.

Chapter 4

When the ratio of CB/CHN is increase to 2:1, the highest PCE reaches 7.31% with an improved Jsc of 16.2 mA/cm^2 and FF reduced to 61 % with the increase CHN ratio in the mixture. Further increasing the ratio of CHN/CB to 1:1, increases Jsc to 16.92 mA/cm^2, but the PCE decreases to 6.80 % due to a dramatically decrease in FF 55%.

Table 4.1 photovoltaic performance of device processed from different solvents

Solvent	V_{oc} (V)	J_{sc} (mA/cm^2)	FF (%)	PCE (PCE average) (%)	R_s (Ω cm^2)	R_{sh} (Ω cm^2)
CB	0.73	14.55	64.5	6.86 (6.72)	1.23	637
CB/CHN (3:1)	0.73	15.24	63.7	7.10 (6.89)	1.16	478
CB/CHN (2:1)	0.74	16.20	61.0	7.31 (7.21)	2.5	901
CB/CHN (1:1)	0.72	16.92	55.8	6.80 (6.68)	3.6	475

Upon increasing the CHN amount in solvent mixture, current density is significantly enhanced. In order to investigate the origin of this enhanced Jsc, we studied the spectral response of the devices with and without CHN treatment (Figure 4.2b) by external quantum efficiency (EQE) measurements. All EQE curves show broad optical response in the entire absorption range from 350 nm to 850 nm. The response in the region from 350 to 600 nm is mainly due to the absorption of PC$_{71}$BM, while the response from 600 to 800 nm is due to the absorption of PTB7 (Figure 4.3). Compared with the device obtained from only CB, EQE values for all devices obtained from CHN/CB solvent mixture show overall improvement in a prominent range from 400 nm to 750 nm spectral range. The highest EQE reaches almost 75 % at 674 and 620 nm for the devices with CHN/CB ratio of 2:1 and 1:1. The calculated Jsc values by integrating the EQE agree well with the increase trend of Jsc values measured above (the calculated Jsc values of 13.35, 14.13, 15.08 and 15.88 mA/cm^2 correspond to the devices treated with CB, CB/CHN (3:1), CB/CHN (2:1) and CB/CHN (1:1), respectively). It is known that enhancement in EQE responds to more efficient charge collection or absorption of photons. [37] The increased current densities imply that the addition of CHN induced a possible more efficient photon harvest or charge collection than with CB treatment.

Chapter 4
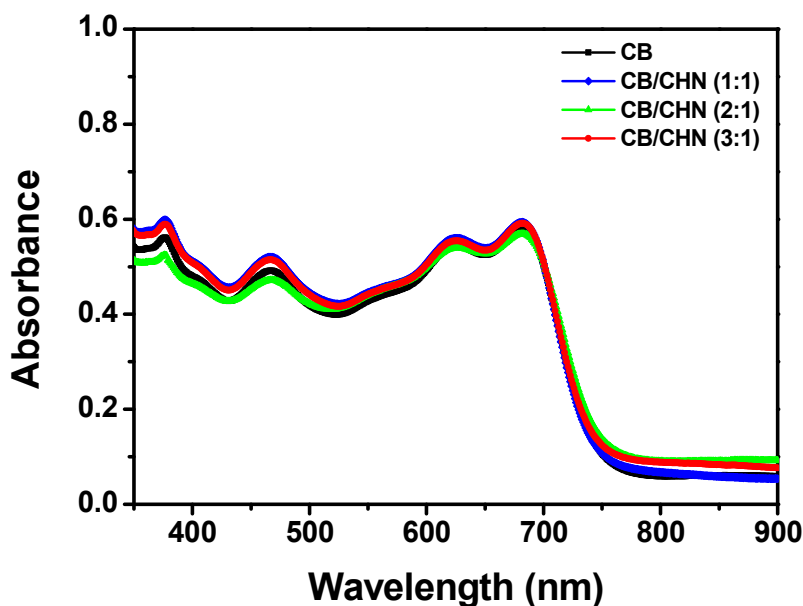
Figure 4.3. UV-Vis absorption spectrum of PTB7:PC$_{71}$BM blend film treated with CB/CHN solvent mixture of different ratio (1:0, 1:1, 2:1 and 3:1) in volume.

4.3.2 Crystallization of polymer-fullerene dispersions from CB and CB/CHN with different solvent mixture ratio

It is worth to note that along with the enhanced Jsc in PSCs obtained from the CB/CHN solvent mixture, the FF dropped significantly when the ratio of CHN increased in the solvent mixture. In fact, Jsc and FF can be influenced by the control of crystallinity and morphology formation of the active layer.

To investigate the effect of the solvent mixture processing on crystallization and molecule orientation alignment of polymer, the crystallinity structure of PTB7:PC$_{71}$BM blend film is evaluated by utilizing the grazing incidence small angle X-ray scattering (GISAXS) and wide angle X-ray scattering (GIWAXS) measurements. Yu and co-workers have detailed reports of the fine crystalline structure of PTB series polymer and its interaction with PCBM. [38-40] In the present study, the original four wet films are coated on a Si substrate from solution containing

81
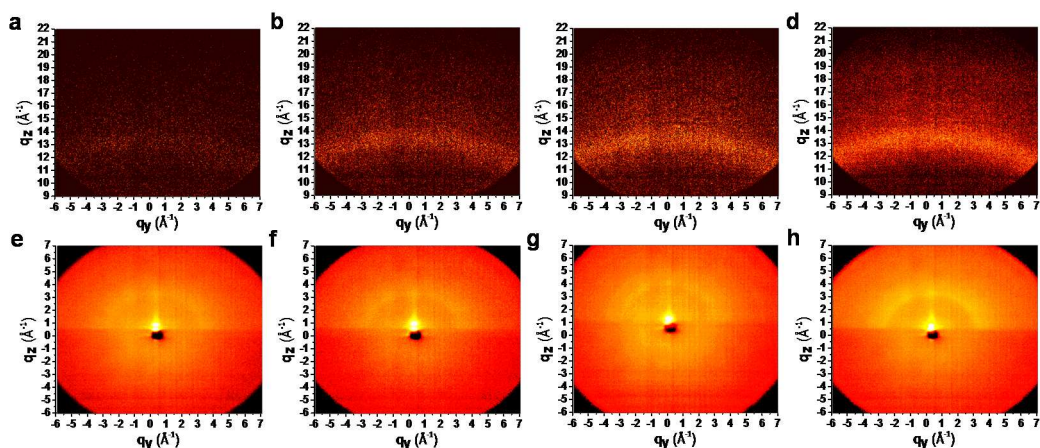
Figure 4.4. GIWAXS (up) and GISAXS (down) images acquired from PTB7: $PC_{71}BM$ blend films fabricated from PTB7:$PC_{71}BM$ blend solutions with different solvent: (a, e) CB, (b, f) CB/CHN (3:1), (c, g) CB/CHN (2:1) and (d, h) CB/CHN (1:1). 3 % DIO in volume is contained in all solvents.
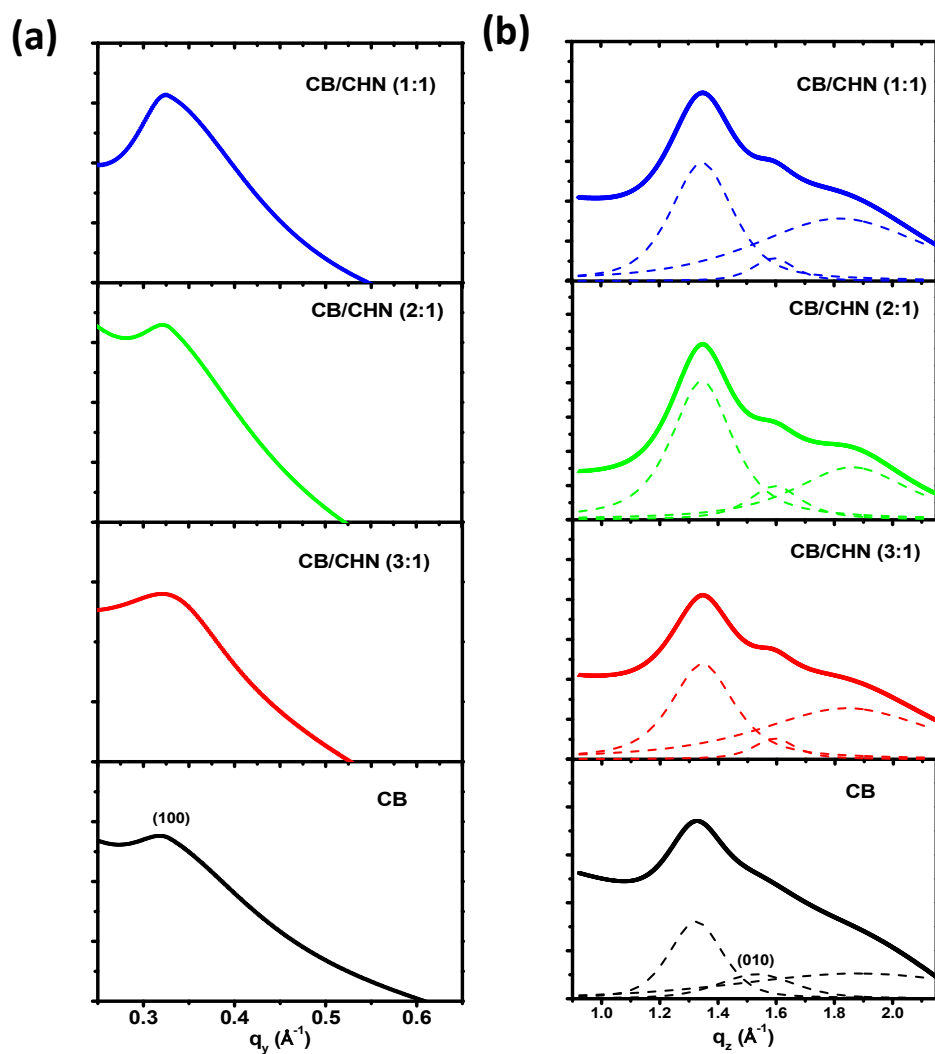
Figure 4.5. The corresponding q_y and q_z scans from the 2-D GISAXS and GIWAXS patterns. Pseudo-Voigt function fits are used to determine the total peak position, the individual peaks and FWHMs.

Chapter 4

the following four solvents mixtures: CB, CB/CHN (3:1), CB/CHN (2:1) and CB/CHN (1:1) and dried slowly in a glove box by covering with a Petri dish without gas flow or heat evaporation. The respective 2-D GIWAXS and GISAXS results for samples from CB and CB/CHN solvent mixture processed are shown in Figure 4.4a-h. The corresponding q_y (in plane) and q_z (out of plane) scans are shown in Figure 4.5. It should be noted that four films show similar scattering profiles. For the film from CB, a distinctive peak at $q_y \approx 0.33$ Å^{-1} arises from the (100) Bragg diffraction of PTB7, which is associated with the inter-stacking of alkyl side chain of PTB7 lamellae. The corresponding d-spacing and crystal size by Bragg equation and Scherrer's analysis are summarized in Table 2. The original scattering peaks along q_z direction resolved with a pseudo-Voigt function in Topas software show three peaks. The peak at 1.53 Å^{-1} (d=4.1 Å) arises from the (010) Bragg diffraction of PTB7, which corresponds to the π-π stacking between polymer backbones parallel to substrate. In addition, the symmetric circle at the scattering vector $q_z \approx 1.33$ Å^{-1} and the wide peak at q_z=1.88 Å^{-1} correspond to the Bragg diffraction of PCBM. For the other three films from CB/CHN solvent mixture, there are not significant peak changes for $q_y \approx 0.33$ Å^{-1} with d-spacing of around 19 Å. However, a large change is observed in the full width at half-maximum (FWHM) of scattering peak that is usually related to the variation of polymer crystallinity and domain size. The FWHM of scattering peak is gradually decreased in company with increased amount of CHN in solvent mixture, indicating the addition of CHN enhances the crystallinity of PTB7. The corresponding domain size calculated from (100) Bragg diffraction peak of PTB7 via Scherrer equation increases from 3.59 nm for sample from CB, 4.18 nm for sample from CB/CHN (3:1), 4.60 nm for sample from CB/CHN (2:1) to 4.97 nm for sample from CB/CHN (1:1) (see Table 2).

Another peak corresponding (010) Bragg diffraction of PTB7 shifts from $q_z \approx 1.53$ Å^{-1} for a sample coated from CB to 1.59 Å^{-1} for the three samples with CB/CHN solvent

mixture treatment, evident in the decrease of inter-stacking spacing from 4.1 Å to 3.9 Å. These shifts indicate the extent of the π-π interaction between PTB7 polymer backbones parallel to the substrate is increase after the addition of CHN, provides a key force for aligning ordered conjugated polymer. [39] Taken the results of crystalline structure measurements together, the decrease of FWHM of scattering peaks and enhanced π-π interaction between PTB7 polymer backbones reveal further crystallization and more ordered orientation of PTB7 polymer when replacing CB with subsequent CHN/CB solvent mixture as solvent, which binds more strongly to the anode interfacial layer. These crystalline polymer domains benefit to promote charge transport and across interface to corresponding electrode and weaken the non-geminate recombination of charge, and consequently, contribute to high photocurrent.

Table 4.2. The scattering parameters obtained for analysis of the domain size of the blend film.

Solvent	Peak position ($Å^{-1}$)	FWHM (°)	d-space (Å)	Domain size (nm)
CB	0.329	2.19	19.07	3.590
	1.324	3.49	4.75	2.281
	1.532	4.2	4.10	1.904
CB/CHN (3:1)	0.331	1.88	18.99	4.182
	1.344	3.36	4.67	2.371
	1.596	2.92	3.94	2.743
CB/CHN (2:1)	0.332	1.71	18.79	4.598
	1.346	3.43	4.67	2.322
	1.591	2.29	3.95	3.498
CB/CHN (1:1)	0.328	1.58	19.19	4.973
	1.346	3.40	4.67	2.343
	1.591	2.26	3.95	3.544

But, by calculation of domain size, we also found that the higher crystallinity PTB7 accompanies with a relatively bigger domain size. The increase in domain size of PTB7 calculated from (010) Bragg diffraction is also observed after addition of CHN (see Table 4.2). It originates from increased inter-chain stacking between PTB7 chains

Chapter 4

and π-π stacking between PTB7 polymer backbones due to increased amount of CHN in solvent mixture. However, the observed negligible change of $PC_{71}BM$ inter-stacking distances and domain size obtained from the Bragg peak at $q_z \approx 1.33$ Å^{-1} after the addition of CHN suggests that the ternary solvent mixture does not affect the interaction between $PC_{71}BM$ and $PC_{71}BM$. In fact, in a blend system including acceptor and donor, the interaction between PTB7 and $PC_{71}BM$ is stronger than between $PC_{71}BM$ and $PC_{71}BM$. In the present research, PCBM is difficult to intercalate PTB7 crystallites due to the increased inter-chain interaction after the use of CHN resulting in limited space between the alkyl side chains of PTB7 lamellae.[39] Hence PCBM molecule accumulation is squeezed out of the PTB7 domain area. This also implies that the polymer crystallization leads to subsequent fullerene aggregation. The GIXS results suggest that the addition of CHN improved crystallinity of polymer, but a big phase separation of PTB7 domains and $PC_{71}BM$ domains in blend film will be predicted due to crystallization of polymer.

Generally, the photo-generated excitons (hole-electron pairs) in donor polymers need to drift to the heterojunction interface of donor and acceptor where the excitons are separated into free charges by built-in electric field. The domain size is a commonly morphology factor for exciton dissociation efficiency. Thus processing with CHN increased the domain size would extend the diffusion length of exciton (exciton diffusion length is ca. 10∼20 nm) and not benefit to reach the interface for the excitons, further inducing possible geminate recombination. Linking with measurements of the performance of the solar cell devices, we conclude that the enhanced crystallinity of polymer due to the use of CHN leaded to the increase in Jsc, but the big domain size contributed to the poor dissociation efficiency of exciton and low FF.

4.3.3 Correlation between surface morphology and device performance

Chapter 4

A bi-continuous donor-acceptor interpenetrating morphology and crystallized polymer chains can effectively increase the charge carrier mobility and decrease exciton recombination and charge trapping. [41, 42] In addition, the morphology of blend film also affects the interfacial area and contact between the active layer and electrode. In order to verify the effect of CB/CHN solvent mixture on the intermixed PTB7 and PC$_{71}$BM of domain, the surface morphology of the active layer is investigated using
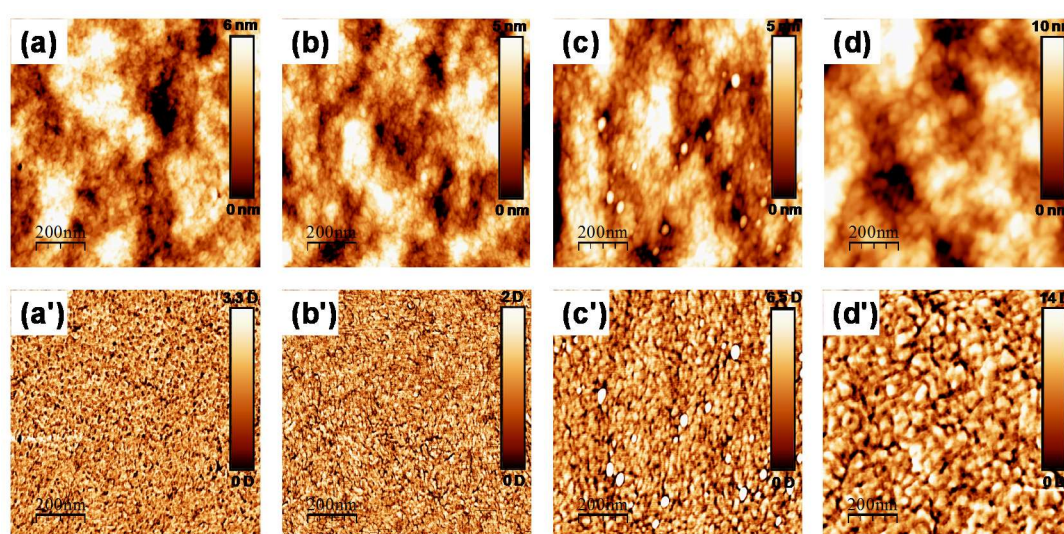
Figure 4.6. AFM topographic (top) and phase images (down) of thin films fabricated from PTB7:PC$_{71}$BM blend solutions with different solvents: (a, a') CB, (b, b') CB/CHN (3:1), (c, c') CB/CHN (2:1) and (d, d') CB/CHN (1:1). 3 % DIO in volume is contained in all solvents.

AFM. Figure 4.6 shows the topography images of PTB7:PC$_{71}$BM film processed from CB (Figure 4.6a) and different ratio CB/CHN mixtures (Figure 4.6b-d) and their corresponding phase images (Figure 4.6a'-d'). The surface topography of the blend film processed from CB shows grains of around several nanometers up to 10 nm size with root-mean-square roughness (RMS) value of 1.5 nm (Figure 4.6a). From the phase image, the surface displays an excellent interpenetrating network and microphase separation (Figure 4.6a'). The bright and dark regions result from two different compositions of the chain/network of polymer crystals and PCBM domains. Following, after using CB/CHN mixture as solvent, a significant change is observed

Chapter 4
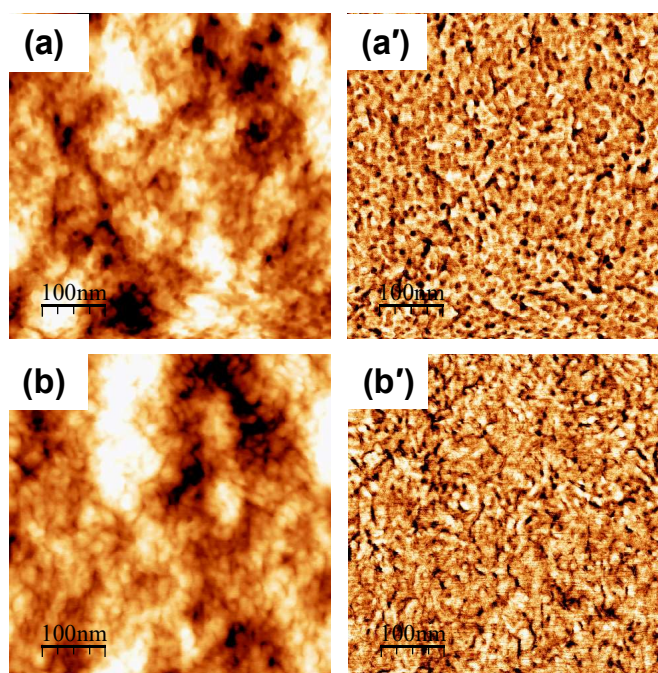
Figure 4.7. AFM topograph (right) and phase image (left) of film treated with CB (a, a') and CB/CHN of 3:1 ratio in volume (b, b').
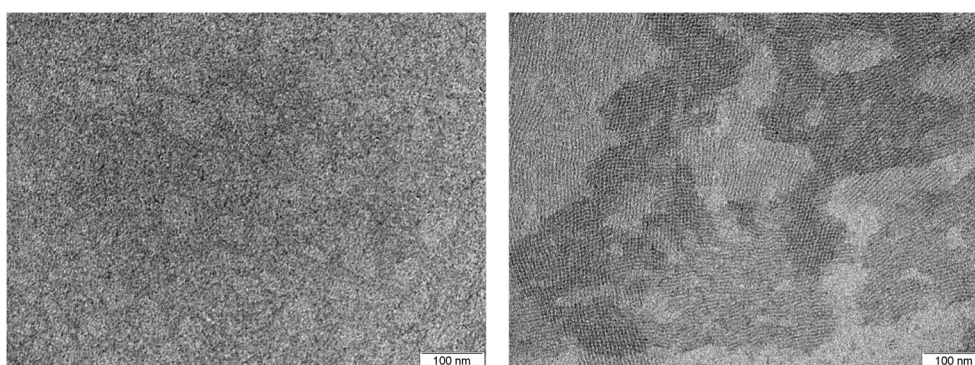
Figure 4.8. Formation of crystalline morphology of polymer by using CB/CHN solvent mixture is mainly happened in solution. The TEM images are obtained from the dillute PTB7:PCBM solution with CB (left) and CB/CHN ratio of 1:1(right). It clearly shows the strong PTB7 polymer chains with regular orientaton and a big aggregation after CB/CHN solvent mixture treatment.

in the surface topography (Figure 4.6b-d). The grains are increased from around 20 nm to 50 nm in diameter with the increased CHN ratio in solvent mixture from 1:3 to 1:1. The corresponding RMS values are 1.32 nm for CB/CHN (3:1), 1.35 nm for CB/CHN (2:1) and 2.3 nm for CB/CHN (1:1). It indicates that the addition of CHN results in bigger grain size but still retaining the smooth film surface. In addition, the

Chapter 4

phase images show that the polymer chain coarsens and aggregates after using CHN. The crystallized morphology and polymer nanowire are more clearly discerned in enlarged AFM images and transmission electron microscopy from high CHN/CB ratio of 1:1 in Figure 4.7 and Figure 4.8, respectively. These results also demonstrate that the polymer chains growth is mainly governed by inter-chain stacking of PTB7 parallel to the substrate. In Figure 4.9, we schematically describe the formation of blend film topography due to polymer coarsening and aggregation after the addition of CHN. Compared to the amorphous morphology, the crystallized morphologies benefit from the charge transport and adverse to the charge geminate recombination further leading to the improvement of photocurrent generation. However, the observed relative big grain size and coarsened polymer chain after addition of CHN in solvent can lead to the reduction of interfacial area between PTB7 and PCBM. For OPV devices, FF is an electron property related to charge separation and collection. We speculate that the reduction of interfacial area and phase separation between polymer and fullerene weakens photo-generated charge separation along with increase of amount of CHN in solvent, and therefore increases the overall series resistance and adversely affects the FF of the patterned device. The result also responds well to the above the GIXS measurements.
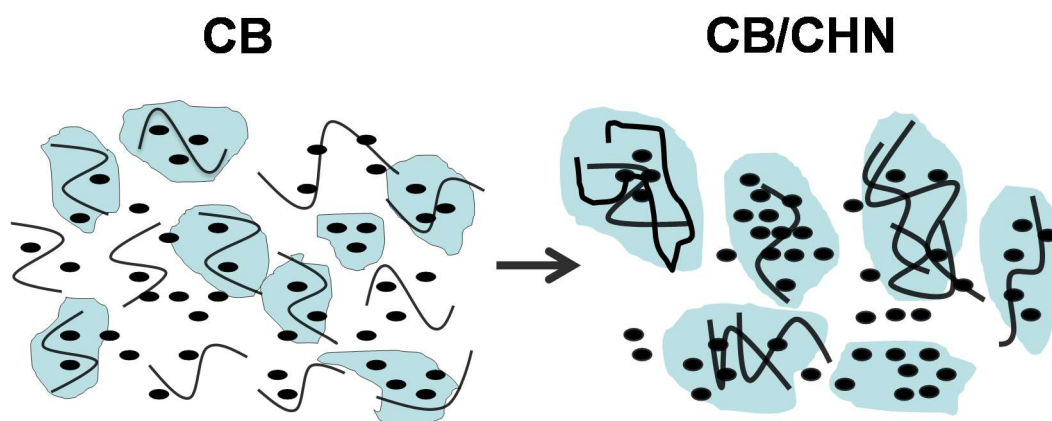
Figure 4.9. Scheme shows the crystalline process of polymer due to the use of CHN.

4.3.4 Charge extraction and recombination kinetics

In a completed device, the crystallinity of polymer and the blend film morphology ultimately affect charge carrier transport, recombination lifetime and charge collection.[31, 43] In order to study the influence of the variation of blend film morphology and polymer crystallinity on the interfacial extraction and recombination of charge carriers in PTB7:PC$_{71}$BM devices, TPV and CE measurements are performed in the devices processed using CB and CB/CHN mixture solvents of 2:1, respectively. These techniques play an important role in determining non-geminate recombination that directly correlates to the photocurrent performance of the devices. The recombination kinetics can be experimentally denoted through a relationship between carrier density and charge-carrier lifetime of the semiconductor.[43, 44] The principle and application of the techniques in solar cells area have also been described elsewhere. [45, 46] The total charge carrier density in the device is measured by the charge extraction (CE) technique at different Voc corresponding to different light intensities as illustrated in Figure 4.10a. At a schematic CE measurement, the cell is first illuminated at open circuit condition with different Voc produced by a light pulse with different light densities (so called light bias). Then, the cell is switched to a short-circuit state and the decay time in the photocurrent is determined (the detailed operation is shown in chapter 2). The extracted charge density can be obtained by integrating the decay with the approximate relations [47]:

$$n = \frac{1}{Aqd}\frac{1}{R}\int V(t)dt$$

The final experimental points are fitted to an exponential equation by geometric capacitance.

$$n = n_0 e^{\gamma Voc}$$

Chapter 4

Where A is the cell effective area, d is the device thickness, R is the resistance connected to the circuit, V is the measured voltage, n is the average charge carrier density and γ is constant.

In present research, the charge carrier densities for the both devices are measured in the region from 0.6 V to 0.76 V close to the Voc (the device Voc of 0.73 V for CB treatment and 0.74 V for CB/CHN treatment). The lower part below 0.6 V is ignored to research since amount of accumulated charges at low light intensities is not possible to estimate with sufficient accuracy, as discussed in previous research. [46] Another reason is that the lower part of measured voltage is mainly dominated by the dielectric properties of device. [46, 48] We observe that the charge carrier density of non-geminate recombination for the devices made from CB/CHN treatment is higher than from CB treatment at a given voltage value to inspect the high voltage region. It suggests that more charge carriers are extracted and accumulated in the cells treated with CB/CHN. It is might attribute to the high crystalline of samples obtained with CB/CHN solvent treatment resulting in a reduced geminate recombination of exciton. However, the results do not mean that these accumulated charges can be directly contribute to effective charge transport in the active layer and collect at corresponding electrode. Charge carrier lifetime is another key factor to affect the charge collection efficiency and performance of device. In order to examine the charge carrier lifetime, we focus on the recombination kinetic analysis by TPV. TPV is a useful technique to understand non-geminate recombination kinetic in working OPV device. Similar to CE, in TPV measurement, the cells is also held at open circuit condition and the Voc is defined by a white light bias. Then, during various constant bias light condition, a small optoelectronic perturbation to particular voltage is applied to measure the carrier lifetime. [47] Adjusting the light density, series of output perturbation are recorded at different light bias.
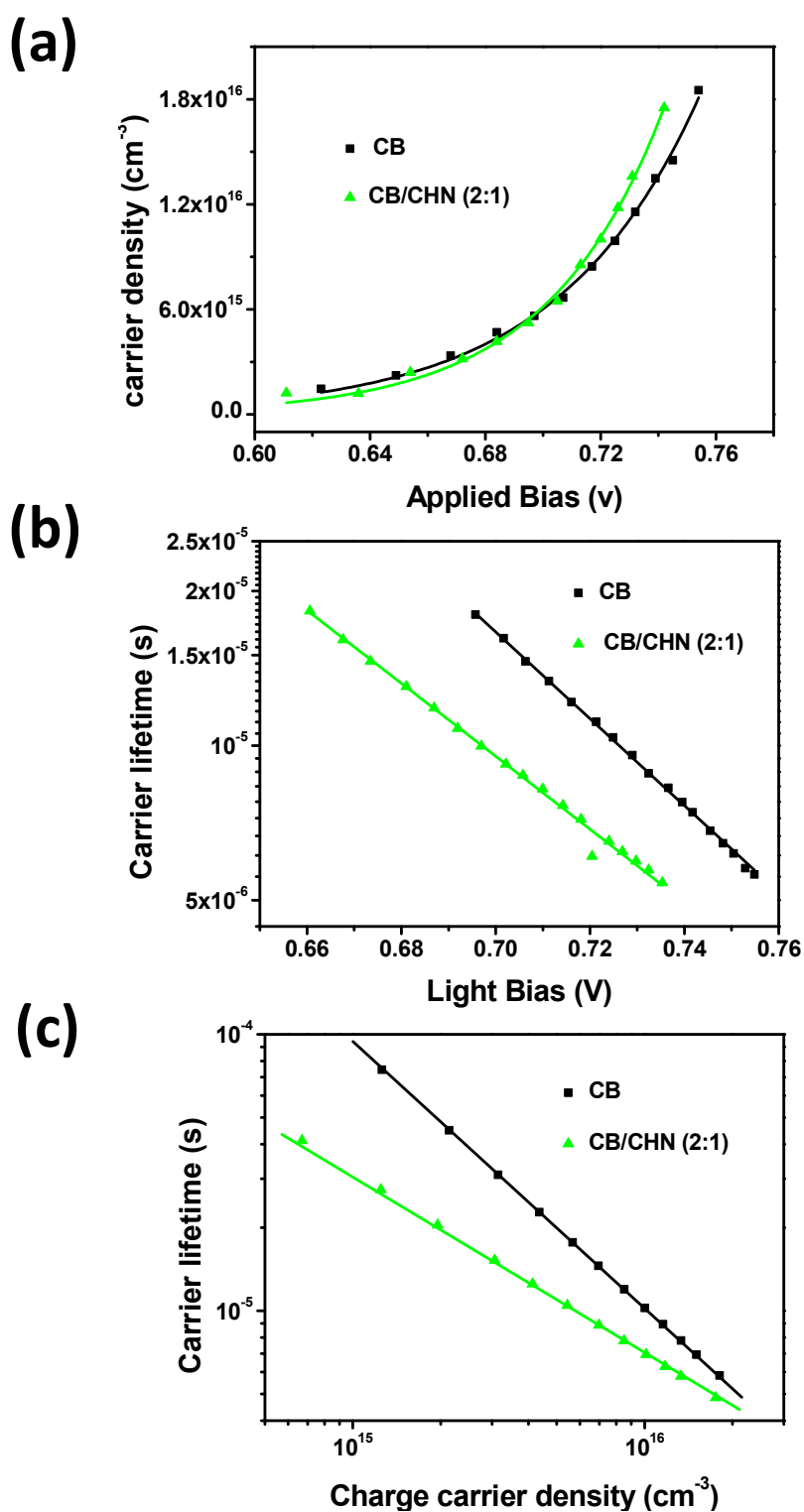
Figure 4.10. The charge carrier density extracted as a function of light induced voltage for devices with CB and CB: CHN (2:1) treatment. The solid line shows the device charge corresponding to a geometrical capacitance (a). Charge recombination lifetime versus light bias for devices treated with CB and CB: CHN (2:1) (b). The corresponding charge carrier recombination life time as a function of charge carrier density for the complete device processed with different solvent (c).

The lifetime of the accumulated charge carriers in a complete cell was obtained from the voltage decay with the respective Voc [45, 47] and shown in Figure 4.10b:

$$\tau_r = \tau_{r0} * e^{-\beta Voc}$$

Where τ_r is the small perturbation obtained from TPV decay to an exponential decay. In order to analyze the recombination of extraction charge, TPV and CE are combined to yield the charge carrier lifetime as a function of charge carrier density under open circuit conditions

In our research, the charge carrier lifetime was measured at a high charge density regime, close to the actual charge density, due to the device geometrical capacitance. At high charge density the measured charge carrier lifetime more truly corresponds to non-geminate recombination kinetics. [48, 49] In Figure 4.10c, the carrier lifetime vs charge carrier density curves for both devices display similar recombination kinetic trends that the recombination lifetime decreases with the increased charge density stored in the device under the working condition. However at the same charge density, both devices show different non-geminate recombination lifetime, which relates to the recombination order (λ+1). In our case the important parameter, power law λ, can be obtained from

$$\tau_r = \tau_{r0} * n^{-\lambda}$$

The value of $-\lambda$ can be taken from the slope in log-log plot. [43, 47] For device with CB treatment, yielding a slope of with $\lambda \approx 0.98$, the corresponding recombination order of ≈ 2 is obtained. The device with CB/CHN mixture shows a slight reduced recombination order of 1.6 corresponding to λ of 0.6. The results illustrate that non-geminate carrier charge lifetime for device processed with CB is minor longer

than for the one with CB/CHN mixture. Takes CE measurement together, the higher the charge carrier density, the shorter the recombination lifetime for the sample treated from CB/CHN mixture. The observed slow recombination kinetics for samples with CB treatment is likely to be attributed to the large interfacial area between PTB7 and $PC_{71}BM$ shown in AFM images, which leads to a rapid charge transport and collection in the corresponding electrode. Moreover, the increased carrier lifetime is also a key factor for the increase of FF in PSCs as discussed in previous research. [50, 51] These results we obtained are in good agreement with measurements of solar cells performance, as the device processed from CB solvent showed higher FF than from CB/CHN (2:1). Combination with the analysis of AFM and GIXS above, we believe that morphology of blend film and crystallinity of polymer are the primary cause for influencing the charge carrier extraction and recombination kinetics.

Chapter 4

4.4 Conclusions

In conclusion, we first employ ternary solvent mixtures in optimization of PTB7:PC$_{71}$BM BHJ solar cells. Addition of marginal solvent CHN to CB:DIO binary solvent system significantly affects the morphology of PTB7:PC$_{71}$BM BHJ film including the interpenetrating network structure, chain alignment and phase separation, leading to a considerably improvement in PSC performance. In-situ observation of the crystallization film by GIXS displays an oriented molecule ordering as well as improvement of inter-chain stacking and π-π stacking between PTB7 polymer backbones along with increase of CHN in solution, which consequently leads to the more efficient Jsc. The increased polymer crystallinity and big phase separation in blend film due to the use of CHN consequently contributed to the enlarged charge extraction density and fast charge non-geminate recombination. All the effects induce a simultaneous increase in short circuit current and decrease in FF after CHN/CB of different ratio treatment. The device from CB/CHN of 2:1 ratio treatment displays an optimal PCE of 7.31%. This work gains understanding correlation between polymer morphology, crystallization, charge extraction and recombination kinetics, and more generally with PSC device performance by multiple solvent processing.

Chapter 4

4.5 Reference

1.   Brabec, C. J.; Gowrisanker, S.; Halls, J. J.; Laird, D.; Jia, S.;Williams, S. P., Polymer–fullerene bulk-heterojunction solar cells. *Adv. Mater.* **2010**, *22*, 3839-3856.

2.   Park, S. H.; Roy, A.; Beaupre, S.; Cho, S.; Coates, N.; Moon, J. S.; Moses, D.; Leclerc, M.; Lee, K.;Heeger, A. J., Bulk heterojunction solar cells with internal quantum efficiency approaching 100&percnt. *Nat. Photonics* **2009**, *3*, 297-302.

3.   You, J.; Dou, L.; Yoshimura, K.; Kato, T.; Ohya, K.; Moriarty, T.; Emery, K.; Chen, C.-C.; Gao, J.;Li, G., A polymer tandem solar cell with 10.6% power conversion efficiency. *Nat. Commun.* **2013**, *4*, 1446.

4.   Dou, L.; You, J.; Yang, J.; Chen, C.-C.; He, Y.; Murase, S.; Moriarty, T.; Emery, K.; Li, G.;Yang, Y., Tandem polymer solar cells featuring a spectrally matched low-bandgap polymer. *Nat. Photonics* **2012**, *6*, 180-185.

5.   He, Z.; Xiao, B.; Liu, F.; Wu, H.; Yang, Y.; Xiao, S.; Wang, C.; Russell, T. P.;Cao, Y., Single-junction polymer solar cells with high efficiency and photovoltage. *Nat. Photonics* **2015**, *9*, 174-179.

6.   Chen, J. D.; Cui, C.; Li, Y. Q.; Zhou, L.; Ou, Q. D.; Li, C.; Li, Y.;Tang, J. X., Single-Junction Polymer Solar Cells Exceeding 10% Power Conversion Efficiency. *Adv. Mater.* **2015**, *27*, 1035-1041.

7.   Dou, L.; Gao, J.; Richard, E.; You, J.; Chen, C.-C.; Cha, K. C.; He, Y.; Li, G.;Yang, Y., Systematic investigation of benzodithiophene-and diketopyrrolopyrrole-based low-bandgap polymers designed for single junction and tandem polymer solar cells. *J. Am. Chem. Soc.* **2012**, *134*, 10071-10079.

8.   Zhou, H.; Yang, L.; Stuart, A. C.; Price, S. C.; Liu, S.;You, W., Development of fluorinated benzothiadiazole as a structural unit for a polymer solar cell of 7% efficiency. *Angew Chem Int Ed Engl* **2011**, *123*, 3051-3054.

9.   Beaumont, N.; Hancox, I.; Sullivan, P.; Hatton, R. A.;Jones, T. S., Increased efficiency in small molecule organic photovoltaic cells through electrode modification with self-assembled monolayers. *Energy & Environmental Science* **2011**, *4*, 1708-1711.

10.   Tan, Z. a.; Zhang, W.; Zhang, Z.; Qian, D.; Huang, Y.; Hou, J.;Li, Y., High-Performance Inverted Polymer Solar Cells with Solution-Processed Titanium Chelate as Electron-Collecting Layer on ITO

Chapter 4

Electrode. *Adv. Mater.* **2012**, *24*, 1476-1481.

11. Liang, Y. Y.; Wu, Y.; Feng, D. Q.; Tsai, S-T.; Son, H-J.; Li, G.; Yu, L.P., Development of New Semiconducting Polymers for High Performance Solar Cells. *J. Am. Chem. Soc. 200*9, *131*, 56–57.

12. Small, C. E.; Chen, S.; Subbiah, J.; Amb, C. M.; Tsang, S.-W.; Lai, T.-H.; Reynolds, J. R.;So, F., High-efficiency inverted dithienogermole-thienopyrrolodione-based polymer solar cells. *Nat. Photonics* **2012**, *6*, 115-120.

13. Peet, J.; Heeger, A. J.; Bazan, G. C., "Plastic" solar cells: self-assembly of bulk heterojunction nanomaterials by spontaneous phase separation. *Acc. Chem. Res.* **2009**, *42*, 1700-1708.

14. Guo, X.; Zhang, M.; Ma, W.; Ye, L.; Zhang, S.; Liu, S.; Ade, H.; Huang, F.; Hou, J., Enhanced Photovoltaic Performance by Modulating Surface Composition in Bulk Heterojunction Polymer Solar Cells Based on PBDTTT-C-T/PC71BM. *Adv. Mater.* **2014**, *26*, 4043-4049.

15. Halls, J.; Walsh, C.; Greenham, N.; Marseglia, E.; Friend, R.; Moratti, S.; Holmes, A., Efficient photodiodes from interpenetrating polymer networks. **1995**.

16. Thompson, B. C.;Frechet, J. M., Polymer–fullerene composite solar cells. *Angew. Chem., Int. Ed.* **2008**, *47*, 58-77.

17. Padinger, F.; Rittberger, R. S.;Sariciftci, N. S., Effects of postproduction treatment on plastic solar cells. *Adv. Funct. Mater.* **2003**, *13*, 85-88.

18. Li, G.; Yao, Y.; Yang, H.; Shrotriya, V.; Yang, G.;Yang, Y., " Solvent annealing" effect in polymer solar cells based on poly (3-hexylthiophene) and methanofullerenes. *Adv. Funct. Mater.* **2007**, *17*, 1636.

19. Li, G.; Shrotriya, V.; Huang, J.; Yao, Y.; Moriarty, T.; Emery, K.;Yang, Y., High-efficiency solution processable polymer photovoltaic cells by self-organization of polymer blends. *Nat. Mater.* **2005**, *4*, 864-868.

20. Wang, D. H.; Morin, P.-O.; Lee, C.-L.; Kyaw, A. K. K.; Leclerc, M.;Heeger, A. J., Effect of processing additive on morphology and charge extraction in bulk-heterojunction solar cells. *J. Mater. Chem. A* **2014**, *2*, 15052-15057.

21. Yao, Y.; Hou, J.; Xu, Z.; Li, G.;Yang, Y., Effects of solvent mixtures on the nanoscale phase separation in polymer solar cells. *Adv. Funct. Mater.* **2008**, *18*, 1783.

22. Schmidt-Hansberg, B.; Sanyal, M.; Klein, M. F.; Pfaff, M.; Schnabel, N.; Jaiser, S.; Vorobiev, A.; Müller, E.; Colsmann, A.;Scharfer, P., Moving through the phase diagram: morphology formation in

Chapter 4

solution cast polymer–fullerene blend films for organic solar cells. *Acs Nano* **2011**, *5*, 8579-8590.

23.   Fan, X.; Wang, J.; Huang, H.;Wang, H., Binary additives regulate the PC71BM aggregate morphology for highly efficient polymer solar cells. *ACS Photonics* **2014**, *1*, 1278-1284.

24.   Su, M. S.; Kuo, C. Y.; Yuan, M. C.; Jeng, U.; Su, C. J.;Wei, K. H., Improving device efficiency of polymer/fullerene bulk heterojunction solar cells through enhanced crystallinity and reduced grain boundaries induced by solvent additives. *Adv. Mater.* **2011**, *23*, 3315-3319.

25.   Liu, F.; Gu, Y.; Wang, C.; Zhao, W.; Chen, D.; Briseno, A. L.;Russell, T. P., Efficient Polymer Solar Cells Based on a Low Bandgap Semi-crystalline DPP Polymer-PCBM Blends. *Adv. Mater.* **2012**, *24*, 3947-3951.

26.   Ye, L.; Zhang, S.; Ma, W.; Fan, B.; Guo, X.; Huang, Y.; Ade, H.;Hou, J., From binary to ternary solvent: morphology fine-tuning of D/A blends in PDPP3T-based polymer solar cells. *Adv. Mater.* **2012**, *24*, 6335-6341.

27.   Liang, Y.; Xu, Z.; Xia, J.; Tsai, S. T.; Wu, Y.; Li, G.; Ray, C.;Yu, L., For the bright future—bulk heterojunction polymer solar cells with power conversion efficiency of 7.4%. *Adv. Mater.* **2010**, *22*, E135-E138.

28.   Hammond, M. R.; Kline, R. J.; Herzing, A. A.; Richter, L. J.; Germack, D. S.; Ro, H.-W.; Soles, C. L.; Fischer, D. A.; Xu, T.;Yu, L., Molecular order in high-efficiency polymer/fullerene bulk heterojunction solar cells. *ACS nano* **2011**, *5*, 8248-8257.

29.   Lou, S. J.; Szarko, J. M.; Xu, T.; Yu, L.; Marks, T. J.;Chen, L. X., Effects of additives on the morphology of solution phase aggregates formed by active layer components of high-efficiency organic solar cells. *J. Am. Chem. Soc.* **2011**, *133*, 20661-20663.

30.   Fu, H.; Tan, L.; Shi, Y.;Chen, Y., Tunable size and sensitization of ZnO nanoarrays as electron transport layers for enhancing photocurrent of photovoltaic devices. *Journal of Materials Chemistry C* **2015**, *3*, 828-835.

31.   Zhou, H.; Zhang, Y.; Seifter, J.; Collins, S. D.; Luo, C.; Bazan, G. C.; Nguyen, T. Q.;Heeger, A. J., High-Efficiency Polymer Solar Cells Enhanced by Solvent Treatment. *Adv. Mater.* **2013**, *25*, 1646-1652.

32.   Li, X.; Zhang, W.; Wang, X.; Gao, F.;Fang, J., Disodium edetate as a promising interfacial material for inverted organic solar cells and the device performance optimization. *ACS applied*

Chapter 4

materials & interfaces **2014**, *6*, 20569-20573.

33.   He, Z.; Zhong, C.; Su, S.; Xu, M.; Wu, H.;Cao, Y., Enhanced power-conversion efficiency in polymer solar cells using an inverted device structure. *Nat. Photonics* **2012**, *6*, 591-595.

34.   Susanna, G.; Salamandra, L.; Ciceroni, C.; Mura, F.; Brown, T.; Reale, A.; Rossi, M.; Di Carlo, A.;Brunetti, F., 8.7% Power conversion efficiency polymer solar cell realized with non-chlorinated solvents. *Sol. Energy Mater. Sol. Cells* **2015**, *134*, 194-198.

35.   Kim, J.-H.; Park, J. H.; Lee, J. H.; Kim, J. S.; Sim, M.; Shim, C.;Cho, K., Bulk heterojunction solar cells based on preformed polythiophene nanowires via solubility-induced crystallization. *J. Mater. Chem.* **2010**, *20*, 7398-7405.

36.   Han, P.; Balderrama, V. S.; Mihi, A.; Formentin, P.; Ferre-Borrull, J.; Pallares, J.;Marsal, L. F., Improving the Efficiency of PTB1: PCBM Bulk Heterojunction Solar Cells by Polymer Blend Solution Aging. *Photovoltaics, IEEE Journal of* **2015**, *5*, 889-896.

37.   Lin, L. B.; Jenekhe, S.;Borsenberger, P., High electron mobility in bipolar composites of organic molecules. *Appl. Phys. Lett.* **1996**, *69*, 3495-3497.

38.   Liang, Y.; Feng, D.; Wu, Y.; Tsai, S.-T.; Li, G.; Ray, C.;Yu, L., Highly efficient solar cell polymers developed via fine-tuning of structural and electronic properties. *J. Am. Chem. Soc.* **2009**, *131*, 7792-7799.

39.   Chen, W.; Xu, T.; He, F.; Wang, W.; Wang, C.; Strzalka, J.; Liu, Y.; Wen, J.; Miller, D. J.;Chen, J., Hierarchical nanomorphologies promote exciton dissociation in polymer/fullerene bulk heterojunction solar cells. *Nano Lett.* **2011**, *11*, 3707-3713.

40.   Szarko, J. M.; Rolczynski, B. S.; Guo, J.; Liang, Y.; He, F.; Mara, M. W.; Yu, L.;Chen, L. X., Electronic Processes in Conjugated Diblock Oligomers Mimicking Low Band-Gap Polymers: Experimental and Theoretical Spectral Analysis†. *J. Phys. Chem. B* **2010**, *114*, 14505-14513.

41.   Zhang, F.; Jespersen, K. G.; Bjoerstroem, C.; Svensson, M.; Andersson, M. R.; Sundström, V.; Magnusson, K.; Moons, E.; Yartsev, A.;Inganäs, O., 38-Influence of solvent mixing on the morphology and performance of solar cells based on polyfluorene copolymer/fullerene blends. *Adv. Funct. Mater.* **2006**, *16*, 667-674.

42.   Moon, J. S.; Takacs, C. J.; Cho, S.; Coffin, R. C.; Kim, H.; Bazan, G. C.;Heeger, A. J., Effect of Processing Additive on the Nanomorphology of a Bulk Heterojunction Material†. *Nano Lett.* **2010**, *10*,

Chapter 4

4005-4008.

43.   Spoltore, D.; Oosterbaan, W. D.; Khelifi, S.; Clifford, J. N.; Viterisi, A.; Palomares, E.; Burgelman, M.; Lutsen, L.; Vanderzande, D.;Manca, J., Effect of polymer crystallinity in P3HT: PCBM solar cells on band gap trap states and apparent recombination order. *Advanced Energy Materials* **2013**, *3*, 466-471.

44.   Foertig, A.; Kniepert, J.; Gluecker, M.; Brenner, T.; Dyakonov, V.; Neher, D.; Deibel, C., Nongeminate and geminate recombination in PTB7: PCBM solar cells. *Adv. Funct. Mater.* **2014**, *24*, 1306-1311.

45.   Albero, J.; Zhou, Y.; Eck, M.; Rauscher, F.; Niyamakom, P.; Dumsch, I.; Allard, S.; Scherf, U.; Krüger, M.; Palomares, E., Photo-induced charge recombination kinetics in low bandgap PCPDTBT polymer: CdSe quantum dot bulk heterojunction solar cells. *Chemical Science* **2011**, *2*, 2396-2401.

46.   Guerrero, A.; Montcada, N. F.; Ajuria, J.; Etxebarria, I.; Pacios, R.; Garcia-Belmonte, G.; Palomares, E., Charge carrier transport and contact selectivity limit the operation of PTB7-based organic solar cells of varying active layer thickness. *J. Mater. Chem. A* **2013**, *1*, 12345-12354.

47.   Shuttle, C. G.; Maurano, A.; Hamilton, R.; O'Regan, B.; Mello, J. C.; Durrant, J. R., Charge extraction analysis of charge carrier densities in a polythiophene/fullerene solar cell: Analysis of the origin of the device dark current. *Appl. Phys. Lett.* **2008**, *93*, 183501.

48.   Etxebarria, I.; Guerrero, A.; Albero, J.; Garcia-Belmonte, G.; Palomares, E.; Pacios, R., Inverted vs standard PTB7: PC70BM organic photovoltaic devices. The benefit of highly selective and extracting contacts in device performance. *Organic Electronics* **2014**, *15*, 2756-2762.

49.   Hawks, S. A.; Deledalle, F.; Yao, J.; Rebois, D. G.; Li, G.; Nelson, J.; Yang, Y.; Kirchartz, T.; Durrant, J. R., Relating recombination, density of states, and device performance in an efficient polymer: fullerene organic solar cell blend. *Advanced Energy Materials* **2013**, *3*, 1201-1209.

50.   Guo, X.G Nan.; Zhou, J.; Lou, S. J.; Smith, J.; Tice, D. B.; Hennek, J. W.; Ortiz, R. P.; Navarrete , J. T. L.; Li, S. Y.; Strzalka, J.; Chen, L. X.; Chang, R. P. H.; Facchetti,   A.; Marks, T. J., Polymer solar cells with enhanced fill factors. *Nat. Photonics* **2013**, *207*, 1-9.

51.   Sanchez-Díaz, A.; Burtone, L.; Riede, M.; Palomares, Emilio., Measurements of Efficiency Losses in Blend and Bilayer-Type Zinc Phthalocyanine/C60 High-Vacuum-Processed Organic Solar Cells. *J. Phys. Chem. C* **2012**, *116*, 16384−16390.

Chapter 5

The Effect of Solvent Mixture Treatment on Surface Composition: Controlling Morphology in Conventional and Inverted Structures Based on PTB7:PC$_{71}$BM

In the chapter, two types of solar cell devices, conventional structure and inverted structure, are prepared based on PTB7:PC$_{71}$BM blend with CB and CB/CHN (2:1, v/v) mixture treatment. Enriched PTB7 on the top surface of active layer connected with metal electrode induces a higher hole selectivity at the anode contact, which is more favorable to i-PSC than c-PSC structure. PCE of 8.05% for i-PSC device from CB treatment is obtained that is significantly higher than the one obtained from c-PSC device (6.86%). Comparison with CB treatment, the use of CB/CHN can affect not only the crystalline morphology and oriented alignment of polymer but also the surface composition of the BHJ active layer. A decrease in PCE for i-PSC device is observed by using CB/CHN as solvent that might be due to the relatively enrichment of PC$_{71}$BM on the top surface and a big phase separation. The result is different to that obtained in c-PSC. In addition, TPV and CE measurements show that after treatment with CB/CHN, i-PSC and c-PSC devices both display fast charge carrier recombination.

Chapter 5

Chapter 5

UNIVERSITAT ROVIRA I VIRGILI
NEW ADVANCES TO CONTROL MORPHOLOGY AND CRYSTALLINITY IN SOLUTION PROCESSED POLYMER SOLAR CELLS.
Peilin Han
Dipòsit Legal: T 256-2016

Chapter 5

Table of content

Chapter 5

Chapter 5

5.1 Introduction

Materials innovation and processing condition optimization in organic solar cells have resulted in the impressive refurbishing in power conversion efficiencies now exceeding 10% over past years. [1, 2] It is known that photo-induced charge generation and transportation in organic photovoltaic are strongly dependent on the morphology of polymer/fullerene blend film. [3-5] A favorable surface morphology provides not only sufficient interfaces for charge separation but also a good percolation pathway for charge transport to the corresponding electrode and for collecting charge. [6-8] For bulk heterojunction (BHJ) solar cells systems, the network interpenetrating morphology of the active layer based on the combination of donor and acceptor plays a key role to effective separation of exciton (hole-electron pairs) in the interface between donor and acceptor. [9, 10] However, carrier extraction selectivity for the dissociated electron collecting in a low work function cathode and hole in high work function anode are more related to the surface composition of the active layer. [11-13] When the acceptor on the surface is enriched and easily bound to the electron transport layer (ETL) then electrons are effectively extracted from the cathode contact. Conversely, when enriched donor on the surface is close to the hole transport layer (HTL), it would benefit to the hole extraction and collection at the anode contact. [12, 14, 15] In previous report, more research have focused on the effect of different interface layer materials (HTL or ETL) on the performance of solar cells. The transport layers with different charge mobility and surface work function have an important role to charge transport, collection and construction of solar cell devices (conventional or inverted structure). [11, 16] However, the effect of surface composition due to the morphologies variation of active layer on interface layer selectivity is much less exploited. In this way, controlling the surface morphologies of blends is more related to the performance of solar cells.

Chapter 5

Use of solvent additives like 1,8-Diiodooctane (DIO) and 1-chloronaphthalene (CN) or multiple solvent mixture treatments during the preparation process of donor and acceptor blend solutions have been proved as useful approaches to control the morphology of the active layer. [17-20] The effect of solvent mixture on morphology is displayed in several ways, such as bi-continuous nanoscale domains of donor and acceptor, improved crystalline of polymer or variation of surface coverage etc.. [21-23] Compared to binary solvent mixtures, ternary solvent mixtures such as dichlorobenzene (DCB)/ chloroform (CF)/DIO give a more favorable domain size and a rougher domain interface and have been successful used in PDPP3T:PC$_{71}$BM solar cells. [20, 24] In chapter 4, we have demonstrated that the photovoltaic performance of PTB7:PC$_{71}$BM solar cells has been dramatically improved by using ternary solvent mixture, including DIO as additive, "friend" solvent chlorobenzene (CB) and "unfriendly" solvent cyclohexanone (CHN). We also proved that the performance improvement mainly stems from addition of CHN leading to the crystalline morphology and oriented molecule alignment of polymer, further increasing short circuit current.

As mentioned above, the surface composition of the active layer plays an important role for the charge transport and charge collection, further influencing the contact selectivity of interface layer between the active layer and the electrode. In the present study, the aim is to investigate the effect of ternary solvent mixture treatment on surface composition as well as correlate the surface composition and selectivity of interface layer. We prepared a series of conventional polymer solar cells (c-PSC) and inverted polymer solar cells (i-PSC) based on PTB7:PC$_{71}$BM blend processed from CB/DIO and CB/CHN/DIO mixtures. Contact angle is used to calculate the surface energy of the blend film and to determine the relative surface components of donor/acceptor. We found the top surface of active layer to be relatively rich in PC$_{71}$BM after using CB/CHN/DIO mixture. The surface potentials and morphologies of the blend film due to variation of surface composition are also surveyed by

employing Kelvin probe force microscopy (KPFM) and AFM. In the end, we use TPV and CE techniques to measure the effect of different solvent mixtures on charge carrier extraction density and charge recombination kinetics in inverted and conventional structures.

5.2 Experimental section

The preparation of PTB7:PC$_{71}$BM blend solution with different solvent mixture and fabrication of the conventional solar cells in the configuration ITO/PEDOT:PSS/PTB7:PC$_{71}$BM(1:1.5, w/w)/Ca/Ag have been described in chapter 4. The inverted device structure are fabricated in the configuration ITO/ZnO/PTB7:PC$_{71}$BM (1:1.5, w/w)/MoO$_3$/Ag. First, the ZnO precursor was prepared by a modified method, [25] the main process is: zinc acetate dihydrate (Zn(CH$_3$COO)$_2$·2H$_2$O) 1.5 g and ethanolamine 0.28 g dissolve in 2-methoxyethanol (CH$_3$OCH$_2$CH$_2$OH) 10 mL under vigorous stirring for 12 h for the hydrolysis reaction in air. Then the precursor solution of ZnO is diluted by methanol with ratio of 1:1 at stirring. Following, this suspension is spin coated on pre-cleaned ITO substrate at 3000 rpm for 30 s. After that, the resulting ZnO film is heated at 200 ℃ for 1 h in air. The PTB7:PC$_{71}$BM composites layer was deposited by spin casting at 1000 rpm for 30s on the ITO/ZnO substrate without further special treatments. Subsequently the samples were transferred into a thermal evaporator located in the same glove box. The final cells are obtained followed the description in chapter 2.

5.3 Results and discussion

### 5.3.1 Performance measurements in different cell structures

In the present study, the devices are fabricated with the configuration ITO/PEDOT:PSS/PTB7:PC$_{71}$BM(1:1.5, w/w)/Ca/Ag for c-PSC structure and

Chapter 5

ITO/ZnO/PTB7:PC$_{71}$BM(1:1.5, w/w)/MoO$_3$/Ag for i-PSC structure. The structures of devices with different types and corresponding level of the materials are shown in Figure 5.1.
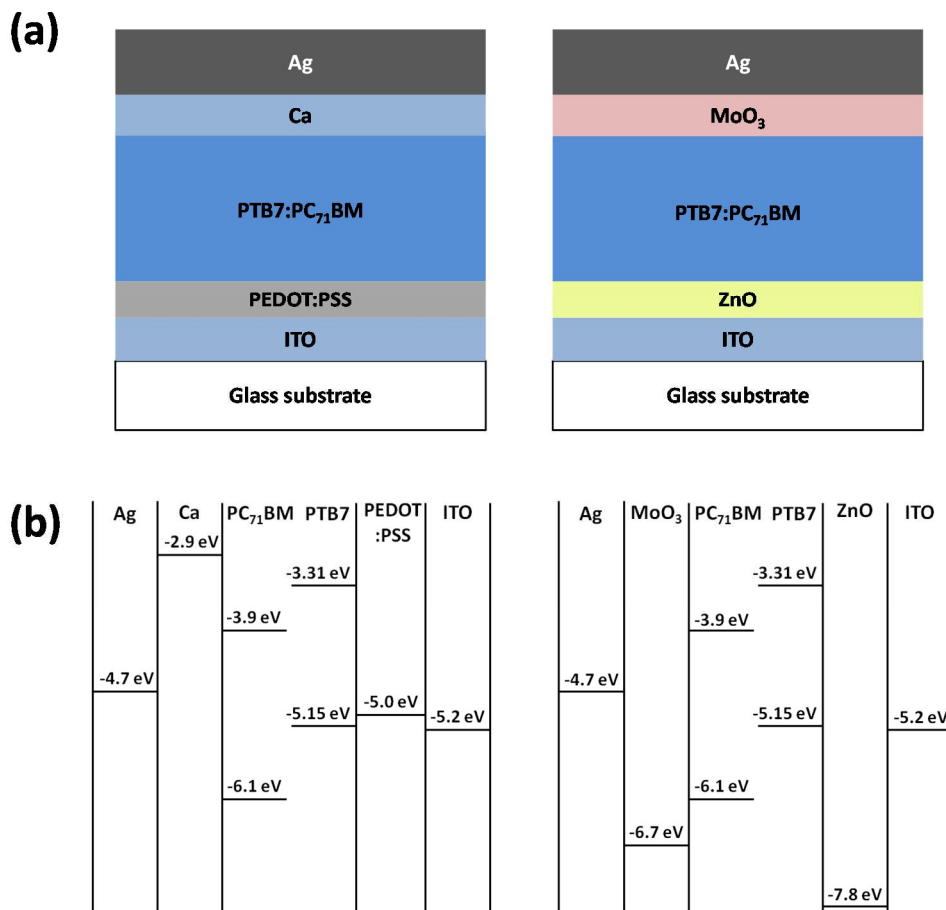

Figure 5.1. The schematic representation of conventional (left) and inversed (right) devices based on PTB7:PC$_{71}$BM (a) and corresponding energy levels of the materials (b).

Since the ternary solvent mixture, including CB/CHN (2:1, v/v) and DIO (3%, v/v in total solvent), has performed an optimal power conversion efficiency (PCE) in conventional solar cells in our previous study, the same solvent mixture is also used in inverted solar cell device. ZnO and MoO$_3$ are selected as the electron transport layer (ETL) and hole transport layer (HTL) in inverted solar cells device, respectively. Figure 5.2 shows the current-voltage curves of PTB7:PC$_{71}$BM solar cells under the illumination of AM 1.5G. The corresponding photovoltaic data of devices are summarized in Table 5.1. As discussed in chapter 4, c-PSCs with CB treatment display a PCE of 6.86% with a Voc of 0.73 V, a Jsc of 14.55 mA/cm^2 and a FF of

64.5%. However, when the inverted device structure replaces the conventional device structure with the same CB treatment, i-PSC shows higher PCE of 8.05% with higher Jsc of 17.20 mA/cm^2 and FF of 66.3%, although a lower Voc of 0.71 V. In addition, it is worth noting that after treatment with CB/CHN of 2:1 ratio, c-PSC displays an obvious increase to 16.2 mA/cm^2 in Jsc, a relatively stable Voc of 0.74 V, thus leading to PCE increasing to 7.31%, although the FF decreases to 61%. In chapter 4, we have demonstrated that the oriented molecule alignment and improved crystallization of polymer, due to addition of CHN, to be the main reasons to induce the enhancement of PCE in c-PSC devices. However, for i-PSC structure, an opposite result is obtained. After treating with CB/CHN (2:1), the PCE decreases to 7.25%, with Jsc decreasing to 16.56 mA/cm^2, FF decreasing to 63.4% and Voc decreasing to 0.69 V.
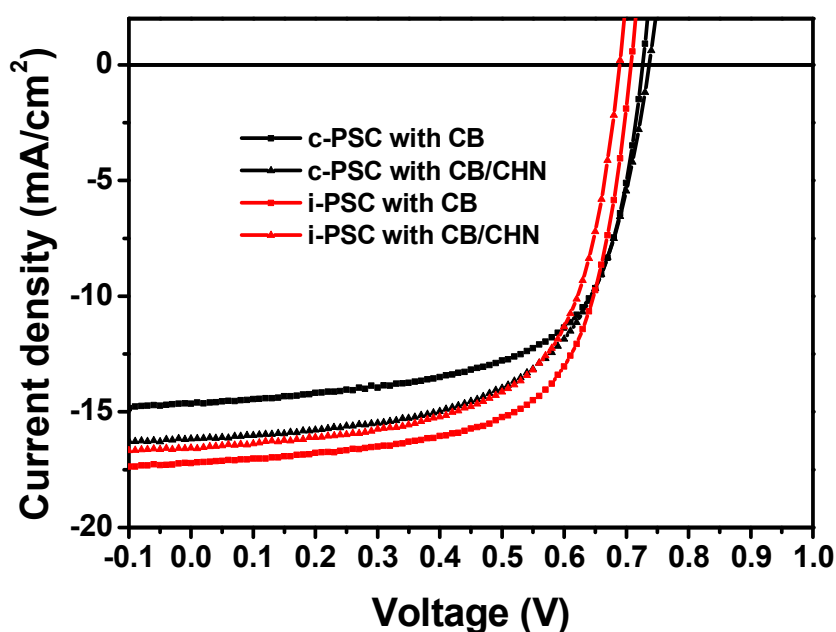
Figure 5.2. J-V curves under AM 1.5 G illumination at 1 sun. Devices based on PTB7:PC$_{71}$BM processed from CB and CB/CHN for conventional and inverted device.

Table 5.1 Photovoltaic performance of device processed from CB and CB/CHN (2:1) for conventional and inverted device.

Device	Solvent	V$_{oc}$ (V)	J$_{sc}$ (mA/cm^2)	FF (%)	PCE (PCE average) (%)
c-PSC	CB	0.73	14.55	64.5	6.86 (6.72)
c-PSC	CB/CHN (2:1)	0.73	16.20	61	7.31 (7.21)
i-PSC	CB	0.71	17.20	66.3	8.05 (7.86)
i-PSC	CB/CHN (2:1)	0.69	16.56	63.4	7.25 (7.16)

Chapter 5

It is clearly observed that when replacing the conventional structure with inverted structure with the same CB treatment, i-PSC shows a higher PCE than c-PSC with higher FF, Jsc. ZnO and MoO$_3$, as ETL and HTL respectively, present improved high charge transport and charge extraction compared to PEDOT:PSS and Ca, thus leading to enhanced solar cells performance, as previously discussed. [26-28] In addition, the different morphologies depend on the top surface composition strongly affect contact selectivity of transport layer and charge extraction in c-PSC and i-PSC devices. [11] It also might be a reason for improvement of solar cell performance in i-PSC devices. However, interestingly, in the our case i-PSC devices exhibit a decrease in PCE that is different to obtained in c-PSC by means of the same CB/CHN mixture treatment. In order to evaluate the morphologies variation from the different solvent processing, we detect the top surface composition of the active layer.

5.3.2 Contact angle measurements and surface energy calculation

The surface energy component of the active layer is surveyed by utilizing advancing contact angle measurements based on different films including ITO, PTB7, PC$_{71}$BM, PTB7:PC$_{71}$BM with CB and CB/CHN mixture treatment. All films are obtained by spin coating solutions on ITO substrate. Surface energy is extracted from a "three-liquid acid-base procedure" developed by van OSS et al, [29, 30] which is defined by the following equation:

$$(1+\cos\theta_{adv})\gamma_L^T = 2\left(\sqrt{\gamma_S^{LW}\gamma_L^{LW}} + \sqrt{\gamma_S^+\gamma_L^-} + \sqrt{\gamma_S^-\gamma_L^+}\right)$$

Where γ^T, γ^{LW}, γ^+, and γ^- denote the total, Lifshitz-van der Waals (dispersive), Lewis acid and base surface energy components, while the subscripts S and L refer to

Chapter 5

the solid surface and probe liquid. The final γ^T of solid film is obtained by

$$\gamma^T = \gamma^{LW} + \gamma^{AB}, \text{ and } \gamma^{AB} \text{ is defined by } \sqrt{\gamma_S^+ \gamma_S^-}$$

Water, ethylene glycol and diiodomethane are selected as three probe liquids in this study. The resultant contact angles of different film are summarized in Table 5.2. The example of calculation processes are displayed in the following description. The surface energy parameters of probe liquids and corresponding transformations to surface energies of different films are summarized in Table 5.3.

For example, the calculation of surface energy of PTB7 as following:

In terms of water as testing liquid:

$$72.8*(1+\cos 88.3) = 2\left(\sqrt{21.8 * \gamma_L^{LW}} + \sqrt{\gamma_S^+ * 22.5} + \sqrt{22.5 * \gamma_S^-}\right)$$

In terms of ethylene glycol as testing liquid:

$$48*(1+\cos 66.5) = 2\left(\sqrt{29 * \gamma_L^{LW}} + \sqrt{\gamma_S^+ * 47} + \sqrt{1.92 * \gamma_S^-}\right)$$

In terms of diiodomethane as testing liquid:

$$50.8*(1+\cos 92) = 2\left(\sqrt{50.8 * \gamma_L^{LW}} + \sqrt{\gamma_S^+ * 0} + \sqrt{0 * \gamma_S^-}\right)$$

Then, combine three equations and the solution of the equation group is calculated to be:

$$\gamma^+ = 3.05$$

$$\gamma^- = 4.87$$

$$\gamma^{AB} = 2\sqrt{\gamma^+\gamma^-} = 7.71$$

$$\gamma^{LW} = 11.83$$

$$\gamma^T = \gamma^{LW} + \gamma^{AB} = 19.54$$

Chapter 5

Table 5.2. Surface energy parameters (in mN/m) of testing liquids

	γ^T	γ^{LW}	γ^{AB}	γ^+	γ^-
Water	72.8	21.8	51	25.5	25.5
Ethylene glycol	48	29	19	1.92	47
Diiodomethane	50.8	50.8	0	0	0

Table 5.3. Advancing contact angles of three probing liquids on various surfaces at initial state, and the calculated surface energies (mN m^{-1})

		ITO	PCBM	PTB7	PTB7:PCBM (CB/CHN-2:1)	PTB7:PCBM (CB)
Catact angle	Water	51.7	73.3	88.3	81.2	85.6
	Ethylene Glycol	39.5	50	66.5	54	61
	diiodomethane	39	23	92	99.4	87
Calculated surface energy component	γ	42.4	48.3	19.54	24.5	22.8
	γ^{LW}	40.2	48.3	11.83	8.9	14
	γ^{AB}	2.2	*	7.71	15.4	8.9
	γ^+	0.83	*	3.05	6.9	3.06
	γ^-	1.41	0.36	4.87	8.57	6.49

Note: *surface energy component found be negligible

It is important to note that the two blend films of PTB7:PC$_{71}$BM with CB treatment ($\sim$22.8 mN m^{-1}) and CB/CHN mixture ($\sim$24.5 mN m^{-1}) have similar surface energies with pure PTB7 film ($\sim$19.5 mN m^{-1}). It confirms that a donor PTB7 enriches on the top surface of active layer compared to acceptor PC$_{71}$BM for both blend films. However, in comparison with the PTB7:PC$_{71}$BM blend film treated with CB, the surface energy is more close to the acceptor PC$_{71}$BM ($\sim$48.3 mN m^{-1}) when CB/CHN mixture is employed as solvent. This indicates that acceptor PC$_{71}$BM relatively enriches on the top surface of the active layer after CB/CHN treatment. This is might due to crystallite reorientation and a large phase separation due to the improved PTB7 crystallization, after CB/CHN treatment lead to the exposure of more PC$_{71}$BM on the surface of active layer.

Chapter 5

As known, in BHJ solar cells, photo-generated electrons are extracted and transported through a channel formed by acceptor material and collected at the cathode and the corresponding holes are transported by donor material and collected at the anode. When the top surface of the blend film is enriched with donor and the top surface connects anode, holes are extracted more efficiently and electrons transport and collection are impeded. In our case, PTB7 enriches at the interface between the active layer and electrode more than $PC_{71}BM$. It implies that the top surface benefits from being covered with HTL layer that connects to the anode, further increasing the hole transport efficiency. Thus the surface formation is more favorable to construct an inverted solar cells structure than conventional structure. It is also a main reason that the solar cells with i-PSC structure displays a higher Jsc and better performance than c-PSC with the same CB treatment. Conversely, after using the CB/CHN mixture as solvent, a relatively increased proportion of $PC_{71}BM$ composition on the surface of blend film benefits the binding with the ETL connected to the cathode. This is more favorable to the electron transport and collection in c-PSC structure than i-PSC structure. In combination with the device performance, i-PSCs show an enhancement in PCE with increased Jsc and FF compared to c-PSCs with CB treatment. Similarly, after the same CB/CHN mixture solvent processed, a decline and decline in Jsc in i-PSCs and in c-PSCs are observed respectively, due to the relatively rich of $PC_{71}BM$ on the top surface. As discussed above, we also conclude that contact selectivity of transport layer and electrode due to the variation of surface composition play a key role in the device performance.

5.3.3 Surface Potential and morphology of active layer

The different surface composition of the active layer or variations in crystallinity and orientation of polymer cause different surface potentials, which correspond to the average work function of active layer surface. [31] This is essential to the selectivity of transport layer materials between the active layer and the electrode. To study the

modification of the CB/CHN mixture treatment on blend surfaces we examine the surface potential by Kelvin probe force microscopy (KPFM). KPFM measures two-dimentional distributions of contact potential difference between the tip and blend film with a resolution in the nanometer range. The surface potential gives some information about surface condition and it is related to some factors such as surface charge density, surface trap or surface reconstruction. [32-34] In this study, KPFM
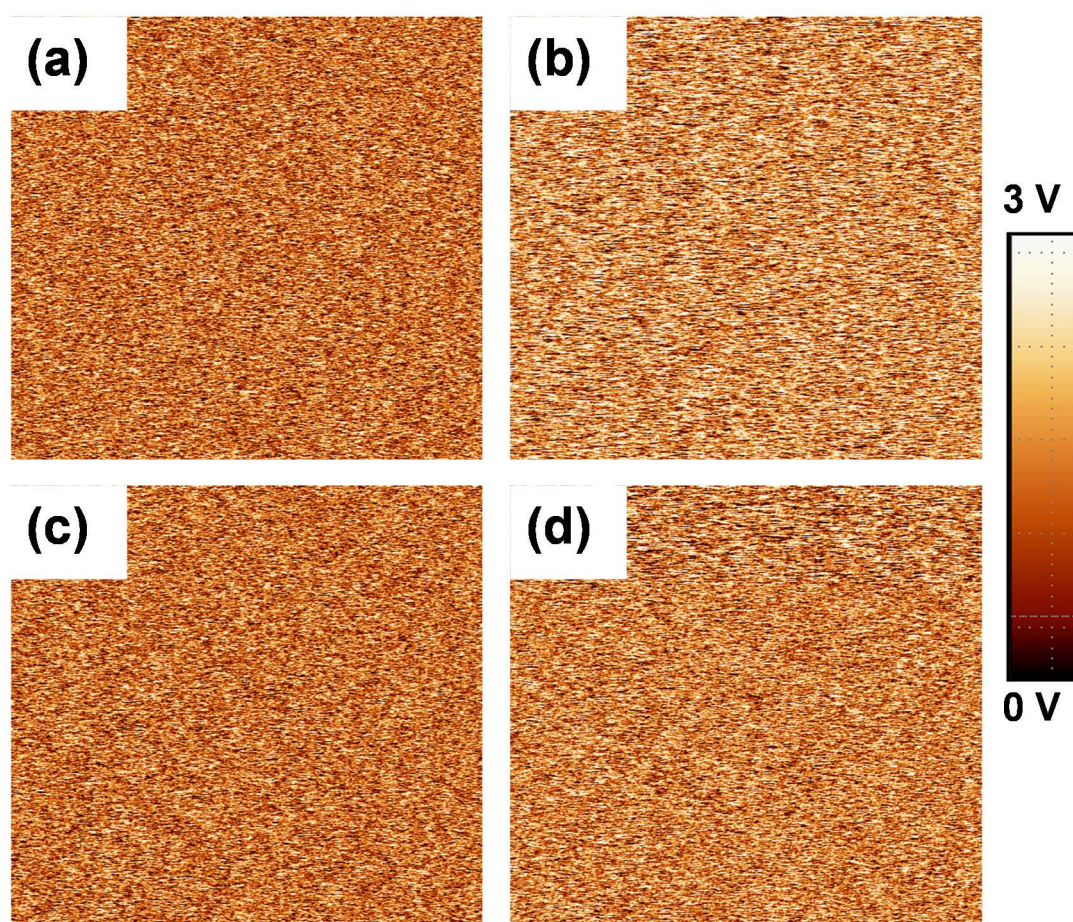
Figure 5.3. The KPFM surface potential images (3μm × 3μm) of PTB7:PC$_{71}$BM blend films processed CB (left) and CB/CHN (2:1) (right) for conventional device (a, b) and inverted device (c, d).

Measurements carried out based on two configurations of ITO/PEDOT:PSS/PTB7:PC$_{71}$BM and ITO/ZnO/PTB7:PC$_{71}$BM, respectively. The average surface contact potentials are deduced with a scale of 3 μm. As shown in
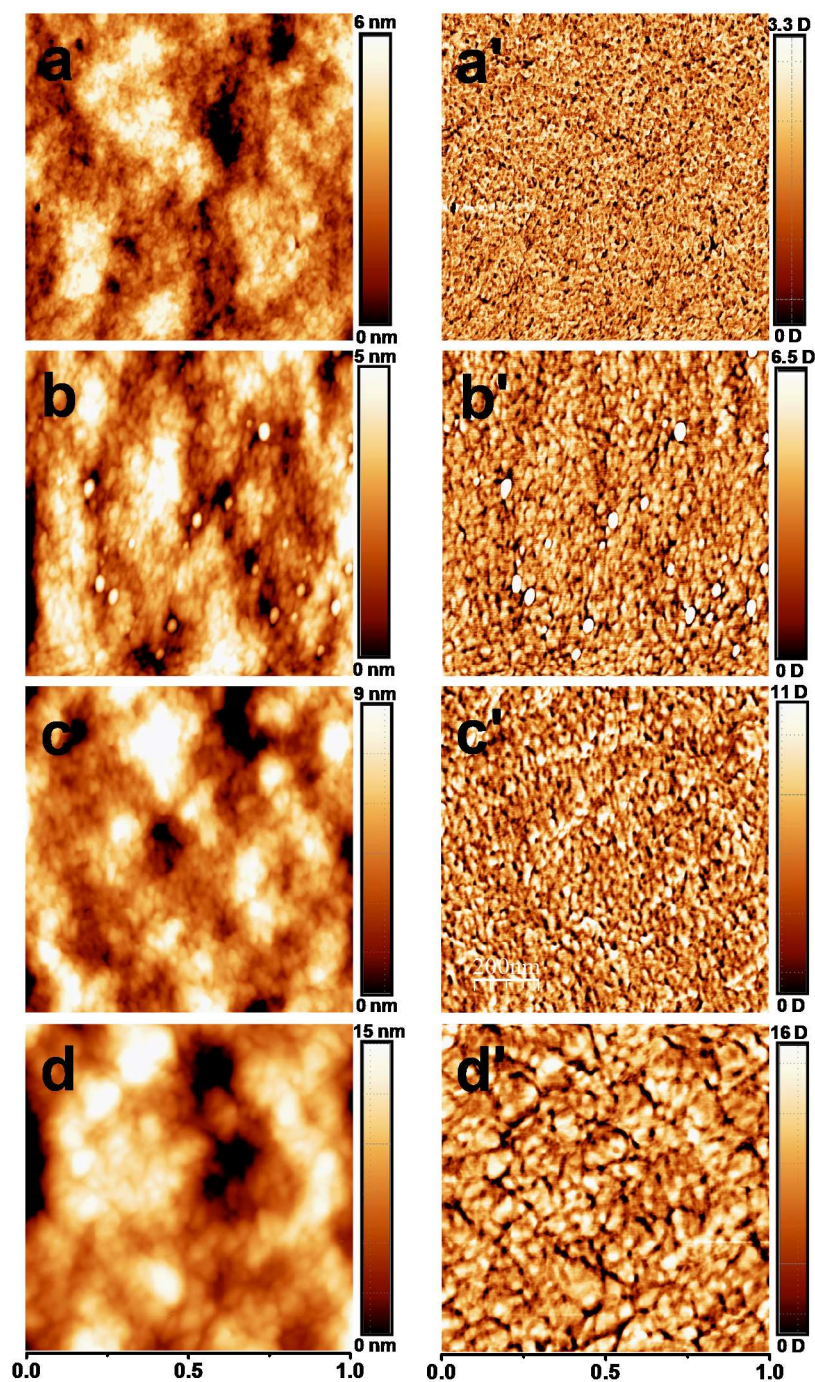
Chapter 5

Figure 5.3, for configuration of ITO/PEDOT:PSS/PTB7:PC$_{71}$BM, a upward shift of 136 mV in average surface potential after CB/CHN treatment is observed relative to that of treatment with CB (Figure 5.3a, b). This result indicates that at the metal electrode/organic interface the vacuum level (VL) of electrode is correspondingly elevated by ～136 mV after the use of CHN, which benefitting to improve the injection of electrons to the cathode in c-PSC device structure and resulting in better device performance. A similar surface potential increase of ～90 mV is also observed in the configuration of ITO/ZnO/PTB7:PC$_{71}$BM (Figure 5.3c, d) after the use of CHN. In combination with surface energy from contact angle analysis, the surface energy of PC$_{71}$BM ($\approx$48.3 mN m^{-1}) is higher than PTB7 ($\approx$19.5 mN m^{-1}) and it relatively enriches on the surface after the use of CHN. The increase of surface potential in both configurations, as measured by KPFM after CB/CHN treatment, might originate from an increase of surface electronic density due to PC$_{71}$BM enriched on the surface of the active layer leading to the surface component reconstruction. [31, 35] It should be noted that the promotion of surface potential after CB/CHN treatment benefits the injection of electron to the cathode for c-PSC, but deteriorates for i-PSC structure, thus causing the regressive device performance. In addition, the surface potentials of the organic layer treated with CB and CB/CHN in i-PSC both are lower than that of the organic layer processed with the same solvents in c-PSC, which should be a main reason for the reduced Voc in i-PSC. [31, 36-38]

We also compare AFM images of PTB7:PC$_{71}$BM blend film on PEDOT:PSS and ZnO surface treated with CB and CB/CHN. Figure 5.4 shows topography images (Figure 5.4a-d) of PTB7:PC$_{71}$BM film treated with CB and CB/CHN mixtures with a ratio of 2:1 for both types of structures, respectively and their corresponding phase image (Figure 5.4a'-d). For both types of solar cells structure with CB treatment, topography images shows a big domain sizes in i-PSC (Figure 5.4c) compared to c-PSC (Figure 5.4a). In addition, a higher surface roughness with a root-mean-square roughness (RMS) value of 2.5 nm is observed in i-PSC device than c-PSC treated with the same
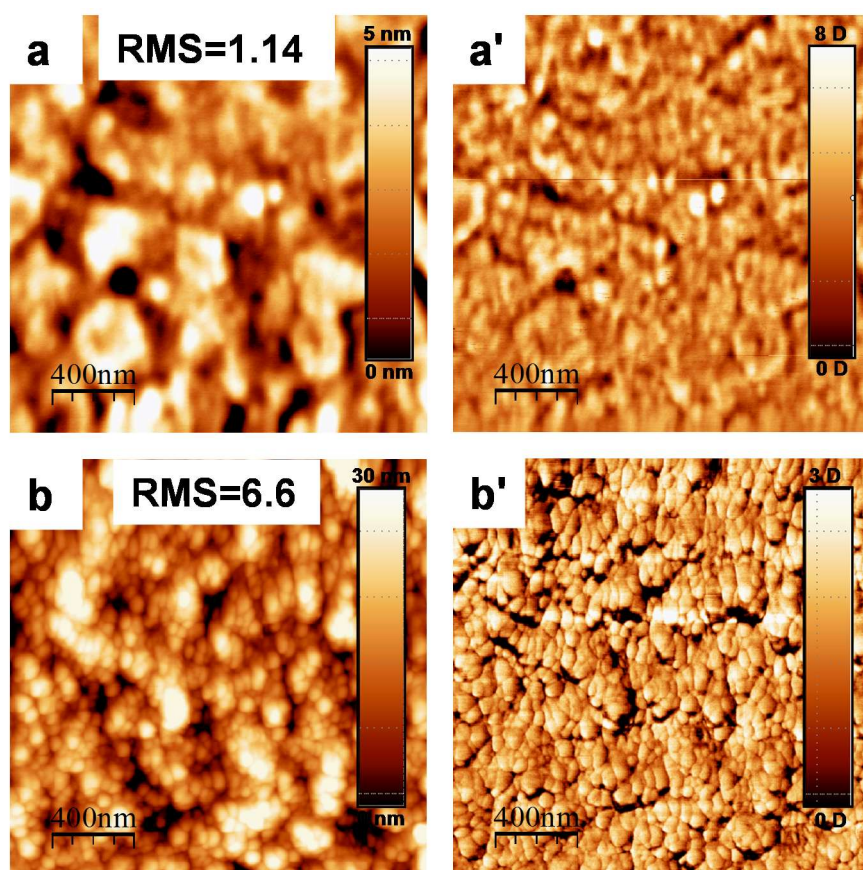
Chapter 5

solvent (RMS of 1.5 nm). This might be explained by the PTB7:PC$_{71}$BM blend spin-coating on different transport layer materials, i.e. PEDOT:PSS for c-PSC and ZnO for i-PSC, which processing different rough surface (Figure 5.5a-d'). After using CB/CHN as solvent, a same phenomenon is observed for i-PSC and c-PSC where

Figure 5.4. AFM topographic (left) and phase images (right) of thin films fabricated from PTB7:PC$_{71}$BM blend solutions with different solvents: (a, a') CB and (b, b') CB/CHN for ITO/PEDOT:PSS/ PTB7:PC$_{71}$BM. (c, c') CB and (d, d') CB/CHN (2:1) for ITO/ZnO/PTB7:PC$_{71}$BM.

116

domain sizes both increase compared to CB treatment. Meanwhile, the phase image displays that the use of CB/CHN leading to polymer chains coarsen and aggregate in i-PSC. The result is similar to that observed in c- PSC and the reason has been discussed in chapter 4. The increased domain sizes and polymer aggregation also imply that more $PC_{71}BM$ is exposed on the top surface of the active layer in devices due to the addition of CHN.

Figure 5.5. AFM topographic (left) and phase images (right) of PEDOT:PSS (a, a') and ZnO (b, b') films.

5.3.4 Charge extraction and recombination kinetics

In chapter 4, we have demonstrated that improved crystallinity of the polymer from CB/CHN treatment is a key to enhance the performance in conventional $PTB7:PC_{71}BM$ solar cells. Large phase separation and polymer aggregation result in a fast non-geminate recombination of extracted photo-generated charge in the interface

Chapter 5

between the active layer and the electrodes, as characterized by TPV and CE techniques. In addition, PTB7 enriched on the top surface in i-PSC structure appears to be more favorable for the hole collection at the corresponding anode. Whereas relatively enriched $PC_{71}BM$ seems to be favorable for the electron collection at cathode in c-PSC. To gain a deeper understanding of the effect of variation of surface composition due to CB/CHN treatment on surface charge in both device types, charge extraction and recombination in the interface between the active layer and the
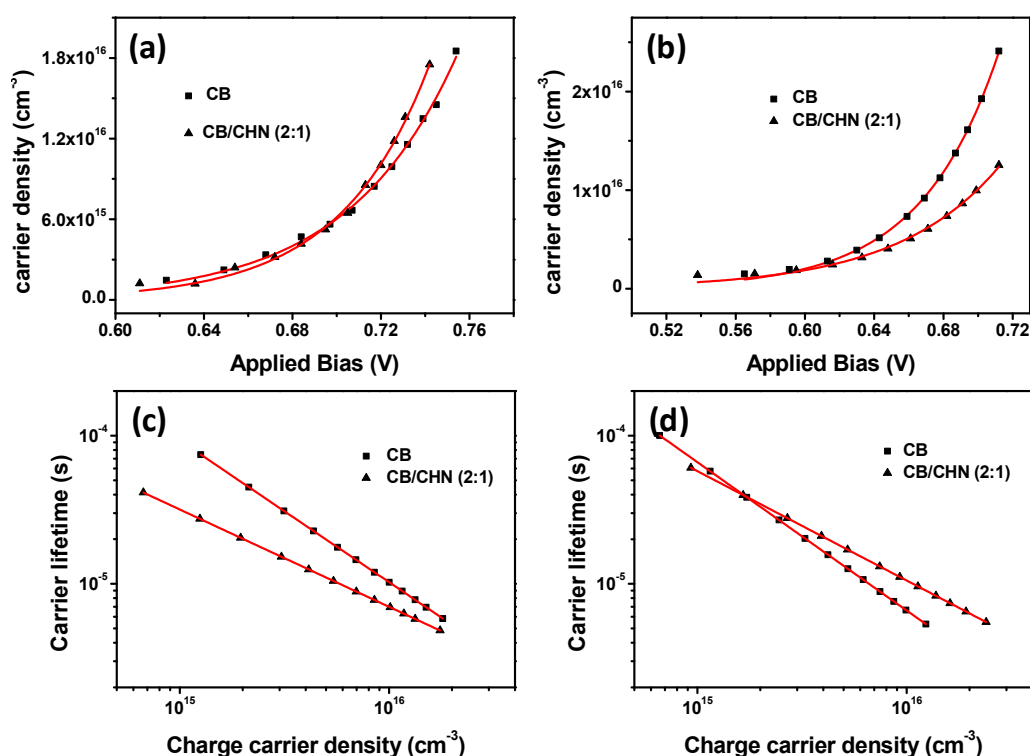

Figure 5.6. Distribution of charge density for different light-induced voltage extracted from CE measurements for PTB7:$PC_{71}BM$ treated with CB and CB/CHN in c-PSC (a) and i-PSC (b). Solid line shows the device charge corresponding to a geometrical capacitance. Charge carrier recombination lifetime vs charge carrier density for the complete PTB7:$PC_{71}BM$ solar cells treated with CB and CB/CHN in c-PSC (c) and i-PSC (d).

electrode are investigated by means of TPV and CE. The two techniques are widely used to research non-recombination in working solar cells and their working mechanism have been described elsewhere [39, 40] and in chapter 4. The average charge carrier density n, under open condition, is collected from different light bias

and the data is corrected by geometry capacitance. Even though discussed in chapter 4, we continue to focus on the charge carrier density in high light intensity for all devices since it is dominated by the dielectric properties of the active layer in low light density. As shown in Figure 5.6a, a different trend emerges for the two types of devices: c-PSC device displays a slight higher charge carrier density when treated with CB/CHN than with CB treatment due to the higher crystalline of the polymer from CB/CHN treatment, as proved by grazing incidence X-ray scattering (Figure 5.7).

Comparing the same solvent treatments in i-PSC device, CB treatment results in a higher charge carrier density even though CB/CHN produces a higher crystallinity of the polymer (Figure 5.6b). As discussed above, yielding a high charge extraction density can be achieved by surface composition restructuring with enriched $PC_{71}BM$ with CB treatment but also by producing polymer of high crystallinity from CB/CHN treatment. In the present study, we demonstrate that the restructuring of the surface composition allows for a more efficient extraction of charge compared to variation of polymer crystallinity.
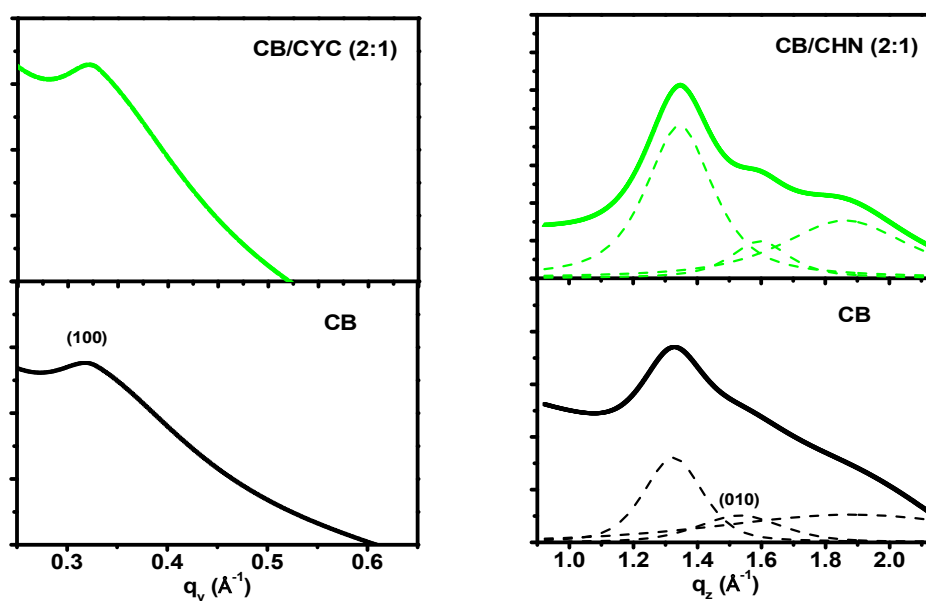
Figure 5.7. The corresponding q_y and q_z scans from the 2-D GISAXS (left) and GIWAXS (right) patterns, which corresponding to film treated with CB and CB/CHN (2:1). Pseudo-Voigt function fits are used to determine the total peak position, the individual peaks and FWHMs.

119

Chapter 5

In order to determine the effective charge carrier lifetime, TPV is performed based on monitoring the photovoltage decay on a small perturbation during constant light bias. Combining the TPV and CE measurements, the charge carrier lifetime τ is represented as a function of charge carrier density under circuit condition according to $\tau(n) = \tau_0 n^{-\lambda}$, as shown in Figure 5.6c, d. The value of $-\lambda$ can be taken from the slope of log-log plot and is related to the non-geminate recombination order ($\lambda+1$). For both c-PSC and i-PSC devices with same CB treatment similar recombination order of 1.95 for c-PSC and 2.1 for i-PSC device are yielded. After using CB/CHN mixture as solvent, the non-geminate recombination lifetime for both devices types is slightly shorter than for CB as solvent, which corresponds to a reduced recombination order of 1.65 and 1.73 for c-PSC and i-PSC, respectively. However, different surface morphologies and surface compositions are obtained for both device types treated with CB, interpenetrating network morphologies for c-PSC and enriched PTB7 on the top surface connecting to the cathode for i-PSC device are both possible contributes to the effective collection of extracted charge at the corresponding electrode, further leading to long non-geminate recombination lifetime. On the other hand, for both device types treated with CB/CHN a big phase separation and isolated domains of PTB7 and $PC_{71}BM$ are obtained from AFM images and might contribute to the relatively fast recombination, resulting in increasing geminate recombination in the same phase. Finally, the relatively fast charge recombination contributes to the decrease in FF, as observed by the performance measurements of device after using CB/CHN as a solvent.

5.4 Conclusions

In summary, two types of solar cell devices, conventional structure and inverted structure, are prepared based on PTB7:PC$_{71}$BM blend with CB and CB/CHN (2:1, v/v) mixture treatments. Enriched PTB7 on the top surface of active layer, detected via surface energy measurements, induces higher hole selectivity at the anode contact and is favorable to i-PSC compared with c-PSC device. Thus, PCE of 8.05% for i-PSC device from CB treatment is obtained that is significantly higher than the one obtained from c-PSC device (6.86%). Comparison with CB treatment, CB/CHN treatment can affect not only the crystalline morphology and oriented alignment of polymer but also the surface composition of the active layer. A decrease in PCE for i-PSC device is observed by using CB/CHN as solvent that might be due to the addition of CHN leading to the relatively enrichment of PC$_{71}$BM on the top surface and a big phase separation. The result is different to that observed in c-PSC. It can be concluded that selection of transport layer between active layer and electrode is related to the variation of surface composition and play a key role in the device performance. In addition, TPV and CE measurements at different light bias show surface composition of active layer and polymer crystallinity are important factors for non-geminate recombination kinetics. After treatment with CB/CHN, i-PSC and c-PSC devices both show fast charge carrier recombination due to a big phase separation and isolated domains polymer PTB7 and PC$_{71}$BM.

Chapter 5

5.5 references

1.   Chen, J. D.; Cui, C.; Li, Y. Q.; Zhou, L.; Ou, Q. D.; Li, C.; Li, Y.;Tang, J. X., Single-Junction Polymer Solar Cells Exceeding 10% Power Conversion Efficiency. *Adv. Mater.* **2015**, *27*, 1035-1041.

2.   You, J.; Dou, L.; Yoshimura, K.; Kato, T.; Ohya, K.; Moriarty, T.; Emery, K.; Chen, C.-C.; Gao, J.;Li, G., A polymer tandem solar cell with 10.6% power conversion efficiency. *Nat. Commun.* **2013**, *4*, 1446.

3.   Chen, S.; Manders, J. R.; Tsang, S.-W.;So, F., Metal oxides for interface engineering in polymer solar cells. *J. Mater. Chem.* **2012**, *22*, 24202-24212.

4.   Xin, H.; Reid, O. G.; Ren, G.; Kim, F. S.; Ginger, D. S.;Jenekhe, S. A., Polymer nanowire/fullerene bulk heterojunction solar cells: how nanostructure determines photovoltaic properties. *Acs Nano* **2010**, *4*, 1861-1872.

5.   Jailaubekov, A. E.; Willard, A. P.; Tritsch, J. R.; Chan, W.-L.; Sai, N.; Gearba, R.; Kaake, L. G.; Williams, K. J.; Leung, K.;Rossky, P. J., Hot charge-transfer excitons set the time limit for charge separation at donor/acceptor interfaces in organic photovoltaics. *Nat. Mater.* **2013**, *12*, 66-73.

6.   Bartelt, J. A.; Beiley, Z. M.; Hoke, E. T.; Mateker, W. R.; Douglas, J. D.; Collins, B. A.; Tumbleston, J. R.; Graham, K. R.; Amassian, A.;Ade, H., The importance of fullerene percolation in the mixed regions of polymer–fullerene bulk heterojunction solar cells. *Advanced Energy Materials* **2013**, *3*, 364-374.

7.   Huang, Y.; Kramer, E. J.; Heeger, A. J.;Bazan, G. C., Bulk heterojunction solar cells: morphology and performance relationships. *Chem. Rev.* **2014**, *114*, 7006-7043.

8.   Dang, M. T.; Hirsch, L.; Wantz, G.;Wuest, J. D., Controlling the morphology and performance of bulk heterojunctions in solar cells. Lessons learned from the benchmark poly (3-hexylthiophene):[6, 6]-phenyl-C61-butyric acid methyl ester system. *Chem. Rev.* **2013**, *113*, 3734-3765.

9.   Chen, H.-Y.; Yang, H.; Yang, G.; Sista, S.; Zadoyan, R.; Li, G.;Yang, Y., Fast-grown interpenetrating network in poly (3-hexylthiophene): methanofullerenes solar cells processed with additive. *J. Phys. Chem. C* **2009**, *113*, 7946-7953.

10. Bertho, S.; Oosterbaan, W. D.; Vrindts, V.; D'Haen, J.; Cleij, T. J.; Lutsen, L.; Manca, J.;Vanderzande, D., Controlling the morphology of nanofiber-P3HT:PCBM blends for organic bulk

Chapter 5

heterojunction solar cells. *Organic Electronics* **2009**, *10*, 1248-1251.

11. Guo, X.; Zhang, M.; Ma, W.; Ye, L.; Zhang, S.; Liu, S.; Ade, H.; Huang, F.;Hou, J., Enhanced Photovoltaic Performance by Modulating Surface Composition in Bulk Heterojunction Polymer Solar Cells Based on PBDTTT-C-T/PC$_{71}$BM. *Adv. Mater.* **2014**, *26*, 4043-4049.

12. Guerrero, A.; Dörling, B.; Ripolles-Sanchis, T.; Aghamohammadi, M.; Barrena, E.; Campoy-Quiles, M.;Garcia-Belmonte, G., Interplay between fullerene surface coverage and contact selectivity of cathode interfaces in organic solar cells. *ACS nano* **2013**, *7*, 4637-4646.

13. Hsu, B. B.; Duan, C.; Namdas, E. B.; Gutacker, A.; Yuen, J. D.; Huang, F.; Cao, Y.; Bazan, G. C.; Samuel, I. D.;Heeger, A. J., Control of Efficiency, Brightness, and Recombination Zone in Light-Emitting Field Effect Transistors. *Adv. Mater.* **2012**, *24*, 1171-1175.

14. Chang, L.; Lademann, H. W.; Bonekamp, J. B.; Meerholz, K.;Moulé, A. J., Effect of trace solvent on the morphology of P3HT: PCBM bulk heterojunction solar cells. *Adv. Funct. Mater.* **2011**, *21*, 1779-1787.

15. Lee, J.; Kaake, L. G.; Cho, J. H.; Zhu, X.-Y.; Lodge, T. P.;Frisbie, C. D., Ion gel-gated polymer thin-film transistors: operating mechanism and characterization of gate dielectric capacitance, switching speed, and stability. *J. Phys. Chem. C* **2009**, *113*, 8972-8981.

16. Cho, S.; Kim, K.-D.; Heo, J.; Lee, J. Y.; Cha, G.; Seo, B. Y.; Kim, Y. D.; Kim, Y. S.; Choi, S.-y.;Lim, D. C., Role of additional PCBM layer between ZnO and photoactive layers in inverted bulk-heterojunction solar cells. *Sci. Rep.* **2014**, *4*.

17. Liang, Y.; Xu, Z.; Xia, J.; Tsai, S. T.; Wu, Y.; Li, G.; Ray, C.;Yu, L., For the bright future—bulk heterojunction polymer solar cells with power conversion efficiency of 7.4%. *Adv. Mater.* **2010**, *22*, E135-E138.

18. Kaake, L. G.; Jasieniak, J. J.; Bakus, R. C.; Welch, G. C.; Moses, D.; Bazan, G. C.;Heeger, A. J., Photoinduced charge generation in a molecular bulk heterojunction material. *J. Am. Chem. Soc.* **2012**, *134*, 19828-19838.

19. Wang, D. H.; Morin, P.-O.; Lee, C.-L.; Kyaw, A. K. K.; Leclerc, M.;Heeger, A. J., Effect of processing additive on morphology and charge extraction in bulk-heterojunction solar cells. *J. Mater. Chem. A* **2014**, *2*, 15052-15057.

20. Ye, L.; Zhang, S.; Ma, W.; Fan, B.; Guo, X.; Huang, Y.; Ade, H.;Hou, J., From binary to ternary

Chapter 5

solvent: morphology fine-tuning of D/A blends in PDPP3T-based polymer solar cells. *Adv. Mater.* **2012**, *24*, 6335-6341.

21. Zhou, Y.; Fuentes-Hernandez, C.; Shim, J.; Meyer, J.; Giordano, A. J.; Li, H.; Winget, P.; Papadopoulos, T.; Cheun, H.;Kim, J., A universal method to produce low–work function electrodes for organic electronics. *Science* **2012**, *336*, 327-332.

22. Collins, B. A.; Tumbleston, J. R.;Ade, H., Miscibility, crystallinity, and phase development in P3HT/PCBM solar cells: toward an enlightened understanding of device morphology and stability. *The Journal of Physical Chemistry Letters* **2011**, *2*, 3135-3145.

23. Wu, J.-L.; Chen, F.-C.; Hsiao, Y.-S.; Chien, F.-C.; Chen, P.; Kuo, C.-H.; Huang, M. H.; Hsu, C.-S., Surface plasmonic effects of metallic nanoparticles on the performance of polymer bulk heterojunction solar cells. *ACS nano* **2011**, *5*, 959-967.

24. Ma, W.; Tumbleston, J. R.; Ye, L.; Wang, C.; Hou, J.; Ade, H., Quantification of Nano-and Mesoscale Phase Separation and Relation to Donor and Acceptor Quantum Efficiency, Jsc, and FF in Polymer: Fullerene Solar Cells. *Adv. Mater.* **2014**, *26*, 4234-4241.

25. Sun, Y.; Seo, J. H.; Takacs, C. J.; Seifter, J.; Heeger, A. J., Inverted Polymer Solar Cells Integrated with a Low-Temperature-Annealed Sol-Gel-Derived ZnO Film as an Electron Transport Layer. *Adv. Mater.* **2011**, *23*, 1679-1683.

26. Etxebarria, I.; Guerrero, A.; Albero, J.; Garcia, G.; Palomares, E.; Pacios, R., Inverted vs tandard PTB7:PC70BM rganic photovoltaic devices. the benefit of highly selective and extracting contacts in device performance. *Organic electronics* **2014**, *15*, 2756-2762.

27. Fu, H.; Tan, L.; Shi, Y.; Chen, Y., Tunable size and sensitization of ZnO nanoarrays as electron transport layers for enhancing photocurrent of photovoltaic devices. *Journal of Materials Chemistry C* **2015**, *3*, 828-835.

28. Tao, C.; Ruan, S.; Zhang, X.; Xie, G.; Shen, L.; Kong, X.; Dong, W.; Liu, C.; Chen, W., Performance improvement of inverted polymer solar cells with different top electrodes by introducing a MoO$_3$ buffer layer. *Appl. Phys. Lett.* **2008**, *93*, 193307-1-193307-3.

29. McIntyre, J. E.; Milburn, A. H., Thermotropic liquid-crystalline polyesters and polyesteramides. *British Polymer Journal* **1981**, *13*, 5-10.

30. Van Oss, C. J.; Chaudhury, M. K.; Good, R. J., Interfacial Lifshitz-van der Waals and polar

Chapter 5

interactions in macroscopic systems. *Chem. Rev.* **1988**, *88*, 927-941.

31. Zhou, H.; Zhang, Y.; Seifter, J.; Collins, S. D.; Luo, C.; Bazan, G. C.; Nguyen, T. Q.; Heeger, A. J., High-Efficiency Polymer Solar Cells Enhanced by Solvent Treatment. *Adv. Mater.* **2013**, *25*, 1646-1652.

32. Zhou, H.; Zhang, Y.; Mai, C.-K.; Seifter, J.; Nguyen, T.-Q.; Bazan, G. C.; Heeger, A. J., Solution-Processed pH-Neutral Conjugated Polyelectrolyte Improves Interfacial Contact in Organic Solar Cells. *ACS nano* **2014**, *9*, 371-377.

33. Pingree, L. S.; Reid, O. G.; Ginger, D. S., Electrical scanning probe microscopy on active organic electronic devices. *Adv. Mater.* **2009**, *21*, 19-28.

34. Nonnenmacher, M.; o'Boyle, M.;Wickramasinghe, H., Kelvin probe force microscopy. *Appl. Phys. Lett.* **1991**, *58*, 2921-2923.

35. Venkatesan, S.; Ngo, E.; Khatiwada, D.; Zhang, C.; Qiao, Q., Enhanced lifetime of polymer solar cells by surface passivation of metal oxide buffer layers. *ACS applied materials & interfaces* **2015**, *7*, 16093-16100.

36. Zhang, S.; Ye, L.; Wang, Q.; Li, Z.; Guo, X.; Huo, L.; Fan, H.; Hou, J., Enhanced photovoltaic performance of diketopyrrolopyrrole (DPP)-based polymers with extended π conjugation. *J. Phys. Chem. C* **2013**, *117*, 9550-9557.

37. Udum, Y.; Denk, P.; Adam, G.; Apaydin, D. H.; Nevosad, A.; Teichert, C.; White, M. S.; Sariciftci, N. S.; Scharber, M. C., Inverted bulk-heterojunction solar cell with cross-linked hole-blocking layer. *Organic electronics* **2014**, *15*, 997-1001.

38. Wu, T.; Hsiao, Y.-C.; Li, M.; Kang, N.-G.; Mays, J. W.; Hu, B., Dynamic Coupling between Electrode Interface and Donor/Acceptor Interface via Charge Dissociation in Organic Solar Cells at Device-Operating Condition. *J. Phys. Chem. C* **2015**, *119*, 2727-2732.

39. Foertig, A.; Kniepert, J.; Gluecker, M.; Brenner, T.; Dyakonov, V.; Neher, D.; Deibel, C., Nongeminate and geminate recombination in PTB7: PCBM solar cells. *Adv. Funct. Mater.* **2014**, *24*, 1306-1311.

40. Sánchez-Díaz, A.; Izquierdo, M.; Filippone, S.; Martin, N.; Palomares, E., The origin of the high voltage in DPM12/P3HT organic solar cells. *Adv. Funct. Mater.* **2010**, *20*, 2695-2700.

Chapter 5

Chapter 6

General Conclusions

Chapter 6

In this thesis, more attention was focused on the preparation and performance optimization of BHJ solar cells based on PTBx:PCBM system by different solution processed approaches. The main effect of these approaches on the performance of the devices origins from the change in the morphology of active layer, domain size and crystallinity of polymer, further leading to the variation of photovoltaic performance parameters, such as short circuit current and fill factor.

In the chapter 3, the method of solution aging was applied in the fabrication of polymer solar cells based on PTB1:PCBM blend. The novel method affects the exciton separation, morphology of blend film and finally impacts device performance. Compared to the blend film without solution aging, the aged films present significantly improved small nanoscale domain in morphology and a bi-continuous interpenetrating network which in turn result in higher interface area and efficient charge generation between the donor and acceptor. GIWAXS and GISAXS of films showed favorable charge transport pathways due to the increase of interaction between PCBM and the thienothiophene unit of PTB1. All effects give rise to the better charge collection and higher short circuit current.

we obtained the best performance of 5.16% with blend solutions aged for 48 h, a significant improvement exceeding 19% over the efficiency of 4.32% obtained in devices without polymer blend solution aging. In addition, we also verify the validity of solution aging by utilizing the approach in P3HT:PCBM system. The fabrication of P3HT:PCBM solar cells is same to PTB1:PCBM solar cells and different aging times are performer with 0 h, 24 h, 48 h and 72 h. The results show that the optimal PCE of 3.5% with Jsc of 9.14 mA/cm^2 is obtained from solution aging for 24 h comparison with PCE of 3.1% obtained without solution aging. We believe that this efficient method can be applied to other organic devices such as photodetectors, field-effect transistors and light emitting diodes.

In the chapter 4, we employ multiple solvent mixtures in morphology optimization of

Chapter 6

the active layer based on PTB7:PC$_{71}$BM BHJ solar cells. Addition of "unfriendly" solvent CHN to CB:DIO binary solvent system significantly affects the morphology of PTB7:PC$_{71}$BM BHJ film including the interpenetrating network structure, chain alignment and phase separation, leading to a considerably improvement in PSC performance. In-situ observation of the crystallization film by GIXS displays an oriented molecule ordering as well as improvement of inter-chain stacking and π-π stacking between PTB7 polymer backbones along with increase of CHN in solution, which consequently leads to the more increment Jsc. The increased polymer crystallinity and big phase separation in blend film due to the use of CHN consequently contributed to the enlarged charge extraction density and fast charge non-geminate recombination. All the effects induce a simultaneous increase in short circuit current and decrease in FF after CHN/CB of different ratio treatment. The device from CB/CHN of 2:1 ratio treatment displays an optimal PCE of 7.31%. This work gains understanding correlation between polymer morphology, crystallization, charge extraction and recombination kinetics, and more generally with PSC device performance by multiple solvent processing.

Following the ternary solvent mixture treatment with the optimal ratio 2:1of CB/CHN, in chapter 6, two types of solar cell devices, conventional structure and inverted structure, are prepared based on PTB7:PC$_{71}$BM blend with CB and CB/CHN (2:1, v/v) mixture treatments. Enriched PTB7 on the top surface of active layer, detected via surface energy measurements, induces higher hole selectivity at the anode contact and is favorable to i-PSC compared with c-PSC device. Thus, PCE of 8.05% for i-PSC device from CB treatment is obtained that is significantly higher than the one obtained from c-PSC device (6.86%). Comparison with CB treatment, CB/CHN treatment can affect not only the crystalline morphology and oriented alignment of polymer but also the surface composition of the active layer. A decrease in PCE for i-PSC device is observed by using CB/CHN as solvent that might be due to the addition of CHN leading to the relatively enrichment of PC$_{71}$BM on the top surface and a big phase separation. The result is different to that observed in c-PSC. It can be concluded that

Chapter 6

selection of transport layer between active layer and electrode is related to the variation of surface composition and play a key role in the device performance. In addition, TPV and CE measurements at different light bias show surface composition of active layer and polymer crystallinity are important factors for non-geminate recombination kinetics. After treatment with CB/CHN, i-PSC and c-PSC devices both show fast charge carrier recombination due to a big phase separation and isolated domains polymer PTB7 and PC$_{71}$BM.

Chapter 6

List of Contributions

Journal Articles

P.L. Han, V.S. Balderrama, A. Mihi, P. Formentin, J.F. Borrull, J. Pallarés, L.F. Marsal, Improving the Efficiency of PTB1: PCBM Bulk Heterojunction Solar Cells by Polymer Blend Solution Aging, *IEEE Journal of photovoltaics,* 2015, 5, 889-896.

P.L. Han, A. Mihi, J.F. borrull, J. Pallarés, L.F. Marsal, Interplay Between Morphology, Optical Properties, and Electronic Structure of Solution-Processed Bi_2S_3 Colloidal Nanocrystals, *J. Phys. Chem. C,* 2015, 119, 10693–10699.

V.S. Balderrama, M. Estrada, P.L. Han, P. Granero, J. Pallarès, J. Ferré-Borrull, L.F. Marsal, Degradation of Electrical properties of PTB1:PCBM solar cells under different environments, *Solar Energy Materials and Solar Cells,* 2014, 125, 155-163.

P.L. Han, J.F. borrull, J. Pallarés, L.F. Marsal, Morphology Formation and Charge Recombination kinetics in Ordered Construction Bulk Heterojunction Solar Cells via the Role of Multiple Solvent Mixture Processing. *Advanced Functional Materials,* (submitted)

P.L. Han, J.G. Sanchez, J.F. borrull, J. Pallarés, L.F. Marsal, The Effect of Solvent Mixture Treatment on Surface Composition: Controlling Morphology in Conventional and Inverted Structures Based on $PTB7:PC_{71}BM$. *Chemical Science,* (submitted)

Communication to conferences

P.L. Han, P. Formentin, J. Pallarés and L.F. Marsal, Fabrication of colloidal B_2S_3 nanocrystals with size tunable from nanodot to nanorod. *Graduate Students Meeting on Electronics Engineering GSMEE 2014*, Poster, Tarragona, Spain, Jun 19th 2014.

P.L. Han, V.S. Balderrama, P. Formentin, J. Pallarés and L.F. Marsal, The effect of solvent on the performance of PTB1:PC$_{61}$BM bulk heterojunction solar cells, *9th International Conference on Organic Electronics ICOE 2013*, Poster, Grenoble, France, Jun 17th 2013.

P.L. Han, V.S. Balderrama, M. Alba, P. Formentin, J. Pallarés and L.F. Marsal, Influence of annealing and the Blend Concentration on the Performances of PTB1: PC$_{61}$BM BHJ Solar Cells, *9th Spanish Conference on Electron Devices CDE-2013*, Poster, Valladolid, Spain, February 12th 2013.

P.L. Han, V.S. Balderrama, P. Formentin, J. Pallarés and L.F. Marsal, Fabrication and Characterization of PTB1:PC$_{61}$BM bulk heterojunction   Solar cells, *9th International Conference on Organic Electronics ICOE 2012*, Presentation, Tarragona, Spain, Jun 6th 2012.

P.L. Han, V.S. Balderrama, M. Alba, P. Formentin, J. Pallarés and L.F. Marsal, Influence of the Blend Concentration on the Performances of PTB1: PC$_{61}$BM BHJ Solar Cells, *Spanish Nanophotonics Conference CEN2012*, Presentation, Carmona, Sevilla, Spain, October 1st 2012.

J. Ferré-Borrull, V.S. Balderrama, P. Granero, P. Han, A. Mihi, J. Pallarès, and L.F. Marsal, Fabrication, modeling and degradation studies of ordered bulk heterojunction organic solar cells with nanostructured interfaces, *Congreso Internacional de Metalurgia y Materiales 14° SAM-CONAMET / IBEROMAT 2014*, Presentation, Santa Fe, Argentina, Oct 21st 2014.

V.S. Balderrama, M. Estrada, P.L. Han, P. Granero, J. Pallarès, J. Ferré-Borrull, L.F. Marsal, Stability analysis of organic solar cells fabricated with PTB1:PCBM in accordance with established ISOS-D1 protocols, *Spanish Nanophotonics Conference CEN2014*, Presentation, Santander, Spain, May 15th 2014.

V.S. Balderrama, P. Granero, P.L. Han, J. Ferré-Borrull, J. Pallarès, and L.F. Marsal, Fabrication, characterization and design modeling of well-ordered interdigitated organic solar cells, *28th European PV Solar Energy Conference and Exhibition EU PVSEC 2013*, Poster, Paris, France, September 29th 2013.

V.S. Balderrama, P.L. Han, P. Granero, J. Pallarès, J. Ferré-Borrull and L.F. Marsal, Performance and degradation of organic solar cells due to air exposure manufactured with low-band gap material, *9th International Conference on Organic Electronics ICOE 2013*, Poster, Grenoble, France, Jun 17th 2013.